Finite Volume Methods for Acoustics and Elasto-plasticity with Damage in a Heterogeneous Medium

Tiernan Fogarty

A dissertation submitted in partial fulfillment of
the requirements for the degree of

Doctor of Philosophy

University of Washington

2001

Program Authorized to Offer Degree: Department of Applied Mathematics

University of Washington

Abstract

Finite Volume Methods for Acoustics and Elasto-plasticity with Damage in a Heterogeneous Medium

by Tiernan Fogarty

Chair of Supervisory Committee:

High-resolution finite-volume numerical methods originally developed for shock capturing in the context of nonlinear conservation laws are found to be very useful for solving acoustic and elasto-plastic problems in heterogeneous media. These methods are based on solving Riemann problems at the interface between grid cells. The solution method is introduced in the context of acoustics problems with periodic or random media in one and two space dimensions. Test problems are used to show how the method can be extended to solve problems that are elasto-plastic in nature and may include material damage. The use of constrained minimization techniques in conjunction with linear elasticity to solve elasto-plastic problems is introduced and found to be useful in multi-dimensional problems. In one dimension exact Riemann solutions can be computed and have been used to validate the minimization approach. The minimization algorithms are then extended to two-dimensional problems and used to find numerical solutions to a variety of physically interesting 2D examples.

TABLE OF CONTENTS

ACKNOWLEDGMENTS

I would like to thank my advisor Randall J. LeVeque. Without him none of this would have been possible. It has been excellent working with Randy, and I hope to continue to have an active correspondence with him in the future.

I would also like to thank my supervisory committee. Ken Bube, Jerry Kevorkian, and Robert Van Dyck. Much of this work was done with the collaboration of George Turkiyyah. I hope that he and I can also continue to work together in the future.

I would like to thank my many friends in the department who gave me help, encouragement, and a lot of valuable criticism. In particular I would like to thank Arnold Kim, Derek Bale, Tricia Burgess, James Rossmanith, and Sorin Mitran.

Finally I would like to thank the many members of my close family and friends: my parents Tom and Jeri Fogarty, my grandfather Tom Fogarty and grandmother Jean Flemming, Jennifer Goodson, Jim Campbell, Kevin Jones, Mark Offord, Karen Holmes, and the 20+ members of the Fogarty, Hourigan, Larsen, and Steltzner clans who have gone out of their way to encourage this endeavor.

This work was supported in part by NSF grant DMS-9803442 and DOE grant DE-FG03-00ER2592.

Chapter 1

INTRODUCTION

The focus of this work is to simulate numerically elasto-plastic waves in heterogeneous media. In the first part of the thesis we use examples of acoustic wave propagation in a heterogeneous material as a means to introduce the numerical solution techniques. The second half of the thesis is devoted to the goal of developing solution methods for problems that are elasto-plastic in nature. In Chapter 2 we introduce the physical systems of interest and the equations we use to model them. We start with a derivation of elasticity in three dimensions and then reduce this general system to find the equations used to model several examples of 1D and 2D acoustics, elasticity, and elasto-plasticity. All the systems we consider are time-dependent hyperbolic problems where the primary feature of interest is the evolution of the wave structure. Throughout this work the fundamental question that we would like to answer is this: Assuming that the initial state of some material is known, can the material be accurately described at a later time by modeling the wave propagation? For example, when considering an acoustic system we assume that the pressure and velocity fields (or **state variables**) are known initially and we want to be able to model these quantities accurately as they evolve via the simulation of acoustic wave propagation. In the 1D acoustic system there are only two variables of interest: pressure and velocity. We introduce our numerical solution technique in the context of this easy to understand example and then expand upon these ideas to solve more complex examples that are multi-dimensional and elasto-plastic in nature. While in these latter systems the state variables are tensorial and the dynamics and solution techniques are much more complicated, many of the tools needed to solve such problems can be defined in terms of 1D acoustics.

1.1 Problems of Interest

This work was initially motivated by the desire to understand better and possibly help model two problems of interest in acoustics: high-frequency ultrasound (HIFU) and lithotripsy. Both these topics are currently under experimental study at the Applied Physics Lab of the University of Washington. Exposure to the (currently) unanswered questions of these two applications led to the investigation resulting in this thesis.

High-frequency ultrasound in this context is the idea of using a continuous train of high-frequency focused sound waves to generate heat and perform non-invasive medical procedures. In this application there are two main difficulties that need to be overcome before a numerical simulation could be possible: heterogeneities in the “elastic” tissue and discontinuities in the equation of state between the blood and tissue. In order to solve such a problem with the techniques we envision using, we need to be able to simulate wave propagation across both of these kinds of discontinuities. See [2], [3], and [53] for examples of the types of problems associated with interfaces across which the equation of state changes. While we do not return to the specific problem of HIFU in the thesis, we do demonstrate the ability to solve problems that contain both such difficulties. See [7],[21], and [55] for details on other approaches to these kinds of problems. The phenomenon of bubbles in the fluid is another related problem that arises often in biological tissue which would need to be accounted for in any accurate model. See [7] and [11] for details.

Lithotripsy is a technique used to destroy kidney stones via high-pressure focused shock-waves. The apparatus consists of a tank of water into which the subject is submerged. Inside the tank is a parabolic dish which is used to focus an electrically generated shock-wave. The patient is oriented so that the focal point of the dish is located inside the body at the location of a kidney stone. After the successive application of many (thousands) of shock waves incident (and focused on) the stones, they are broken up. While it is clear that the continuous bombardment of the stones will (and does) eventually destroy them, the mechanism responsible for the destruction is not entirely clear. The two main plausible explanations at this time are bubble cavitation in the fluid at the surface or the long term build up of stress and plastic deformation resulting in failure. The type of dynamics associated with the latter of these two mechanisms is the primary topic of interest in this thesis. Once the numerical methods we use are introduced in the context of heterogeneous media in the early parts of the thesis, we use the bulk of this work to model elasto-plastic wave propagation and the associated physics in a solid. Later in the thesis it helps to keep the example of lithotripsy in the back of ones mind as a motivation for understanding and modeling plastic-deformation and damage via wave propagation. In this work we do not address the issue of cavitation. There is however, a vast amount of literature on the subject. See [13], [42], [45], and [64] for an introduction to the subject.

1.2 Solution Obstacles

As we mentioned above, there are several obstacles we would like to surmount with our solution method. The software that is the basis of all our simulation is CLAWPACK, a very robust package that can numerically simulate wave propagation for a large variety of physical systems. The software is designed to solve time-dependent hyperbolic systems of partial differential equations in one, two, and three space dimensions. While the algorithms were originally developed to study shock-waves in the context of conservation laws for gas-dynamics, the methods can be directly applied to systems in nonconservative form (heterogeneous acoustics for example). Examples of the systems CLAWPACK can handle include acoustics, elasticity, advection, Burgers' equation, and the Euler equations. Extensive documentation about the software can be found on the following web-page: (`http://www.amath.washington.edu/~claw/`). See [34],[35], and [36] for details. As CLAWPACK does an extremely good job at modeling the wave propagation in the type of problems we are interested in, the software is a perfectly suited tool to start our investigations. One can down-load CLAWPACK and start with a working 1D or 2D model of the systems listed above. From here, the challenge is to derive the appropriate physical model to use for a given example and then incorporate this added physical content into the numerics by altering and adding to the base algorithms of CLAWPACK.

After the introductory chapter, a derivation of the three-dimensional linear elastic system is given. The linear system assumes that the elastic deformations are small (infinitesimal) rather then large (finite). The key point here is that, prior to the onset of plastic deformation, the assumption that deformation is infinitesimal renders the system linear. Finite deformation is a separate topic that is not considered in any detail in this thesis. An introduction to the topic of finite deformation in this context can be found in [30], [50], [52] and [56]. The basics of elasticity and how underlying physical assumptions can be found in a great number of references. A few of that I have found particularly valuable are [26], [35], and [51]. The 3D elastic system is then used to derive several other systems which are examples in elasticity and acoustics of special cases of the general system in 2D and 1D under different assumptions of how the reduction from 3D was made. See [9], [10], and [59] for more discussion of 2D and 1D elastic reductions.

1.2.1 Numerical Wave Propagation

Once the 1D acoustic system is derived, we use it as an example in Chapter 3 to introduce the wave propagation algorithm CLAWPACK. Each system of interest is viewed in a Lagrangian frame of reference where the domain is partitioned into a computational grid of "cells". For the acoustic example above, we assign an initial cell-wise constant value of pressure and velocity in all the cells within the domain. We then solve for the future cell values of the state variables by modeling the wave propagation throughout the domain via CLAWPACK. CLAWPACK exploits the inherent wave structure of hyperbolic systems by solving **Riemann** problems at all the cell boundaries. Variation of the state variables from cell to cell and the equations of interest define a Riemann problem at each cell interface. Waves generated by the solution of these Riemann problems are the basis of high-resolution, finite-volume, cell-wise update scheme. To first order the algorithm can be shown to be the same as the **Godunov** method and for special cases in the absence of **wave-limiters** it can be shown how the scheme reduces to the **Lax-Wendroff** method. An important aspect of this solution method is that material discontinuities and inhomogeneities can be automatically accounted for. See [18], [27], and [33] for more details.

1.2.2 Acoustics in Heterogeneous Material

The first example we investigate is the 1D acoustic system in a heterogeneous material. In Chapter 4 we first show how the standard solution method fails to model the long time behavior of an acoustic wave propagating in a special case of a periodic medium. This particular medium has a constant sound speed and periodic layers of different impedance. See [17], [31], and [47] for details. As an acoustic wave moves through this medium it is partially reflected and partially transmitted at each impedance mismatch. See [14] and [29]. The wave propagation algorithm uses wave-limiters to help prevent the introduction of numerical dispersion that tends to be introduced in the regions of discontinuities. In the example of the periodically layered medium, we assume that the scale of the material discontinuity is much smaller then the wavelength of the acoustic wave. One expects that in this case there will be a high degree of numerical dispersion as a wave is always in a region of multiple discontinuities. We find that this is in fact the case and that if care is not taken in the wave-limiting method, numerical dispersion will completely degrade the solution. We introduce a new method of wave-limiting that is useful for wave propagation in heterogeneous materials and then show how it works in both periodic and random acoustic examples. See [1], [22], [63], and [38] for related work. After various one-dimensional acoustics problems in heterogeneous media are used to introduce the details of the method, we briefly show how these techniques work in two-dimensional acoustics and go into the details of a 2D acoustic Riemann solution in the presence of material inhomogeneities. See [4], [5], [6], [41], and [48] for a very small sample of problems of interest in this field.

1.2.3 Elasto-Plasticity

Once we have confidence that the solution method can properly simulate acoustic and elastic wave propagation in heterogeneous media, we move on to a discussion of the elasto-plastic regime. In the sections on elasto-plasticity there are several problems that must be first defined and then incorporated into the model and solution procedure. We first give examples of how the solution method solves the one-dimensional elastic system. We then introduce the concepts associated with elasto-plastic behavior. Plasticity refers to permanent strain in a material once the stress exceeds an elastic yield-criterion. An introduction to the theory of plasticity can be found in [19], and [23]. We introduce and give solution procedures for both linear plasticity and non-linear plastic response as well as introducing the concept of damage and solving examples where damage is present. After these concepts are all clearly defined we solve multiple examples which include the elastic, linearly-plastic, nonlinearly-plastic, and damage regimes with heterogeneities in both the stress-strain relation and the plastic yield condition. The main thrust of this discussion is that the material responds elastically to stress until some material-specific yield condition is satisfied. Once the yield condition is satisfied, the constitutive equation or "physics" changes and the material no longer responds to stress in the same fashion. Plastic response implies that a fraction of the strain energy is converted into permanent plastic-deformation that remains after the elastic energy has dissipated. See [25], [32], and [49]for more information on the yield conditions. Before a set of equations can be defined one must first make assumptions about the type of constitutive equations used to govern the plastic response. There is a great supply of literature on the subject of constitutive relations in the plastic regime. See [12], [20], [40], and [44] for a variety of special cases.

1.2.4 Damage

If the amplitude of the plastic deformation is large enough, it can cause an additional phenomenon known as damage. In the context of this work, damage is a measure of the change in the "strength" of the elastic response. An undamaged material can undergo elastic and plastic deformations indefinitely without changing the elastic response or ever "breaking". A material that reaches a value of damage $D = 1$ is assumed to have failed and is no longer capable of elastic behavior. For a material that is plastically deformed but undamaged, the elastic response is the same regardless of the plastic deformation. While the range of stress and strain values that the material responds to elastically is different after plastic deformation has occurred, the nature of the elastic response is unchanged as long as the material remains undamaged. However, in a material that is damaged, the nature of both the elastic and plastic response is permanently altered. A sample of the concerns that arise in this aspect of plasticity can be found in [8], [15], [60], and [62].

1.2.5 Elasto-Plastic Riemann Solution

As will be shown later, the 1d elasto-plastic system can be derived directly by combining the definition of strain with Newton's second law in the following form:

$$\begin{aligned} \epsilon_t - v_x \quad &= 0, \\ \rho(x) v_t - \sigma_x \quad &= 0. \end{aligned} \tag{1.1}$$

Here ρ is the density, and v is the velocity. The system is closed by a constitutive, or **stress-strain** relation between the stress σ and the strain ϵ. Linear elasticity assumes a **Hooke's Law** relation given as

$$\sigma = \beta\epsilon. \tag{1.2}$$

Here β is a constant that is material specific. As long as the stress does not satisfy the yield condition the material will respond elastically and the system above provides an accurate description of the physics. However, if the amplitude of the stress is large enough, the material will undergo a phase-change from elastic to plastic response. The most basic elasto-plastic constitutive relation assumes that the plastic response is also linear but with a much smaller ability to withstand stress. To model elasto-plastic behavior one can assume a stress-strain relation given as

$$\sigma = \beta\epsilon \;\text{ if }\; \sigma < \sigma_y \;\text{ and }\; \sigma = \beta_p\epsilon \;\text{ if }\; \sigma = \sigma_y. \tag{1.3}$$

Note that plastic deformation changes the definition of σ_y.

The nature of this dual constitutive relation can be seen clearly via the example shown in the figures 1.1–1.3. Here we show a 2d example with two clearly separated elastic and plastic waves. A long thin 2d material is pulled apart so that the entire left-hand side moves to the left while the entire right-hand side moves to the right. Here we are solving a Riemann problem where every point in the slab to the left of center moves at an initial velocity of $v = -10$ while every point to the right of the center moves with initial velocity $v = +10$. The velocity is great enough that the induced stress causes the yield condition to be satisfied. Two elastic and two plastic waves are generated in the center and move outwards. The elastic wave speed is greater than the plastic wave speed so that the waves clearly separate the material into 3 distinct regions after a short time. In this example we use no-traction boundary conditions so that the upper and lower boundaries only exhibit stress in the x-direction. See Figure 1.1 and Figure 1.2. Note also how the material is "pulled in" vertically while it is stretched out horizontally. Also note that while the calculations are performed in Lagrangian coordinates, these figures show material deformation in greatly exaggerated Eulerian coordinates. Here the color represents the amount of plastic deformation in the material.

In addition to the propagating waves, in the center of the domain one can see that there is also a "dip" in the upper and lower boundaries at the position of the initial velocity jump. The nature of this dip is still an open question. At this point we believe the phenomenon to be an accurate feature of the two-dimensional solution and not a numerical artifact. Since no-traction boundary conditions are used at the upper and lower boundaries, this does not correspond exactly to a one-dimensional Riemann problem, but gives a good feel for the nature of such a solution. Figure 1.4 shows the Riemann structure for this example. Here we can see the correspondence of the two elastic and plastic waves that would arise in a single Riemann problem with the numerical example.

In one dimension we develop two solution techniques to solve this problem. The first solution method is based on solving exact elasto-plastic Riemann problems for elastic and plastic waves and then using these waves to find the new cell values of our state variables, stress σ and velocity v. See [37], [57] and [58] for details on this type of Riemann solution. The second solution method solves purely elastic Riemann problems and then compares the new cell values with the yield condition. If the yield condition is found to be exceeded then the algorithm uses **minimization techniques** to adjust the stress and plastic strain and redefine the yield condition. The solution procedure based on solving exact elasto-plastic Riemann problems can be shown to give solutions which are correct. While this exact Riemann solution technique works extremely well in 1D, unfortunately it does not appear that the method can be extended to 2D. The method based on minimization of free energy subject to the constraint of the yield condition gives the same results as the exact elasto-plastic Riemann method in 1D, and can be extended in a straight-forward manner to 2D and 3D. In Chapters 6 and 7 we show how both methods give the proper results in 1D and then show how the method based on minimization techniques extends to 2D and gives what we believe are accurate solutions.

1.2.6 New in This Work

As stated above, the original motivation for this investigation was the lithotripsy problem. The goal was to develop a numerical model that could simulate elastic and elasto-plastic wave propagation along with the effects of non-linear plasticity and damage. While in future work we hope to model cell-wise plastic deformation as a tensorial quantity, in this work we have modeled plastic deformation and damage as scalar quantities. Here the plastic deformation π, models the amount plastic-strain energy that is converted into permanent material deformation. The damage D, models the reduction in strength of the material via an alteration of the material coefficients. While the modeling of plastic deformation and damage in this fashion is not new to the field, the use of this type of physical model with a time-dependent multi-dimensional wave propagation method to solve problems in heterogeneous media is, to the best of our knowledge, original. See [39], [43], [61], [56], and [57] for other examples of Godunov-type methods applied to similar problems.

In this work we have used high-resolution finite-volume methods to successfully develop two solution methods capable of solving elasto-plasticity with damage in one dimension. The first method we have developed uses exact Riemann solutions to solve for elastic and plastic waves in the case of linear and non-linear elasto-plasticity with damage. The second approach, which is novel to this work, is the use of minimization techniques in conjunction with linear-elastic Riemann solutions to model both one-dimensional and two-dimensional elasto-plastic wave propagation with damage. We use the fact that the two methods give the same results for a series of one-dimensional experiments with a variety of differing heterogeneities as a way to prove the validity of the technique based on minimization. We then use specialized examples which allow comparison between the 1D and 2D solution methods as a way to ensure the accuracy of the 2D solution method. The most important contribution of this work is the ability to solve what was the most difficult problem: the numerical modeling of 2D plastic behavior. The solution method based on minimization not only gives accurate results in 1D but is shown to be easily extendible to 2D and 3D.

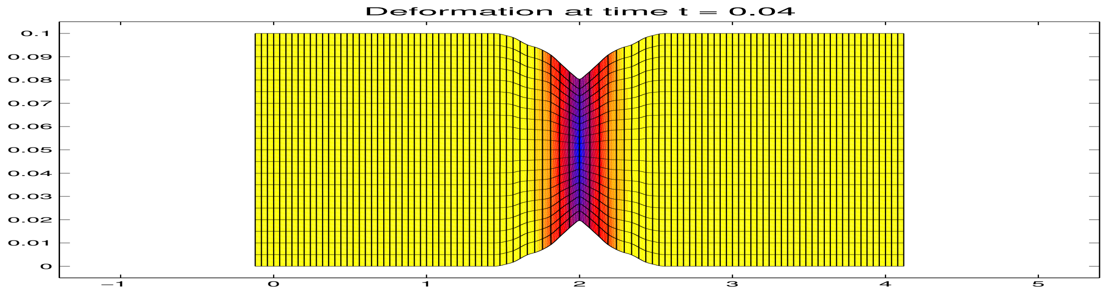

Figure 1.1: Here we see a 2D slab of material in greatly exaggerated Eulerian coordinates. The left-half of the slab is being pulled to the left while the right-half is being pulled to the right.

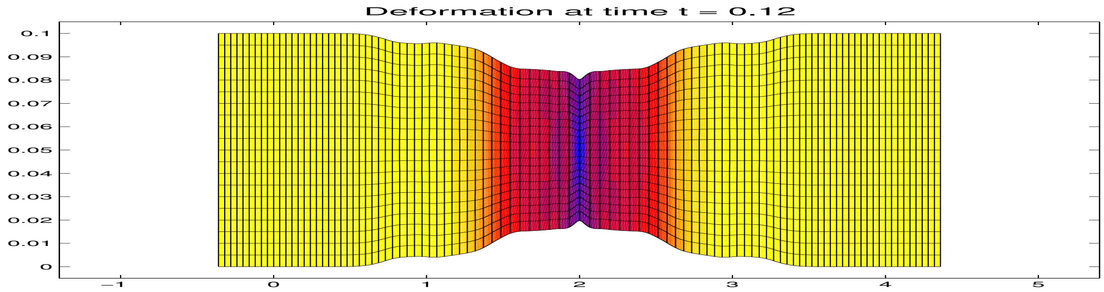

Figure 1.2: Elastic and Plastic waves are generated by the velocity differential at the center of the slab. Note that behind the two plastic wave fronts the velocity must be zero.

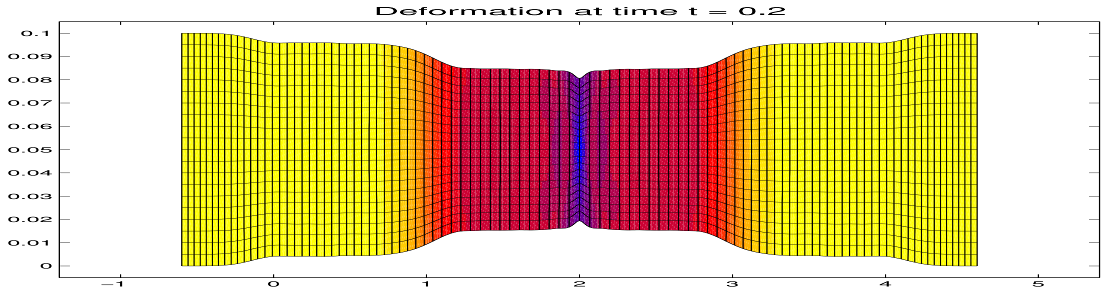

Figure 1.3: Final time in the calculation. The two elastic and two plastic waves are fully separate and clearly visible

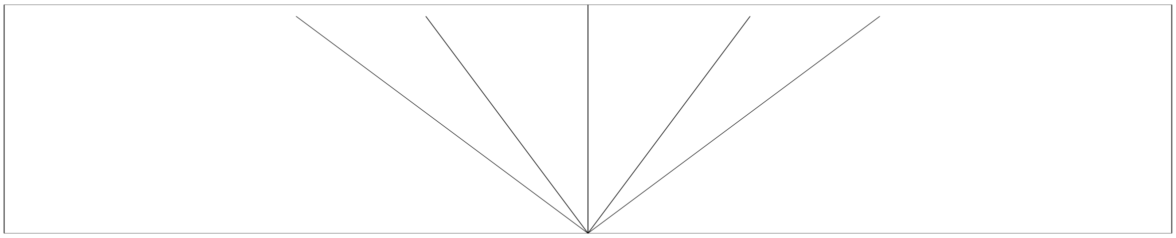

Figure 1.4: Riemann structure for this example: two elastic and two plastic waves.

Chapter 2

EQUATIONS OF INTEREST

In this chapter the general 3D system of conservation laws for elasticity is derived by combining the equations of motion with a constitutive equation and the definition of strain. From the 3D conservation law system for elasticity we show how to derive elastic and acoustic systems in both 2D and 1D. If we make certain assumptions on the variation in the third dimension then the 3D system simplifies to either the plane-strain or plane-stress 2D elastic equations. The distinction between the plane-strain and plane-stress systems and the necessary reductions needed to arrive at them are thoroughly examined. Further assumptions show how the the 2D systems can be reduced to the equations of 1D elasticity and 1D acoustics. Finally 1D acoustics are used as a means to introduce the basics of finite volume methods and of the specific finite volume solver used throughout this work: CLAWPACK.

2.1 Conservation Laws

The elasticity equations may be derived via a conservation law, which in three space dimensions takes the form,

$$\frac{\partial}{\partial t}q(x,y,z,t)+\frac{\partial}{\partial x}f(q(x,y,z,t))+\frac{\partial}{\partial y}f(q(x,y,z,t))+\frac{\partial}{\partial z}f(q(x,y,z,t))=0, \tag{2.1}$$

As we will show later, $q(x,y,z,t$ here is a vector of state variables. See [33] and [34] for details.

If we apply a force balance on a cubic element in a continuum that is undergoing internal motions. Newton's second law gives a set of three equations known as the equations of motion for a continuum. These equations, in the absence of source terms or body forces, can be written as

$$\rho\frac{\partial^2}{\partial t^2}u_i=\frac{\partial}{\partial x_j}\sigma_{ij},\quad i=1,2,3,\quad j=1,2,3. \tag{2.2}$$

Note that we use summation notation. Here (2.2) is a system of three equations where u_i is the component of displacement in the i'th direction and the partial derivatives of the components (σ_{ij}) of the stress tensor are summed over j. If we denote the i'th component of velocity as

$$v_i=\frac{\partial u_i}{\partial t} \tag{2.3}$$

we see that (2.2) is a conservation law of the form (2.1).

In order to solve this system we need a constitutive equation which relates σ_{ij} to u_i. Hooke's Law is the most general form of a constitutive law for linear elasticity. Hooke's law for an isotropic linear elastic material can be written as

$$\sigma_{ij} = \lambda \epsilon_{kk} \delta_{ij} + 2\mu \epsilon_{ij}, \quad i = 1,2,3 \quad j = 1,2,3. \tag{2.4}$$

Here ϵ_{kk} is the trace of the strain tensor. Note that this is a tensorial relation that we can write in matrix form as

$$\begin{bmatrix} \sigma_{11} \\ \sigma_{22} \\ \sigma_{33} \\ \sigma_{12} \\ \sigma_{23} \\ \sigma_{13} \end{bmatrix} . = \begin{bmatrix} \lambda + 2\mu & \lambda & \lambda & 0 & 0 & 0 \\ \lambda & \lambda + 2\mu & \lambda & 0 & 0 & 0 \\ \lambda & \lambda & \lambda + 2\mu & 0 & 0 & 0 \\ 0 & 0 & 0 & 2\mu & 0 & 0 \\ 0 & 0 & 0 & 0 & 2\mu & 0 \\ 0 & 0 & 0 & 0 & 0 & 2\mu \end{bmatrix} \begin{bmatrix} \epsilon_{11} \\ \epsilon_{22} \\ \epsilon_{33} \\ \epsilon_{12} \\ \epsilon_{23} \\ \epsilon_{13} \end{bmatrix} . \tag{2.5}$$

See [26] and [29] for details. Here λ and μ are called the Lamé constants, with $\lambda = (\kappa - 2\mu/3)$ where κ is the bulk modulus or $1/\kappa$ is the coefficient of compressibility and μ is the shear modulus or rigidity, δ_{ij} is the Kronecker delta. The strain-displacement relationship can be written as

$$\epsilon_{ij} = \frac{1}{2}\left(\frac{\partial u_i}{\partial x_j} + \frac{\partial u_j}{\partial x_i}\right), \quad i = 1,2,3 \quad j = 1,2,3. \tag{2.6}$$

Substitute (2.6) into (2.4) and combine Hooke's law with the equations of motion to get the following system of equations

$$\rho \frac{\partial}{\partial t} v_i = \frac{\partial}{\partial x_j} \sigma_{ij}, \quad i = 1,2,3 \quad j = 1,2,3 \tag{2.7}$$

and

$$\sigma_{ij} = \lambda(u_{k,k})\delta_{ij} + \mu(u_{i,j} + u_{j,i}), \quad i = 1,2,3 \quad j = 1,2,3. \tag{2.8}$$

Here $u_{i,j} = \sum_{j=1}^{3} \frac{\partial u_i}{\partial x_j}$. The six equations (2.3), (2.7) for $i = 1,2,3$ plus the definition (2.8) for σ_{ij} describe the equations of the displacements u_i and velocities v_i. Note that all the systems of equations in this work are assumed to be in a Lagrangian (computational) frame of reference. While some figures in later sections show deformation in an Eulerian frame of reference so that one can visualize how material is spatially altered, unless otherwise stated the default frame of reference is Lagrangian.

2.2 Three Dimensional Elasticity Equations

To solve the system given by (2.3), (2.7) and (2.8) we need to have expressions for the time derivatives of the stresses. We take the time derivative of (2.5), (2.6), and (2.8) and combine with (2.7) to obtain the hyperbolic conservation law which governs 3D isotropic elasticity.

$$
\begin{aligned}
&\sigma_{11t} - (\lambda + 2\mu)v_{1x} - \lambda v_{2y} - \lambda v_{3z} = 0 \\
&\sigma_{22t} - \lambda v_{1x} - (\lambda + 2\mu)u_{2y} - \lambda v_{3z} = 0 \\
&\sigma_{33t} - \lambda v_{1x} - \lambda v_{2y} - (\lambda + 2\mu)v_{3z} = 0 \\
&\sigma_{12t} - \mu(v_{1x} + v_{2y}) = 0 \\
&\sigma_{23t} - \mu(v_{1z} + v_{3y}) = 0 \\
&\sigma_{13t} - \mu(v_{1z} + v_{3x}) = 0 \\
&\rho v_{1t} - \sigma_{11x} - \sigma_{12y} - \sigma_{13z} = 0 \\
&\rho v_{2t} - \sigma_{12x} - \sigma_{22y} - \sigma_{23z} = 0 \\
&\rho v_{3t} - \sigma_{13x} - \sigma_{23y} - \sigma_{33z} = 0
\end{aligned}
\tag{2.9}
$$

This can be written as the hyperbolic system:

$$q_t + Aq_x + Bq_y + Cq_z = 0 \tag{2.10}$$

Here

$$
q = \begin{bmatrix} \sigma_{11} \\ \sigma_{22} \\ \sigma_{33} \\ \sigma_{12} \\ \sigma_{23} \\ \sigma_{13} \\ v_1 \\ v_2 \\ v_3 \end{bmatrix}
\qquad
A = \begin{bmatrix}
0 & 0 & 0 & 0 & 0 & 0 & -(\lambda+2\mu) & 0 & 0 \\
0 & 0 & 0 & 0 & 0 & 0 & -\lambda & 0 & 0 \\
0 & 0 & 0 & 0 & 0 & 0 & -\lambda & 0 & 0 \\
0 & 0 & 0 & 0 & 0 & 0 & 0 & \mu & 0 \\
0 & 0 & 0 & 0 & 0 & 0 & 0 & 0 & 0 \\
0 & 0 & 0 & 0 & 0 & 0 & 0 & 0 & \mu \\
-1/\rho & 0 & 0 & 0 & 0 & 0 & 0 & 0 & 0 \\
0 & 0 & 0 & -1/\rho & 0 & 0 & 0 & 0 & 0 \\
0 & 0 & 0 & 0 & 0 & -1/\rho & 0 & 0 & 0
\end{bmatrix}
\tag{2.11}
$$

and B and C are similar matrices with the nonzero elements shifted to different locations. Recall that this system is hyperbolic if the matrices A, B, and C and any linear combination of them are diagonalizable with real eigenvalues and a complete set of linearly independent eigenvectors.

For the spatially-homogeneous isotropic case, any linear combination of the matrices A, B, and C has nine eigenvalues that correspond to the wave speeds of the six different waves that can occur as well as the three zero-speed waves.

$$\lambda^1 = -c_p, \quad \lambda^2 = c_p, \quad \lambda^3 = -c_s, \quad \lambda^4 = c_s, \quad \lambda^5 = -c_s, \quad \lambda^6 = c_s, \quad \lambda^7 = \lambda^8 = \lambda^9 = 0.$$

Here c_p is the speed of the P-waves (or pressure waves) and c_s is the speed of the S-waves (or shear waves). Note that there are 2 sets of S-waves in the 3D case. The wave speeds are given by

$$c_p = \sqrt{\frac{\lambda + 2\mu}{\rho}}, \qquad c_s = \sqrt{\frac{\mu}{\rho}}. \tag{2.12}$$

It is important to note that in a heterogeneous material all of the material constants used above may very spatially. For example λ, μ, and ρ become $\lambda(x, y, z)$, $\mu(x, y, z)$, and $\rho(x, y, z)$. In this more general case the system is still hyperbolic in a given domain as long as the above condition is true at any given point (x, y, z).

2.3 Two Dimensional Elasticity Equations

We can reduce the three-dimensional equations to two space dimensions if we assume there is no variation in the z-direction. In this case the system of nine equations (2.10) reduces to two decoupled systems of equations,

$$\begin{aligned} &\sigma_{11t} - (\lambda + 2\mu)v_{1x} - \lambda v_{2y} = 0 \\ &\sigma_{22t} - \lambda v_{1x} - (\lambda + 2\mu)v_{2y} = 0 \\ &\sigma_{12t} - \mu(v_{1x} + v_{1y}) = 0 \\ &\rho v_{1t} - \sigma_{11x} - \sigma_{12y} = 0 \\ &\rho v_{1t} - \sigma_{12x} - \sigma_{22y} = 0 \end{aligned} \tag{2.13}$$

and

$$\begin{aligned} &\sigma_{23t} - \mu v_{3y} = 0 \\ &\sigma_{13t} - \mu v_{3x} = 0 \\ &\rho v_{3t} - \sigma_{13x} - \sigma_{23y} = 0. \end{aligned} \tag{2.14}$$

The system given by (2.13) is known as the **plane-strain two-dimensional elasticity equations**, where $v_1 = u_{1t}$ is the x component of velocity, $v_2 = u_{2t}$ is the y component of velocity, and σ_{ij} is the component of stress in the ij direction. The second system given by (2.14) models shear waves with motion orthogonal to the x-y plane and will not be investigated in this work.

Similarly we can define a **plane-stress** problem by assuming that there are no non-zero stresses caused by forces which lie outside of the plane. Specifically this means that for the plane-stress case we assume that $\sigma_{13} = \sigma_{23} = \sigma_{33} = 0$. With this formulation the constitutive relation for 2D plane stress is given as

$$\begin{bmatrix} \epsilon_{11} \\ \epsilon_{22} \\ \epsilon_{33} \\ \epsilon_{12} \end{bmatrix} = \begin{bmatrix} \frac{\lambda+\mu}{\mu(3\lambda+2\mu)} & -\frac{\lambda}{2\mu(3\lambda+2\mu)} & -\frac{\lambda}{2\mu(3\lambda+2\mu)} & 0 \\ -\frac{\lambda}{2\mu(3\lambda+2\mu)} & \frac{\lambda+\mu}{\mu(3\lambda+2\mu)} & -\frac{\lambda}{2\mu(3\lambda+2\mu)} & 0 \\ -\frac{\lambda}{2\mu(3\lambda+2\mu)} & -\frac{\lambda}{2\mu(3\lambda+2\mu)} & -\frac{\lambda}{2\mu(3\lambda+2\mu)} & 0 \\ 0 & 0 & 0 & \frac{1}{2\mu} \end{bmatrix} \begin{bmatrix} \sigma_{11} \\ \sigma_{22} \\ 0 \\ \sigma_{12} \end{bmatrix}. \tag{2.15}$$

This gives the **plane-stress two-dimensional elasticity equations**,

$$\begin{aligned} &\sigma_{11t} - \frac{4\mu(\lambda+\mu)}{\lambda+2\mu} v_x - \frac{2\lambda\mu}{\lambda+2\mu} v_{2y} = 0 \\ &\sigma_{22t} - \frac{2\lambda\mu}{\lambda+2\mu} u_x - \frac{4\mu(\lambda+\mu)}{\lambda+2\mu} v_{2y} = 0 \\ &\sigma_{12t} - \mu(v_{2x} + v_{1y}) = 0 \\ &\rho v_{1t} - \sigma_{11x} - \sigma_{12y} = 0 \\ &\rho v_{2t} - \sigma_{12x} - \sigma_{22y} = 0 \end{aligned} \tag{2.16}$$

Note that while the plane-strain (2.13) and plane-stress (2.16) systems have the same structure, they have differing effective material constants. The difference in the two systems gives solutions that (as we will see later) are quantitatively different but qualitatively identical. We will return and explore the differences between the plane-strain and plane-stress systems in later sections.

In order to implement a numerical solution via CLAWPACK we rewrite the plane-strain problem (for example) as the following variable-coefficient hyperbolic system:

$$q_t + A(x,y)q_x + B(x,y)q_y = 0, \tag{2.17}$$

where

$$q = \begin{bmatrix} \sigma_{11} \\ \sigma_{12} \\ \sigma_{22} \\ v_1 \\ v_2 \end{bmatrix}, \quad A = -\begin{bmatrix} 0 & 0 & 0 & (\lambda(x,y)+2\mu(x,y)) & 0 \\ 0 & 0 & 0 & 0 & \mu(x,y)) \\ 0 & 0 & 0 & \lambda(x,y) & 0 \\ 1/\rho(x,y) & 0 & 0 & 0 & 0 \\ 0 & 1/\rho(x,y) & 0 & 0 & 0 \end{bmatrix}, \tag{2.18}$$

$$B = -\begin{bmatrix} 0 & 0 & 0 & 0 & \lambda(x,y) \\ 0 & 0 & 0 & \mu(x,y)) & 0 \\ 0 & 0 & 0 & 0 & (\lambda(x,y)+2\mu(x,y)) \\ 0 & 1/\rho(x,y) & 0 & 0 & 0 \\ 0 & 0 & 1/\rho(x,y) & 0 & 0 \end{bmatrix}. \tag{2.19}$$

If we define $\hat{A} = \alpha A + \beta B$, where $\alpha^2 + \beta^2 = 1$ (*i.e.*, $\alpha = \cos\theta$ and $\beta = \sin\theta$) then we can combine A and B above into a more compact system which is more open to study. We have

$$q = \begin{bmatrix} \sigma_{11} \\ \sigma_{22} \\ \sigma_{12} \\ v_1 \\ v_2 \end{bmatrix}, \qquad \hat{A} = -\begin{bmatrix} 0 & 0 & 0 & \alpha(\lambda+2\mu) & \beta\lambda \\ 0 & 0 & 0 & \alpha\lambda & \beta(\lambda+2\mu) \\ 0 & 0 & 0 & \beta\mu & \alpha\mu \\ \alpha/\rho & 0 & \beta/\rho & 0 & 0 \\ 0 & \beta/\rho & \alpha/\rho & 0 & 0 \end{bmatrix}. \tag{2.20}$$

The eigenvalues of $\hat{A}$ are

$$\lambda^1 = -c_p, \quad \lambda^2 = c_p, \quad \lambda^3 = -c_s, \quad \lambda^4 = c_s, \quad \lambda^5 = 0. \tag{2.21}$$

The P-wave eigenvectors are

$$r^1 = \begin{bmatrix} \lambda+2\mu\alpha^2 \\ \lambda+2\mu\beta^2 \\ 2\mu\alpha\beta \\ \alpha c_p \\ \beta c_p \end{bmatrix}, \quad r^2 = \begin{bmatrix} \lambda+2\mu\alpha^2 \\ \lambda+2\mu\beta^2 \\ 2\mu\alpha\beta \\ -\alpha c_p \\ -\beta c_p \end{bmatrix}, \tag{2.22}$$

while the S-wave eigenvectors $r^{3,4}$ and the stationary wave r^5 are

$$r^3 = \begin{bmatrix} -2\alpha\beta\mu \\ 2\alpha\beta\mu \\ (\alpha^2-\beta^2)\mu \\ -\beta c_s \\ \alpha c_s \end{bmatrix}, \quad r^4 = \begin{bmatrix} -2\alpha\beta\mu \\ 2\alpha\beta\mu \\ (\alpha^2-\beta^2)\mu \\ \beta c_s \\ -\alpha c_s \end{bmatrix}, \quad r^5 = \begin{bmatrix} \beta^2 \\ \alpha^2 \\ -\alpha\beta \\ 0 \\ 0 \end{bmatrix}. \tag{2.23}$$

Here we see the five eigenvalues correspond to the wave speeds of the five waves given by the system above. In this case we there are two pressure waves that move in the direction of r^1 and r^2 with speeds $\pm c_p$, two shear waves that move in the direction of r^3 and r^4 with speeds $\pm c_s$, and a zero speed wave. Note that if we set $(\alpha, \beta) = (1, 0)$ or $(0, 1)$ we recover the matrices A and B separately. Observe that P-waves $r^{1,2}$ have velocity components directed in the $\pm(\alpha, \beta)$-direction, the direction in which the plane wave propagates. The S-waves, on the other hand, have motion in the orthogonal direction $\pm(-\beta, \alpha)$. Note also that a P-wave in the x- or y-direction has $\sigma_{12} = 0$, but that a P-wave propagating in any other direction has $\sigma_{12} \neq 0$.

2.4 Two-Dimensional Acoustic Equations

The two-dimensional elastic and acoustic equations are differentiated by the notion of shear stress. An elastic medium can support shear stress while an acoustic medium can not. Once the elastic equations are known we may derive the acoustic equations simply by setting $\mu = 0$ in (2.13) as,

$$\begin{aligned}
&\sigma_{11t} - (\lambda)v_{1x} - \lambda v_{2y} = 0 \\
&\sigma_{22t} - \lambda v_{1x} - (\lambda)v_{2y} = 0 \\
&\sigma_{12t} = 0 \\
&\rho v_{1t} - \sigma_{11x} - \sigma_{12y} = 0 \\
&\rho v_{2t} - \sigma_{12x} - \sigma_{22y} = 0
\end{aligned} \tag{2.24}$$

Note that it does not make sense to derive the 2D acoustic equations from the plane-stress elastic equations, as the plane-stress elastic equations contain assumptions that are incompatible with 2D acoustics.

We can rewrite the system in terms of the pressure p, where $\sigma_{11} = \sigma_{22} = -p$, as

$$\begin{aligned}
p_t &= -\lambda(v_{1x} + v_{2y}) \\
v_{1t} &= -\frac{1}{\rho} p_x \\
v_{2t} &= -\frac{1}{\rho} p_y.
\end{aligned} \tag{2.25}$$

As with the elastic equations we can rewrite the system as a variable-coefficient hyperbolic system. Note that for $\mu = 0, \lambda = k$

$$q_t + A(x, y)q_x + B(x, y)q_y = 0, \tag{2.26}$$

where

$$q = \begin{bmatrix} p \\ v_1 \\ v_2 \end{bmatrix}, \quad A = \begin{bmatrix} 0 & k(x,y) & 0 \\ 1/\rho(x,y) & 0 & 0 \\ 0 & 0 & 0 \end{bmatrix}, \tag{2.27}$$

$$B = \begin{bmatrix} 0 & 0 & k(x,y) \\ 0 & 0 & 0 \\ 1/\rho(x,y) & 0 & 0 \end{bmatrix}. \tag{2.28}$$

Given the definition of $\hat{A}$ above we can combine A and B for this system as,

$$q = \begin{bmatrix} p \\ v_1 \\ v_2 \end{bmatrix}, \qquad \hat{A} = -\begin{bmatrix} 0 & \alpha k & \beta k \\ \alpha/\rho & 0 & 0 \\ \beta/\rho & 0 & 0 \end{bmatrix}. \tag{2.29}$$

Here the eigenvalues of $\hat{A}$ are

$$\lambda^1 = -c_p, \quad \lambda^2 = c_p, \quad \lambda^3 = 0. \tag{2.30}$$

While the P-wave eigenvectors are

$$r^1 = \begin{bmatrix} -c_p \\ \alpha/\rho \\ \beta/\rho \end{bmatrix}, r^2 = \begin{bmatrix} cp \\ \alpha/\rho \\ \beta/\rho \end{bmatrix}, r^3 = \begin{bmatrix} 0 \\ 1 \\ 0 \end{bmatrix}, \tag{2.31}$$

Note that in an acoustic medium there are no shear waves.

2.5 One-Dimensional Elasticity Equations

We can reduce the two-dimensional plane-strain equations to one space dimension if we make the further assumption that there is no variation in the y-direction. In this case the system of five equations (2.13) reduces to the following:

$$\begin{aligned} \sigma_{11t} - (\lambda + 2\mu)v_x &= 0 \\ \rho v_t - \sigma_{11x} &= 0. \end{aligned} \tag{2.32}$$

In matrix notation this system takes the form,

$$\begin{bmatrix} \sigma_{11} \\ v \end{bmatrix}_t + \begin{bmatrix} 0 & -(\lambda + 2\mu) \\ -1/\rho & 0 \end{bmatrix} \begin{bmatrix} \sigma_{11} \\ v \end{bmatrix}_x = 0. \tag{2.33}$$

As in the 2D system there is also a separate 1D system of equations which models shear waves which is omitted here.

Similarly the plane-stress equations can be reduced to 1D by the assumption that $\sigma_{22} = \sigma_{12} = 0$. This gives the 1D reduction of the plane-stress equations as,

$$\begin{aligned} \tfrac{\sigma_{11t}}{E} - v_x &= 0 \\ \rho v_t - \sigma_{11x} &= 0 \end{aligned} \tag{2.34}$$

or in the notation used above,

$$\begin{bmatrix} \sigma_{11} \\ v \end{bmatrix}_t + \begin{bmatrix} 0 & -\frac{\mu(3\lambda+2\mu)}{\lambda+\mu} \\ -1/\rho & 0 \end{bmatrix} \begin{bmatrix} \sigma_{11} \\ v \end{bmatrix}_x = 0. \tag{2.35}$$

As in 2D, the difference between these two systems can be seen to be a quantitative difference in the eigenvectors and eigenvalues. Note that the system given by (2.32) has eigenvalues $\pm c_p$ with $c_p = \sqrt{\frac{\lambda+2\mu}{\rho}}$, while the system given by (2.34) has eigenvalues $\pm c_p$ where $c_p = \sqrt{\frac{\mu(3\lambda+2\mu)}{\rho(\lambda+\mu)}}$.

2.6 One-Dimensional Acoustic Equations

Before investigating the two-dimensional elastic and acoustic systems we introduce the numerical method and CLAWPACK via study of the one-dimensional acoustic system. We assume no variation in y in the two-dimensional acoustic system to find the 1D system,

$$q_t + A(x)q_x = 0, \tag{2.36}$$

where

$$q = \begin{bmatrix} p \\ v \end{bmatrix}, \quad A = \begin{bmatrix} 0 & k(x) \\ 1/\rho(x) & 0 \end{bmatrix}. \tag{2.37}$$

In a heterogeneous medium we may have the material parameters ρ (density) or k (bulk modulus) change with location x.

CLAWPACK is a finite volume method. These methods divide the computational domain into cells that are separated by cell interfaces. State variables are typically defined as piecewise constant so that within a given cell all the state variables are constant. Cell interfaces separate cells so that all the variability lies in the form of piecewise constant jumps that are always located at cell interfaces. In the setting of CLAWPACK we define cells at integer values. For example in 1D, the cell centered at i lies between the cell interfaces $x_{i-1/2}$ and $x_{i+1/2}$. In 1D acoustics the i'th cell has material parameters ρ_i and k_i. Here we set

$$A_i = \begin{bmatrix} 0 & k_i \\ 1/\rho_i & 0 \end{bmatrix}, \tag{2.38}$$

with the sound speed in the ith cell given by $c_i = \sqrt{\mu_i/\rho_i}$. The system can be diagonalized to find

$$R = \begin{bmatrix} r_i^1 & r_i^2 \end{bmatrix} = \begin{bmatrix} -\rho_i c_i & \rho_i c_i \\ 1 & 1 \end{bmatrix}, \quad \Lambda = \begin{bmatrix} -c_i & 0 \\ 0 & c_i \end{bmatrix}, \quad R^{-1} = \frac{1}{2c_i}\begin{bmatrix} -1 & \rho_i c_i \\ 1 & \rho_i c_i \end{bmatrix}. \tag{2.39}$$

Here the eigenvalues of $A(x)$ are the wave speeds $\lambda_i^1 = -c_i$ and $\lambda_i^2 = +c_i$, while $\rho_i c_i$ is the impedance in the i'th cell.

Ideally, we would like to have the interface between layers of different media aligned with cell interfaces. While in 1D one can see that material interfaces must lie at cell interfaces by definition, in 2D we may have material interfaces at some angle to the grid.

For example in 1D we set ρ_i to the cell average of $\rho(x)$ and k_i to the harmonic average of $k(x)$. This formulation allows spatially varying parameters to be represented numerically as piecewise constant functions. The value of ρ in the ith cell is $\rho_i = \rho(\bar{x}_i)$ where $\rho(\bar{x}_i)$ is the average value of $\rho(x)$ in the ith cell

$$\rho_i = (1/\triangle x)\int_{x_{i-1/2}}^{x_{i+1/2}} \rho(x)dx.$$

See figure 2.1 and [17].

Figure 2.1 shows density as piecewise constant in each cell. For 1D acoustics we have 2 state variables that are also piecewise constant in each cell: velocity and pressure. At

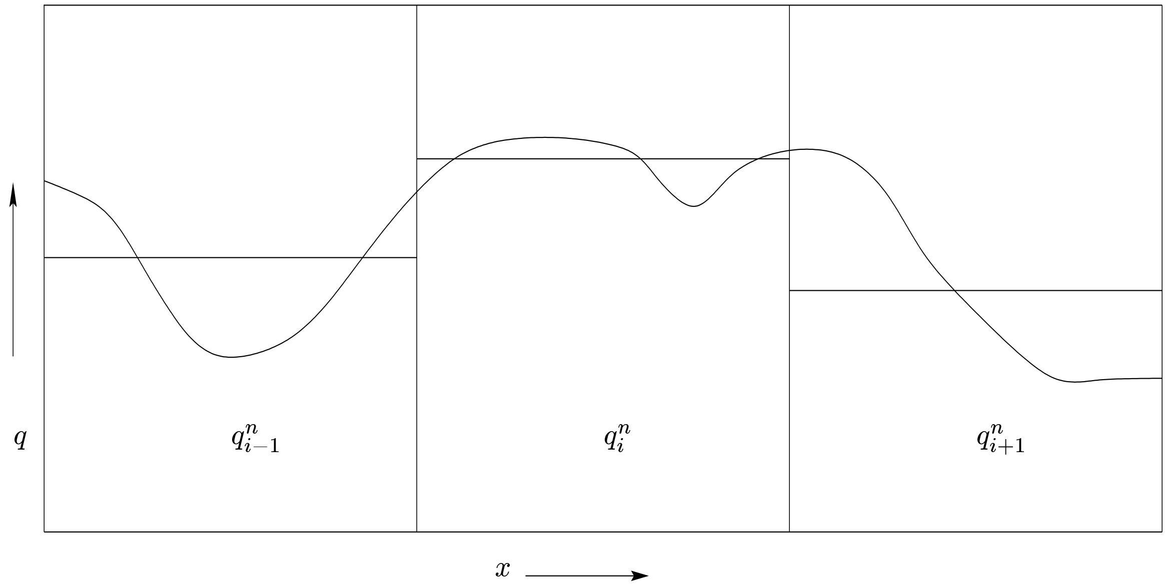

Figure 2.1: Example of cell averaging.

each cell interface we have a difference in the state variables which is governed by equation (2.36). This is the definition of a Riemann problem. The numerical solution methods used to solve all of the problems which fall into the scope of this work are based on solving these Riemann problems.

Chapter 3

NUMERICS VIA CLAWPACK

This chapter contains more of the details needed to use CLAWPACK to solve hyperbolic systems. The discussion of one-dimensional acoustics is continued to illustrate the most basic of concepts used in our solution method: the Riemann problem. Solution techniques of the Riemann problem and wave propagation are discussed in the framework of flux-differencing and Godunov methods. Standard flux limiting methods are introduced and applied in the form of wave limiters.

3.1 Riemann Problem

In the preceding chapter we went to great lengths to put all the elastic and acoustic systems of interest into a particular form. Each of the systems is a hyperbolic system that we have rendered in the form:

$$q_t + A(x,y,z)q_x + B(x,y,z)q_y + C(x,y,z)q_z = 0. \tag{3.1}$$

In all these systems we have presented the eigenvalues and eigenvectors of the matrices A, B, and C so that we may more readily explore their **Riemann structure**. The definition of a Riemann problem is, *the system of interest with piecewise constant initial data having a single discontinuity.* As the Riemann problem is the most fundamental tool used in the solutions of all the systems that we study, we will go into the 1-D acoustic Riemann solution in detail. The more complicated 2-D, 3-D and elasto-plastic systems are extensions of this most basic Riemann problem.

Recall that for 1-D acoustics we have the following system in each cell:

$$q_t + A(x)q_x = 0, \qquad \text{where} \quad A_i = \begin{bmatrix} 0 & k_i \\ 1/\rho_i & 0 \end{bmatrix}$$

The **eigenvalues** and **eigenvectors** of this matrix are given by,

$$\begin{aligned} \lambda_i^1 &= -c_i & \qquad \lambda_i^2 &= c_i \\ r_i^1 &= \begin{bmatrix} -\rho_i c_i \\ 1 \end{bmatrix} & \qquad r_i^2 &= \begin{bmatrix} \rho_i c_i \\ 1 \end{bmatrix} \end{aligned}$$

Here $c_i = \sqrt{k_i/\rho_i}$ is the **sound speed** in i'th cell. Also at the interface between any two cells a Riemann problem is specified. For example between the (i) and $(i-1)$ cells we have the hyperbolic equation $q_t + A(x)q_x = 0$ given above with the following piecewise constant initial data:

$$q(x_i, 0) = \begin{cases} q_{i-1}, & \text{if } x < x_{i-1/2}, \\ q_i, & \text{if } x > x_{i-1/2}. \end{cases} \tag{3.2}$$

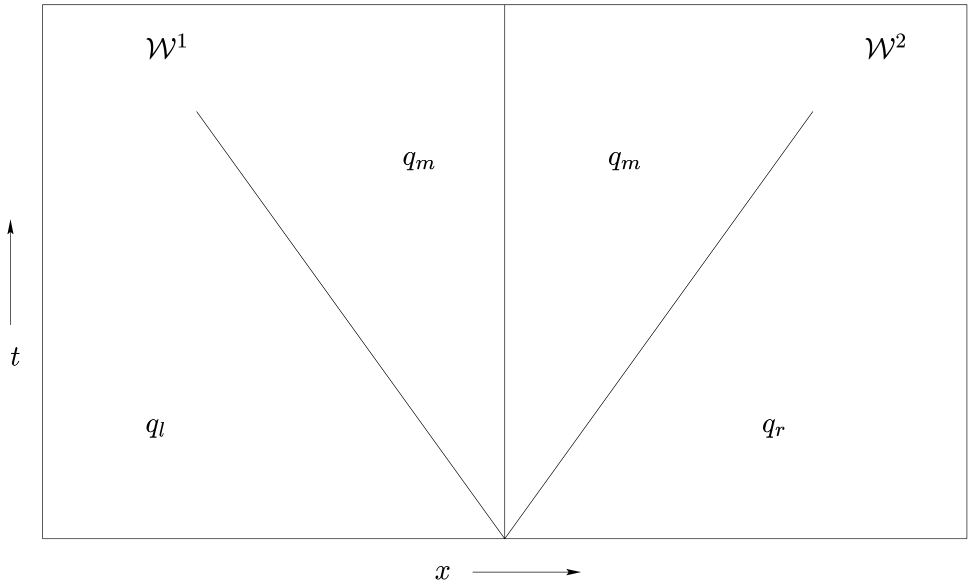

Figure 3.1: Example of cell updating by 1D Riemann Waves (x-t space)

The difference between the averaged state variables, (see figure 2.1) causes a wave to propagate in each direction. These waves must propagate along the direction of the characteristics in each cell. The right-going wave (or 2-wave) moves in the direction of the right eigenvector of the matrix A_i while the left-going wave (or 1-wave) moves in the direction of the left eigenvector of the matrix A_{i-1}. As the difference in Q_i and Q_{i-1} must be the sum of these two waves, one must only determine the waves to find the solution (or mid-state) to the Riemann problem. See Figure 3.1.

Since these characteristic directions (or eigenvectors) are known, we need only find the amplitude of the waves to uniquely determine the solution. Recall that the difference between q_r and q_l is given as the sum of the two waves,

$$q_r - q_l = \mathcal{W}^1 + \mathcal{W}^2. \tag{3.3}$$

These waves must be eigenvectors with some unknown amplitude α,

$$\mathcal{W}^1_{i-1/2} = \alpha^1_{i-1/2} \begin{bmatrix} -\rho_{i-1}c_{i-1} \\ 1 \end{bmatrix} \equiv \alpha^1_{i-1/2} r^1_{i-1} \tag{3.4}$$

$$\mathcal{W}^2_{i-1/2} = \alpha^2_{i-1/2} \begin{bmatrix} \rho_i c_i \\ 1 \end{bmatrix} \equiv \alpha^2_{i-1/2} r^2_i. \tag{3.5}$$

For the 1-D acoustic system this leads to the following 2×2 system to solve for $\alpha^1_{i-1/2}$ and $\alpha^2_{i-1/2}$:

$$\begin{bmatrix} p_i - p_{i-1} \\ v_i - v_{i-1} \end{bmatrix} = \begin{bmatrix} -\rho_{i-1}c_{i-1} & \rho_i c_i \\ 1 & 1 \end{bmatrix} \begin{bmatrix} \alpha^1_{i-1/2} \\ \alpha^2_{i-1/2} \end{bmatrix} \tag{3.6}$$

Once the waves are determined we can find the mid-state q_m of the Riemann problem. Recall that the difference between q_l and q_r is given as,

$$q_r - q_l = \alpha^1 r_l^1 + \alpha^2 r_r^2. \tag{3.7}$$

We can find q_m by either of the following two equations:

$$q_m \quad = \quad q_r - \mathcal{W}^2 \quad \text{or} \quad q_m \quad = \quad q_l + \mathcal{W}^1. \tag{3.8}$$

See Figures 3.2 and 3.3 for a comparison of the waves in x-t space and phase space (p-v for this example). One can see how the mid-state q_m obtained by the jump across the waves in x-t space is the same as the state q_m obtained by the intersection of the Hugoniot locus in phase space. See [33] and [18] for more details. Now that the Riemann problem is well understood we can move on to a brief description of the numerical high-resolution method and the CLAWPACK software.

3.2 Introduction to Clawpack

CLAWPACK can be broken down into two separate parts: **wave propagation** and **wave limiting**. In general flux differencing and wave propagation are not the same. See [35] for more details.

3.2.1 Wave Propagation

In the previous section we resolved the difference of q between cells into waves. Figure 3.4 shows the waves that emanate from the interfaces between cells $i-1$, i, and $i+1$.

One can see that to obtain the value of q_i^{n+1}, one only needs to add in the contributions of the appropriate waves as

$$q_i^{n+1} = q_i^n - \frac{\triangle t}{\triangle x}(\lambda_{i-1/2}^2 \mathcal{W}_{i-1/2}^2 + \lambda_{i+1/2}^1 \mathcal{W}_{i+1/2}^1). \tag{3.9}$$

In general (2-D acoustics or elasticity for example) there will be more than one left and one right going wave at each interface. The term **fluctuations** can be used to measure the net effect of all the left or right-going waves. If we assume that there are m waves emanating to the left and right of a given interface then we can define the left-going fluctuation as

$$\mathcal{A}^- \triangle q_{i-1/2} = \sum_{p=1}^{m} (\lambda^p)^- \mathcal{W}_{i-1/2}^p. \tag{3.10}$$

Similarly, the right-going fluctuation would be written as

$$\mathcal{A}^+ \triangle q_{i-1/2} = \sum_{p=1}^{m} (\lambda^p)^+ \mathcal{W}_{i-1/2}^p. \tag{3.11}$$

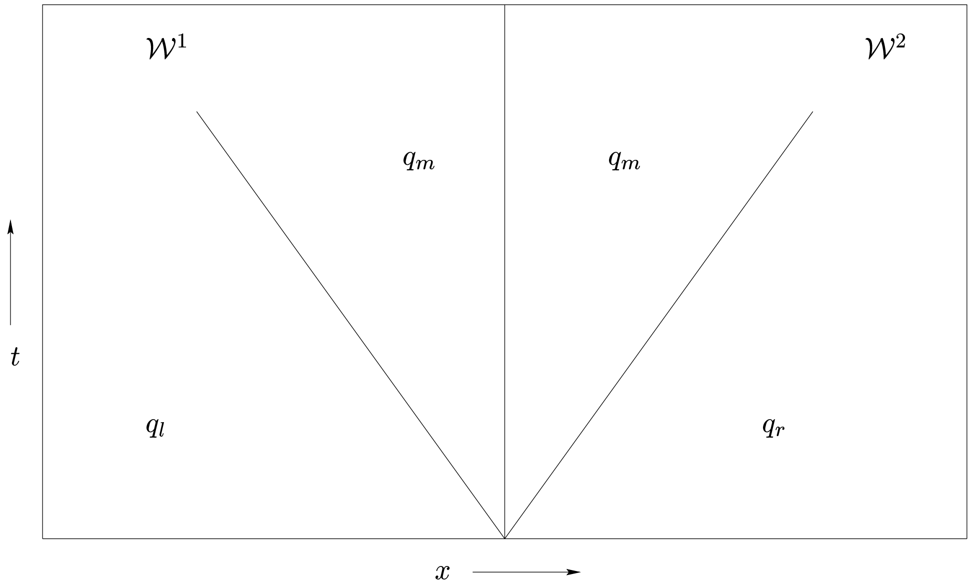

Figure 3.2: 1-D Riemann Waves (x-t space)

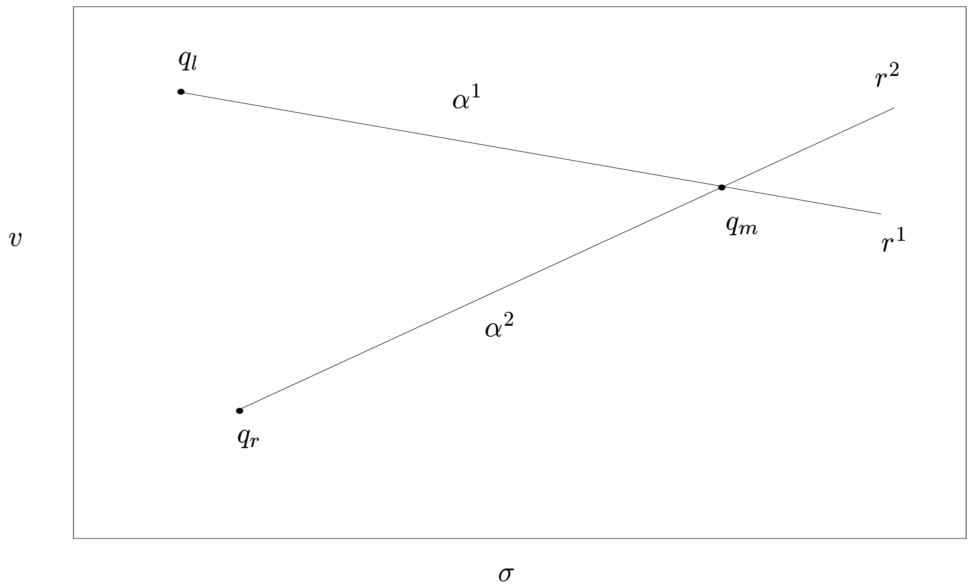

Figure 3.3: 1-D Riemann Waves (σ-v space)

With this notation we can see that propagating these waves and updating Q by adding in the appropriate waves just gives the wave-propagation form of Godunov's method in the form,

$$q_i^{n+1} = q_i^n - \frac{\triangle t}{\triangle x}[\mathcal{A}^+ \triangle q_{i-1/2} + \mathcal{A}^- \triangle q_{i+1/2}]. \tag{3.12}$$

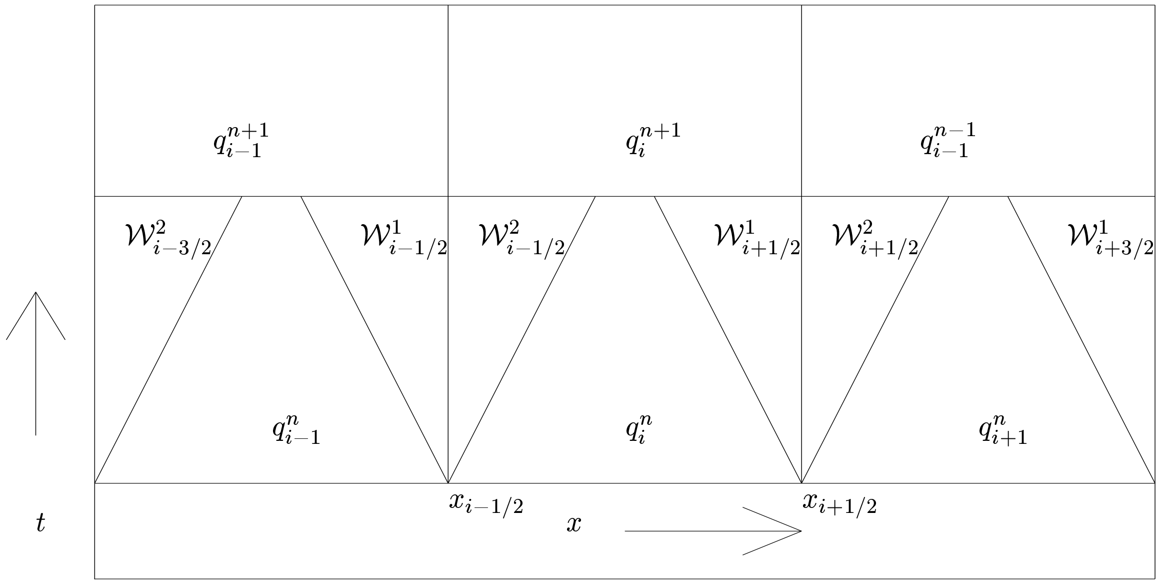

Figure 3.4: Propagated Waves used for cell updating.

Recall that Godunov's method is only first-order accurate. We use a second-order accurate numerical scheme where higher order is achieved via the introduction of **second-order correction terms**.

The introduction of second-order correction terms can be motivated by the Lax-Wendroff method applied to the constant-coefficient case. The method can be written as a correction to the first-order upwind method in terms of the following **correction fluxes**:

$$\tilde{F}_{i-1/2} = \frac{1}{2}\sum_{p=1}^{2} |\lambda_{i-1/2}^p| \left(1 - \frac{\triangle t}{\triangle x}|\lambda_{i-1/2}^p|\right) \mathcal{W}_{i-1/2}^p, \tag{3.13}$$

The second-order method takes the form

$$q_i^{n+1} = q_i^n - \frac{\triangle t}{\triangle x}(\lambda_{i-1/2}^2 \mathcal{W}_{i-1/2}^2 + \lambda_{i+1/2}^1 \mathcal{W}_{i+1/2}^1) - \frac{\triangle t}{\triangle x}(\tilde{F}_{i+1/2} - \tilde{F}_{i-1/2}). \tag{3.14}$$

This is the update formula used in the CLAWPACK software. In the special case where $A_i = A$ is constant, equation (3.14) reduces to the standard Lax-Wendroff method. Note that in this case $\lambda^1 = -c$ and $\lambda^2 = c$ are constant and

$$\tilde{F}_{i-1/2} = \frac{1}{2}(|A| \triangle q_{i-1/2} - \frac{\triangle t}{2 \triangle x} A \triangle q_{i-1/2}). \tag{3.15}$$

If we substitute this form of $\tilde{F}_{i-1/2}$ and $\tilde{F}_{i+1/2}$ into the update formula we find

$$q_i^{n+1} = q_i^n - \frac{\triangle t}{2 \triangle x} A(q_{i+1} - q_{i-1}) + \frac{\triangle t^2}{2 \triangle x^2} A^2 (q_{i+1} - 2q_i + q_{i-1}). \tag{3.16}$$

Here we have used the fact that $|A| = A^+ - A^-$, where $A^\pm = R\Lambda^\pm R^{-1}$. See [34] for more details.

3.2.2 *Wave Limiter*

Standard flux limiting methods are based on the idea that the waves used in the second order corrections can be directly **limited** or cut off in some appropriate manner. In this section we will introduce the standard method of limiting and show examples of when this method fails. In the next section we give an alternate method of wave limiting that is especially useful in rapidly varying heterogeneous material.

Recall that the update formula (3.14) decomposes the update to Q into a first-order accurate upwind update and a second-order correction. The upwind method is known to be excessively dissipative while the second-order Lax-Wendroff method is numerically dispersive and leads to the appearance of spurious oscillations in the solution. A high-resolution method is obtained by applying a nonlinear **limiter** to the second-order corrections to obtain a method with much better properties than either the upwind or Lax-Wendroff methods. These characteristics suggest a limiting method, which favors the full Lax-Wendroff method in regions where q is smooth (locally), and reduces to, or at least favors, the upwind method when q has steep gradients or discontinuities (locally). A simple way to introduce such a limiter is to replace each wave $\mathcal{W}^p_{i-1/2}$ by a limited version

$$\tilde{\mathcal{W}}^p_{i-1/2} = \Phi^p_{i-1/2}\mathcal{W}^p_{i-1/2}$$

for some scalar value $\Phi^p_{i-1/2}$, (for $p = 1, 2$). Here the limiter is determined by comparing each wave with the corresponding wave at the adjacent cell interface in the upwind direction. We compare $\mathcal{W}^1_{i-1/2}$ with $W^1_{i+1/2}$ and $W^2_{i-1/2}$ with $\mathcal{W}^2_{i-3/2}$. In regions where the solution is smoothly varying these waves will differ by very little and we should use unmodified waves to achieve second-order accuracy. We want $\Phi^p_{i-1/2} \approx 1$ in this case. If the waves differ greatly then we must be near a discontinuity in the solution, or at least large values of q_{xx}. In this case the second-order corrections can lead to numerical dispersion and in these regions the waves should be limited by choosing $\Phi^p_{i-1/2}$ closer to zero. We take

$$\Phi^p_{i-1/2} = \phi(\theta^p_{i-1/2})$$

where $\theta^p_{i-1/2}$ is some measure of the ratio of wave strengths. For example, we might take

$$\theta^1_{i-1/2} = \frac{\|W^1_{i+1/2}\|}{\|W^1_{i-1/2}\|}, \qquad \theta^2_{i-1/2} = \frac{\|\mathcal{W}^2_{i-3/2}\|}{\|W^2_{i-1/2}\|} \tag{3.17}$$

where $\|\cdot\|$ is some norm such as the Euclidean norm. Usually this method of limiting works very well. However for certain examples in rapidly varying heterogeneous materials numerical artifacts arise which completely degrade the solution. In the next section we will discuss the solution to this problem via alterations to the standard limiting method. See [16] and [33] for more details.

Chapter 4

ONE DIMENSIONAL ACOUSTICS IN HETEROGENEOUS MATERIAL

In this chapter we start with a brief introduction to 1D acoustics in a heterogeneous medium. We then look at an example of acoustics in a 1D rapidly varying periodic medium. Shortcomings of the standard wave limiter methods applied to this test case are explored. We end the chapter with a discussion of new limiting methods applied successfully on the same 1D periodic acoustic problem followed by examples in random media. This method was first explained in my Masters Thesis [16] and the paper [17].

4.1 Heterogeneous Media

We first consider a one-dimensional problem with a single discontinuity in the density. The medium to the left of the interface is characterized by material parameters ρ_1, μ_1, and c_1 while the medium on the right is characterized by ρ_2, μ_2, and c_2. A wave propagating in either medium can be characterized by an impedance Z where $Z_1 = \rho_1 c_1$ and $Z_2 = \rho_2 c_2$ are the characteristic wave impedances. See [14] for details. Note that Z_1 is defined by the medium that the wave is in before hitting the interface. For a right-going wave, Z_1 is the impedance of the medium to the left of the interface while Z_2 is the impedance of the medium to the right of the interface. The amplitude of reflection and transmission (refraction) coefficients are found as,

$$R_a = \frac{Z_2 - Z_1}{Z_2 + Z_1} \text{ and } T_a = \frac{2Z_2}{Z_2 + Z_1}. \tag{4.1}$$

The coefficients given above determine the exact solution of the single interface problem. As an initial test we use CLAWPACK to solve the interface problem and check against the true solution. Figures 4.1-4.3, show the numerical solution as '+' and the "exact solution" with a resolution of 1000 grid points as a solid line. In the following section we explore an example with multiple interface that gives rise to a numerical instability.

4.2 Periodic Media

In the previous section we saw that our numerical scheme works extremely well on problems with an isolated heterogeneity. In this section we explore a problem with a periodic rapidly-varying heterogeneity motivated by an example given in [47]. We assume the medium has material properties that are periodic with period $2\theta L$. Here ρ and μ satisfy the following: $\rho(x + 2\theta L) = \rho(x)$ and $k(x + 2\theta L) = k(x)$. In [47], results were found for the following set

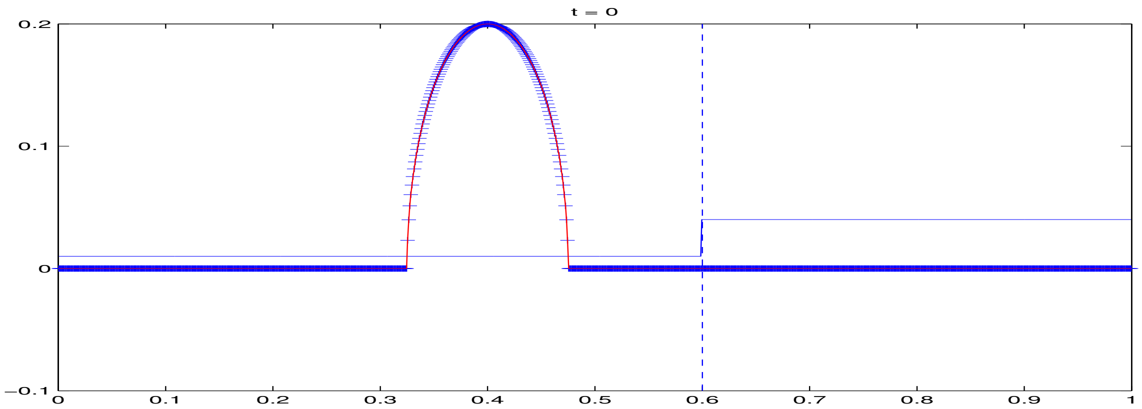

Figure 4.1: true solution(-) and numerical solution (+), time=0, N=1000.

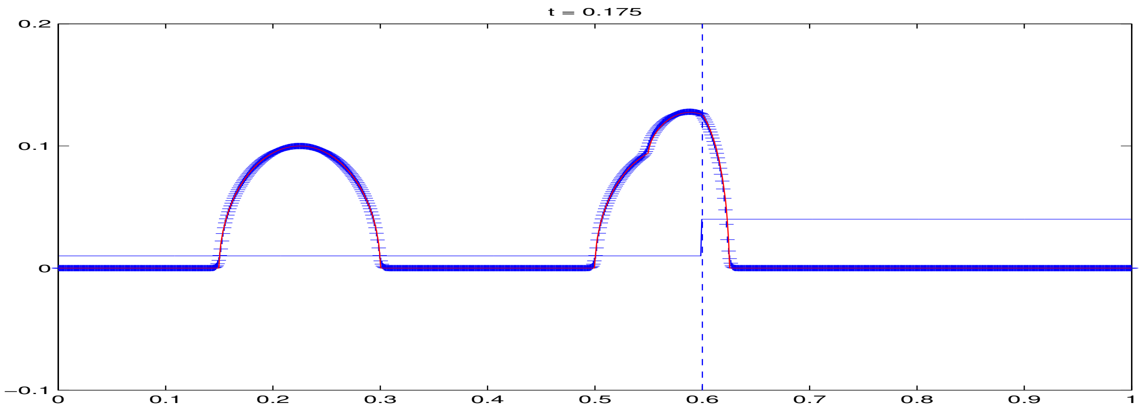

Figure 4.2: true solution(-) and numerical solution (+), time=0.175, N=1000.

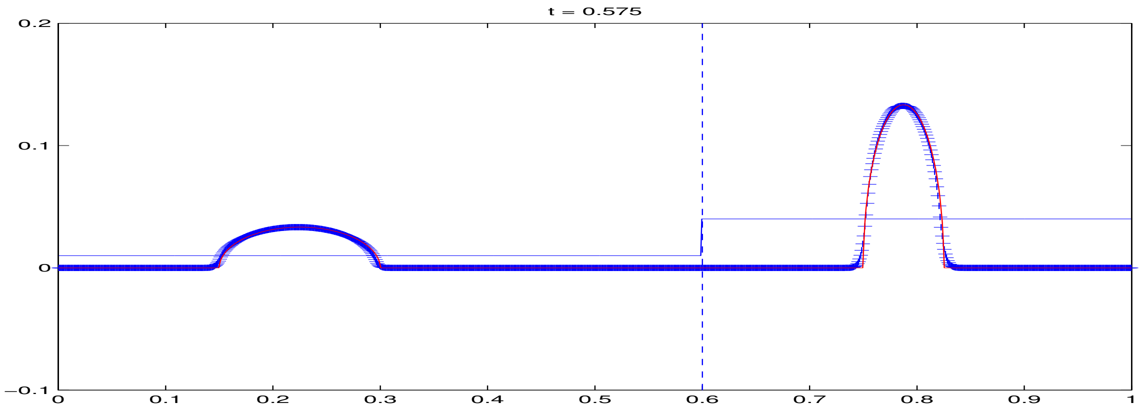

Figure 4.3: true solution(-) and numerical solution (+), time=0.575, N=1000.

up:

$$\rho(x) = \begin{cases} \rho_1 = 1 = \mu_1, & \text{for } 0 < x < \theta L \\ \rho_2 = 3 = \mu_2, & \text{for } \theta L < x < L \end{cases} \tag{4.2}$$

There are three properties of this example that make it a great problem to test our numerical solver: there is an exact solution that exhibits dispersion an effective wave speed different from the wave speed at any point in the medium.

If we assume that the scale of the variation is small compared to the wavelength of waves propagating in the medium, then a dispersion relation can be derived via homogenization techniques. One can use this dispersion relation to predict when a wave propagating in the medium should start to exhibit dispersive behavior. If the numerics are working as intended we expect a wave to propagate relatively unchanged for a certain number of wavelengths before the dispersive behavior becomes noticeable. As we will show below, an effective wave-speed or sound-speed can be derived. For this example it turns out that while the sound speed has a value of 1.0 at all points in the medium, a sound wave traveling in the medium should move at the effective wave speed 0.866. Again if the numerical scheme is working correctly one expects to recover this nonintuitive result. Finally since the sound speed is 1.0 everywhere we can actually solve this problem exactly via the method of characteristics. As we will generally not have an exact solution for problems in heterogeneous material, this example is ideally suited as a numerical test problem.

The dispersion relation can be derived via homogenization techniques applied to this system in the form of a second order wave equation. Recall the 1D acoustic system given by,

$$\begin{aligned} p_t - kv_x &= 0 \\ \rho v_t - p_x &= 0. \end{aligned} \tag{4.3}$$

We can eliminate either p or u from 4.3 to find the second order wave equation. In this case we eliminate p to find the following equation for u,

$$\rho(x)u_{tt}(x,t) = (k(x)u_x(x,t))_x. \tag{4.4}$$

We assume that (4.4) has initial data $u(x,0) = f(x)$ and $u_t(x,0) = 0$. To make use of the homogenization theory we must also assume that $f(x)$ is band-limited,

$$f(x) = \frac{1}{2\pi}\int_{\xi \le T} F(\xi)e^{i\xi x}d\xi,$$

so that the shortest wavelength of the Fourier components of $f(x)$ is $\lambda = 2\pi/T$. We can find a valid homogenized solution to $u(x,t)$ so long as $\epsilon = \theta L/\lambda \ll 1$. As long as the frequency, λ^{-1} of the initial data $f(x)$ is much greater than the period of the medium, we will have a valid solution. Given a periodic, heterogeneous medium Bloch or Floquet expansion can be used to find an effective dispersion relation for the homogenized medium. For a complete discussion of Bloch expansion theory see [1] and [46]. Extensive details of the following results can also be found in [16]. Application of homogenization theory leads to an effective dispersion relation for a wave moving in the homogenized medium, given by

$$\omega_0(\xi) = \Omega_1\xi + (1/6)\epsilon^2\Omega_3\xi^3 + \cdots \tag{4.5}$$

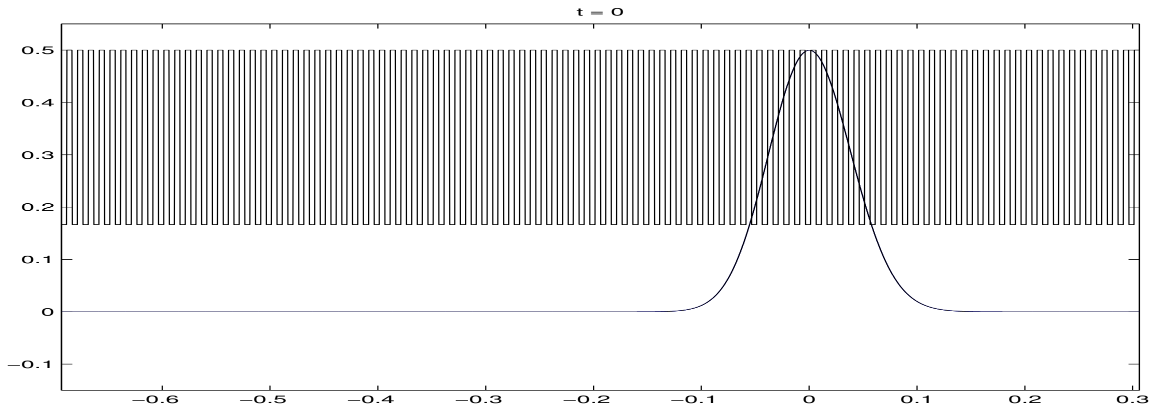

Figure 4.4: density profile and initial position of right-going pulse, time=0, N=4000. Note that in this and the following figures the density and bulk modulus profile is scaled by 1/6. The density is periodic with a value of either $\rho = 1$ or $\rho = 3$ and $\mu = \rho$ everywhere.

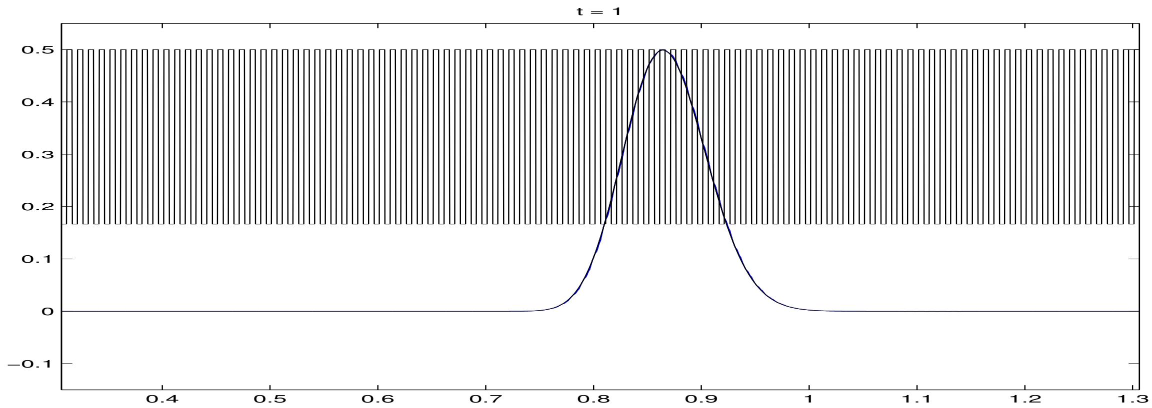

Figure 4.5: comparison of “exact” solution with $\triangle t = \triangle x$ and “numerical” solution with $\triangle t < \triangle x$, right-going pulses, original limiter, time=1, N=4000.

Thus as $\epsilon \to 0$ we have an effective medium propagation vector given by $\omega_0(k) = \Omega_1 k$. Here Ω_1 is the effective speed of the homogenized medium given by

$$\Omega_1^2 = \left[\bar{\rho}\left(\bar{\frac{1}{\mu}}\right)\right]^{-1}.$$

Note that this effective wave speed is given by the usual formula $c = \sqrt{\mu/\rho}$ but using the average of ρ and the harmonic average of μ over the interval.

If this line of analysis is continued one can derive the governing equation in “homogenized” form as,

$$u_{tt} = \Omega_1^2 u_{xx} + \frac{\Omega_1 \Omega_3}{3} a^2 u_{xxxx}, \tag{4.6}$$

recall that $a = 2\theta L$ is the period. See [47] for details. This homogenized equation has no term of order ϵ, is dispersive, and fourth order in x. Note that this same equation is derived in [22] via multiple scale techniques. An extension of multiple scale homogenization theory applied to signaling problems in heterogeneous media can also be found in [63].

For this example we find the effective wave speed

$$\Omega_1^2 = \left[\bar{\rho}\left(\bar{\frac{1}{\mu}}\right)\right]^{-1} = 2/(2(1+1/3)) \;\Rightarrow \Omega_1 = 0.8660. \tag{4.7}$$

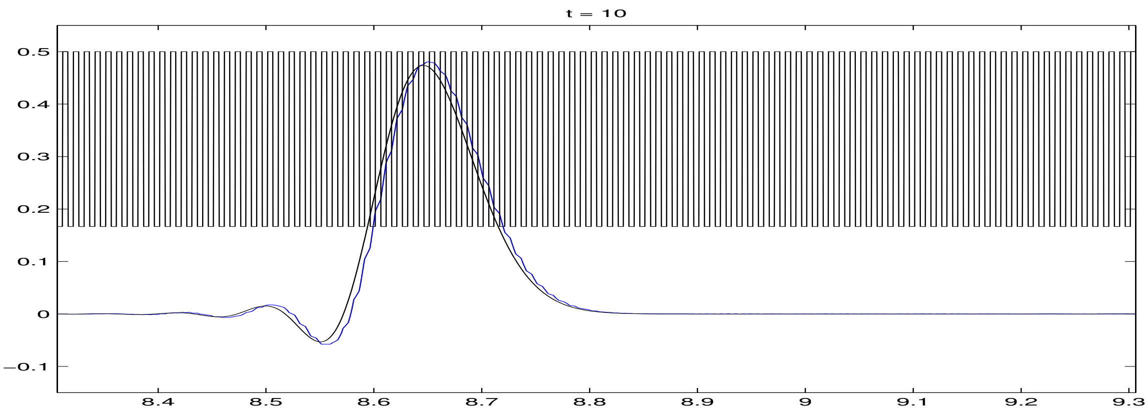

Figure 4.6: comparison of "exact" solution with $\triangle t = \triangle x$ and "numerical" solution with $\triangle t < \triangle x$, right-going pulses, original limiter, time=10, N=4000.

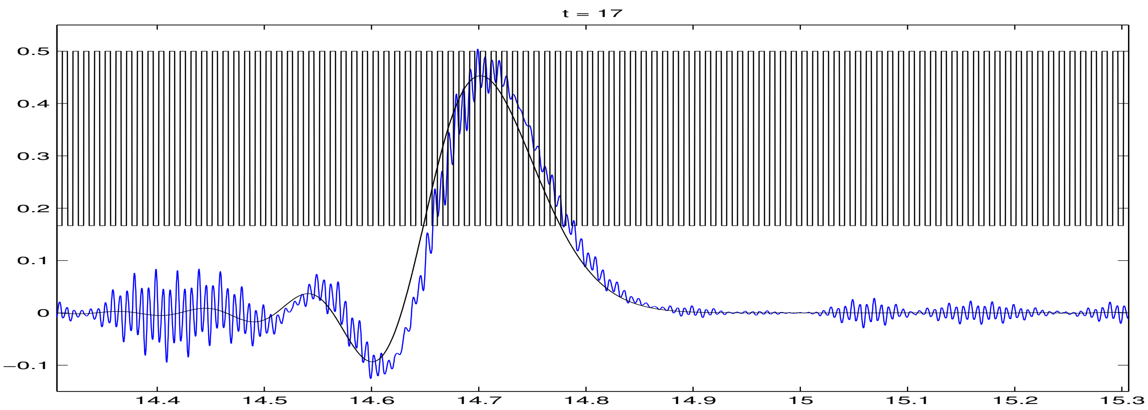

Figure 4.7: comparison of "exact" solution with $\triangle t = \triangle x$ and "numerical" solution with $\triangle t < \triangle x$, right-going pulses with numerical instability, original limiter, time=17, N=4000. Note that much better results are obtained with modified limiter, see Section 4.4.

Note that although the density and bulk modulus are varying periodically, they are chosen in such a way that $c = 1$ everywhere. A consequence of $c = 1$ everywhere is that one can compare numerical results to the exact solution which can be found via the (numerical) method of characteristics.

To replicate the results found in [47] we input the given density and bulk modulus and solve problem with a large wavelength Gaussian velocity pulse and a very small period (so that $\epsilon \approx 0$). A simple way to test the effective wave speed is to let the pulse advect with periodic boundary conditions until it has traveled 1 time unit. So long as the pulse is traveling at the correct speed then the distance traveled should be .866, or after traveling for 10 time units the pulse should move a distance of 8.66. Figures 4.4-4.6 show that CLAWPACK does in fact reproduce the expected effective propagation speed. Note that even though we have a sound wave propagating in a material that has sound speed $c = 1$ at every point, the sound wave is moving with the predicted effective speed of $c = .866$.

Even though the sound speed is constant everywhere, the medium is still dispersive. There is an impedance contrast across interfaces separating layers of different material parameters. From the definition of impedance one can see that alternating layers have an impedance of either $Z = 3$ or $Z = 1$. Recall equation (4.5). One expects a wave to suffer from dispersion for nonzero Ω_3. In this example $\Omega_3 = -.01353$. In addition to the effective wave speed, Figures 4.6- 4.9 show the effective dispersion of the homogenized medium. It should be clear that like the effective wave speed this dispersion is physical and not a numerical artifact. If the problem is run for a much longer time we experience a severe numerical instability, see Figure 4.7. The investigation and resolution of this instability is explained in detail in the following section.

4.3 Transmission Based Limiting Method

Recall our previous discussion of wave limiters. The standard approach is to limit waves by comparing each wave with the corresponding wave at the adjacent cell interface in the upwind direction. For variable-coefficient problems, the eigenvectors may change from cell to cell (and will change whenever the impedance differs), and hence the waves $\mathcal{W}^1_{i-1/2}$ and $\mathcal{W}^1_{i+1/2}$, for example, will not be collinear in phase space. In this case simply comparing the magnitudes, as done in (3.17), may give an insufficient limiter. The two waves could be very different even if they have the same magnitude. In the CLAWPACK software the standard approach is to instead compare the projection of $\mathcal{W}^1_{i+1/2}$ onto $\mathcal{W}^1_{i-1/2}$ with the wave $\mathcal{W}^1_{i-1/2}$, defining

$$\theta^1_{i-1/2} = \frac{\mathcal{W}^1_{i+1/2} \cdot \mathcal{W}^1_{i-1/2}}{\mathcal{W}^1_{i-1/2} \cdot \mathcal{W}^1_{i-1/2}}, \tag{4.8}$$

where $\cdot$ denotes the inner product, in place of (3.17) (and similarly for $\theta^2_{i-1/2}$). We have found that this works well for most problems, but in some cases this results in an unstable method when calculations are run to large times. The instability shown in Figure 4.7 appears to be the result of a resonance phenomenon in the numerical solution introduced by the limiter. This is related to physical resonances that have been investigated by Kevorkian and Bosley [22] in weakly-nonlinear acoustics. Here the resonance is do to the interaction of

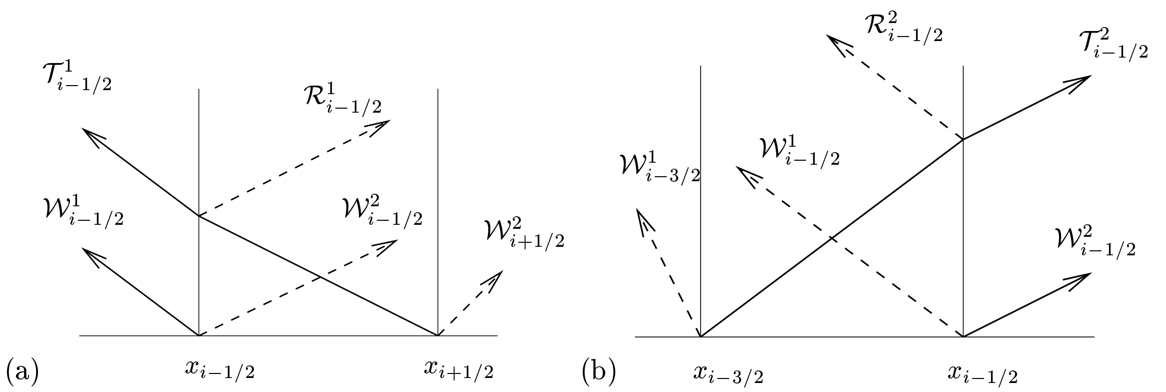

Figure 4.8: Decomposition of waves into transmitted and reflected parts used in defining the transmission-based limiter in 4.9 and 4.10.

the initial data with the medium. Such resonances can arise in both the weakly-nonlinear and linear case. See [63] for a related discussion.

A more robust limiter is motivated by Figure 4.8. In Figure 4.8 one can see that the left-going wave which emanates from the interface at $x_{i-1/2}$ splits into a transmitted wave $\mathcal{T}^1_{i-1/2}$ and a reflected wave $\mathcal{R}^1_{i-1/2}$. The figure suggests that only the transmitted wave $\mathcal{T}^1_{i-1/2}$ should be compared to $\mathcal{W}^1_{i-1/2}$. The transmission coefficient for a left-going wave is $2Z_{i-1}/(Z_{i-1}+Z_i)$ and so we take

$$\theta^1_{i-1/2} = \frac{\|\mathcal{T}^1_{i-1/2}\|}{\|\mathcal{W}^1_{i-1/2}\|} = \left(\frac{2Z_{i-1}}{Z_{i-1}+Z_i}\right)\left(\frac{\alpha^1_{i+1/2}}{\alpha^1_{i-1/2}}\right), \tag{4.9}$$

where $Z_i = \rho_i c_i$ is the impedence in the i'th cell. Similarly, we take

$$\theta^2_{i-1/2} = \frac{\|\mathcal{T}^2_{i-1/2}\|}{\|\mathcal{W}^2_{i-1/2}\|} = \left(\frac{2Z_{i}}{Z_{i-1}+Z_i}\right)\left(\frac{\alpha^2_{i-3/2}}{\alpha^2_{i-1/2}}\right), \tag{4.10}$$

as suggested by Figure 4.8(b). We call this a *transmission-based limiter*. For more details see [16]. Note that for a right-going wave at the same interface the transmission coefficient is $2Z_i/(Z_{i-1}+Z_i)$.

This idea is closely related to what is done in the positivity-preserving scheme of Liu and Lax [28], [38]. Let $R_{i-1/2}$ be the matrix of right eigenvectors found by diagonalizing the matrix

$$A_i = \begin{bmatrix} 0 & k_i \\ 1/\rho_i & 0 \end{bmatrix}. \tag{4.11}$$

Here $R_{i-1/2}$ is given by

$$R_{i-1/2} = \begin{bmatrix} -Z_{i-1} & Z_i \\ 1 & 1 \end{bmatrix}, \tag{4.12}$$

and let $L_{i-1/2}$ be the inverse

$$L_{i-1/2} = \frac{1}{Z_{i-1}+Z_i}\begin{bmatrix} -1 & Z_i \\ 1 & Z_{i-1} \end{bmatrix} \equiv \begin{bmatrix} \ell^1_{i-1/2} \\ \ell^2_{i-1/2} \end{bmatrix}. \tag{4.13}$$

Then solving (3.6) gives

$$\begin{aligned} \alpha^1_{i-1/2} &= \ell^1_{i-1/2} \cdot (Q_i - Q_{i-1}) \\ \alpha^2_{i-1/2} &= \ell^2_{i-1/2} \cdot (Q_i - Q_{i-1}), \end{aligned} \tag{4.14}$$

where $\ell^p_{i-1/2}$ are the row vectors of $L_{i-1/2}$. The naive limiter (3.17) corresponds to setting

$$\theta^1_{i-1/2} = \frac{\|\ell^1_{i+1/2} \cdot (Q_{i+1} - Q_i)\, r^1_{i+1/2}\|}{\|\ell^1_{i-1/2} \cdot (Q_i - Q_{i-1})\, r^1_{i-1/2}\|}. \tag{4.15}$$

The Lax-Liu limiter instead uses the same eigenvectors to split both jumps:

$$\theta^1_{i-1/2} = \frac{\|\ell^1_{i-1/2} \cdot (Q_{i+1} - Q_i)\, r^1_{i-1/2}\|}{\|\ell^1_{i-1/2} \cdot (Q_i - Q_{i-1})\, r^1_{i-1/2}\|} = \frac{\ell^1_{i-1/2} \cdot (Q_{i+1} - Q_i)}{\ell^1_{i-1/2} \cdot (Q_i - Q_{i-1})}. \tag{4.16}$$

Our transmission-based limiter is similar but applies $\ell^1_{i-1/2}$ only to the wave $\mathcal{W}^1_{i+1/2}$ which is approaching the interface, not to all of $Q_{i+1} - Q_i$:

$$\theta^1_{i-1/2} = \frac{\ell^1_{i-1/2} \cdot \mathcal{W}^1_{i+1/2}}{\ell^1_{i-1/2} \cdot (Q_i - Q_{i-1})}. \tag{4.17}$$

Similarly,

$$\theta^2_{i-1/2} = \frac{\ell^2_{i-1/2} \cdot \mathcal{W}^2_{i-3/2}}{\ell^2_{i-1/2} \cdot (Q_i - Q_{i-1})}. \tag{4.18}$$

In the following section we show how the application of this new limiting method can be successfully applied to the periodic example studied above.

4.4 Periodic Media Revisited

Recall the example studied in Section 4.2. The material parameters ρ and k are piecewise constant with

$$(\rho(x),\ k(x)) = \begin{cases} (\rho_1,\ k_1) & \text{if } 0 < x < \theta L \\ (\rho_2,\ k_2) & \text{if } \theta L < x < L \end{cases} \tag{4.19}$$

and repeated periodically, where L is the period and θ the fractional volume of Material 1. Long wavelengths propagate with the effective speed

$$\bar{c} = \sqrt{\hat{k}/\bar{\rho}},$$

where $\hat{k}$ is the harmonic average of k and $\bar{\rho}$ the arithmetic average of ρ over each period.

We return to the case studied in Section 4.2 where $\bar{c} \approx 0.866$ even though the wave speed $c \equiv 1$ everywhere. In this case taking $\Delta t = \Delta x$ results in the exact solution being computed as CLAWPACK reduces to the numerical method of characteristics. We use this to test a truly numerical result obtained with our method using $\Delta t < \Delta x$. Figure 4.9 shows a comparison of the exact solution and the numerical solution using $\Delta t = 0.9\Delta x$ on a very fine grid, for a propagating Gaussian pulse. The two solutions lie on top of one another to plotting accuracy. Note that the wave is observed to move at speed $\bar{c}$ (*e.g.*, at time $t = 1$ it is at $x = 0.866$) and that for large t the dispersive nature of the effective equation is evident.

The problem is initialized by creating a Gaussian velocity pulse within the periodic medium on a large domain. The pulse splits with half of the perturbation energy traveling each direction. Once the two pulses have separated, the right-going pulse is used as initial data in the computational domain. Periodic boundary conditions are imposed and the x-axis is relabeled at each time to indicate distance traveled since initialization.

Figure 4.10 shows a comparison of numerical results obtained at $t = 4$ using $\Delta t = 0.9\Delta x$ on several coarser grids for both limiting methods, and Figure 4.11 shows a log-log plot of the norm of the error vs. Δx. This indicates that the method converges with an order of accuracy roughly 1.3 in the max-norm, when using the transmission-based limiter. The order of accuracy observed in in Figure 4.11 may seem low for this computation since the solution appears to be smooth.

Figure 4.12 shows the exact solution at a sequence of times between $t = 0$ and $t = 0.015$. The solution appears smooth at the beginning and end (and later at each multiple of 0.015), but in between these times it is not smooth. The observed propagation at speed $\bar{c}$ arises only because of constant reflection and cancellation of waves moving within each material slice at the local speed $c = 1$. At most times the solution has a discontinuous first derivative at the material interfaces and so the loss of second-order accuracy is not surprising. In the next section we move on to examples where the media has random material properties. We first look at a special case where the exact solution can still be caluculated, then move onto more interesting exaples with no exact solutoin.

4.5 Random Media

We now consider a random medium in one dimension where $\rho(x)$ and $K(x)$ are taken to be piecewise constant. The medium is defined by choosing 100 layers with random values of ρ and K in each layer according to some distribution. We then fix this medium with 100 layers and solve the equations on a sequence of finer grids in order to perform grid-refinement studies of convergence.

We start with a case where $\rho = K$ in each layer, so that $c \equiv 1$ everywhere and taking $\Delta t = \Delta x$ gives the exact solution for comparison. We choose the 100 values of ρ from a uniform distribution over the interval $0.1 \leq \rho \leq 1.9$ so that the average density is 1 as shown in Figure 4.13. We calculate the effective wave speed as described in Section 4.2 to be $\bar{c} = 0.74$. Figure 4.14 shows a pressure pulse which has propagated to the right from the point $x = t = 0$ in the above medium. Shown in both plots is the exact solution and numerical solution with a resolution of 6400 cells and the numerical solution on a grid with 100 cells. Note that in addition to recovering the effective wave speed, the exact solution and the numerical solutions on the finer grids are visually identical. On the coarsest grid there is some visible difference, but the solution is quite good considering there is only one grid cell per layer on this grid. As in the periodic medium, we can perform a grid refinement study. For the results shown in Figure 4.14 we found the order of accuracy to be 1.2.

For a more challenging test, we chose a layered medium with 2000 layers in which values of ρ and K are chosen in the same way as in the previous example. In this case the sound speed also varies randomly in each layer while the effective sound speed is calculated to be $\bar{c} = 0.92$. Figure 4.15 shows the density, bulk-modulus, and sound-speed profiles along with a pressure pulse which has propagated through this medium from the point $x = t = 0$. The pressure perturbation was initalized as an amplitude 1 Gaussian hump with zero velocity, centered at $x = t = 0$. The initial pulse split into two pulses which propagate to the left and to the right with the predicted effective wave speed of $\bar{c} = .92$. Note that results are shown for 3 resolutions of a 2000 layer medium: N=2000, N=4000, and N=8000. For this example, as with the periodic medium, we have used the modified limiting method to avoid an instability which develops with the standard CLAWPACK limiting methods.

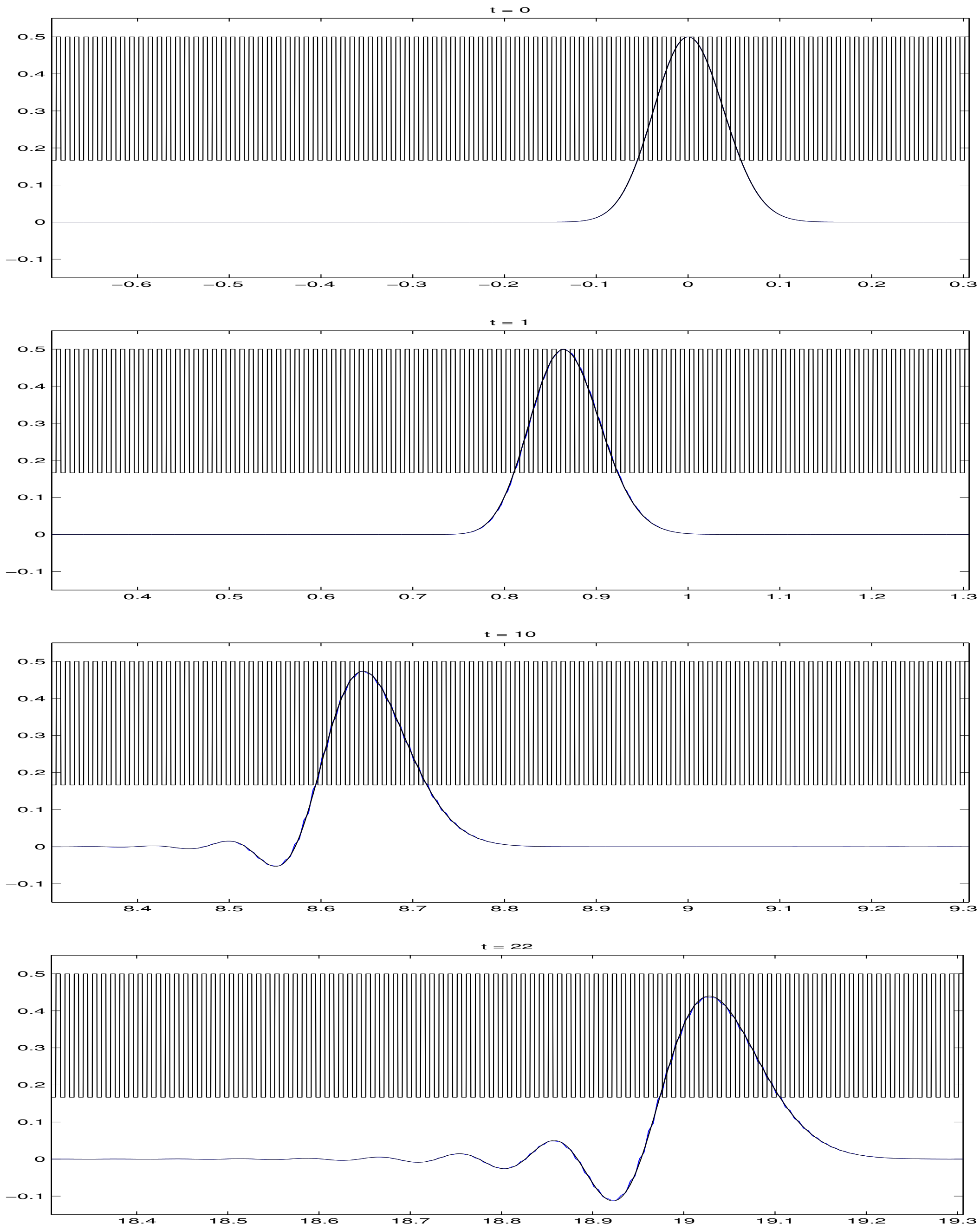

Figure 4.9: Comparison of "exact" solution computed using $\triangle t = \triangle x$ and "numerical" solution with $\triangle t < \triangle x$, at four different times, on a fine grid with $\Delta x = 1/4000$. . The structure of the periodic medium is also indicated by the step function. Note that periodic boundary conditions are used and the x-axis is relabeled at each time to indicate distance traveled since the initial time.

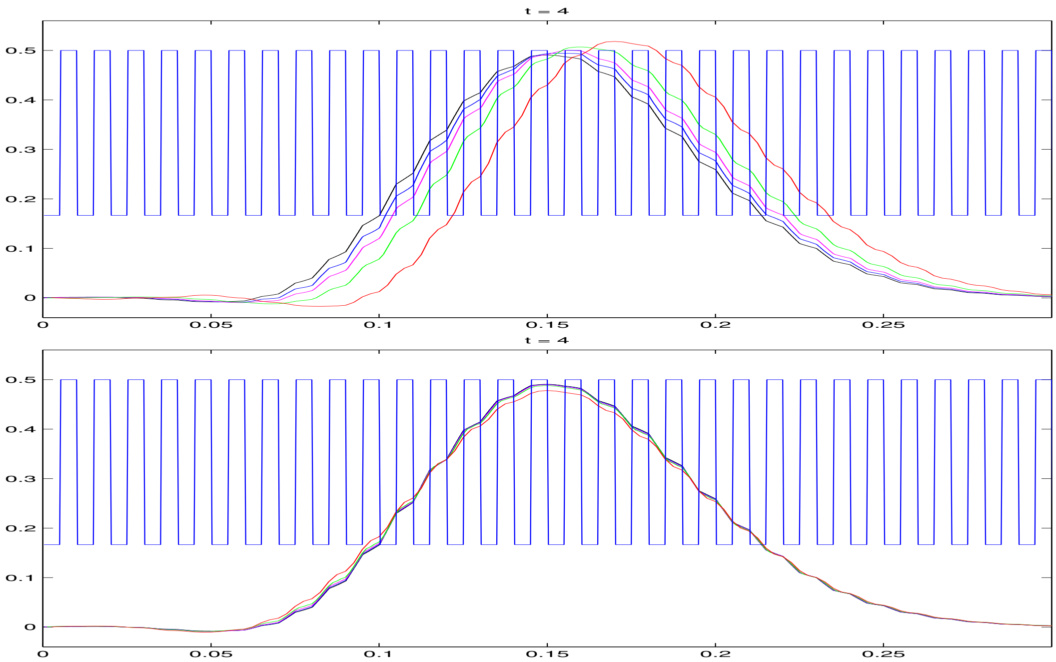

Figure 4.10: $\triangle t = .9 \triangle x$ Numerical solutions with the standard CLAWPACK limiter (upper figure) and the new transmission-based limiter (lower figure). In both figures the pulse is shown at five grid resolutions N=400, 800, 1600, 3200, and 6400. In the upper figure the highest resolution is the pulse farthest to the left.

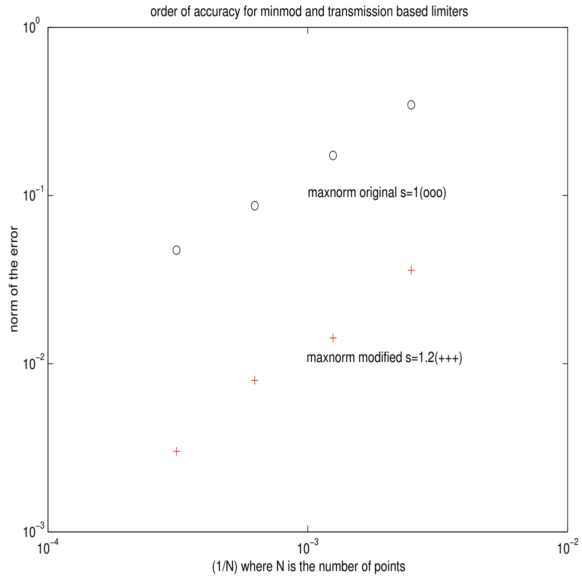

Figure 4.11: Order of accuracy for numerical solutions of figure 4.10. N=400,800,1600,3200 are compared with numerical solution at N=6400, max-norm shown for both methods of limiting, original shown as (ooo), modified shown as (+++). The computed order of accuracy is near 1.2 for the transmission-based limiter and 1.0 for the original limiter.

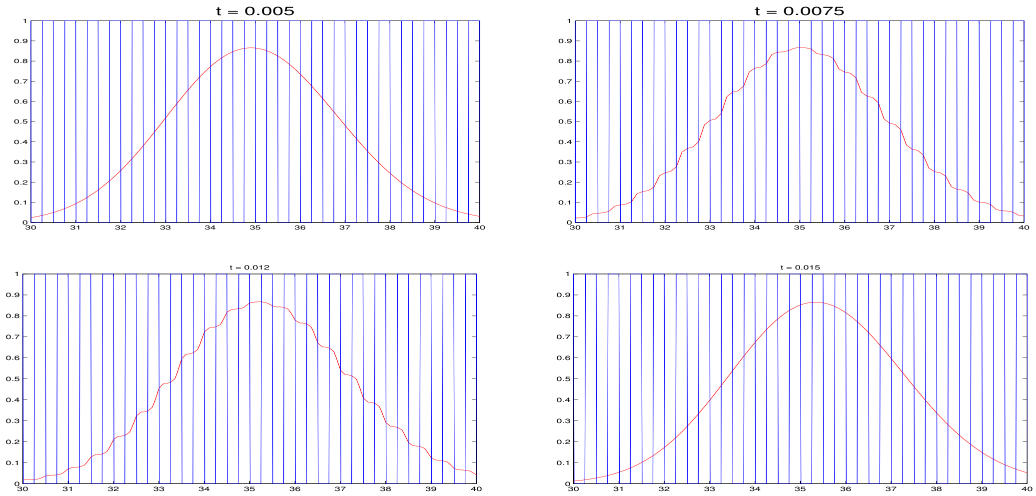

Figure 4.12: Close up of right moving pulse between $t = 0$ and $t = 0.015$.

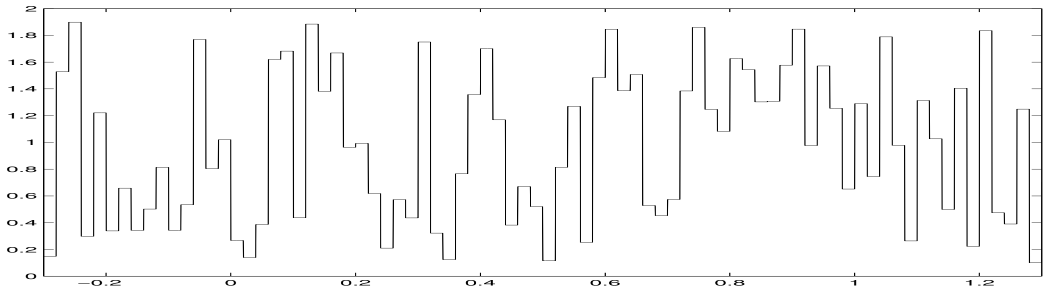

Figure 4.13: Density and bulk modulus profile in layered random medium.

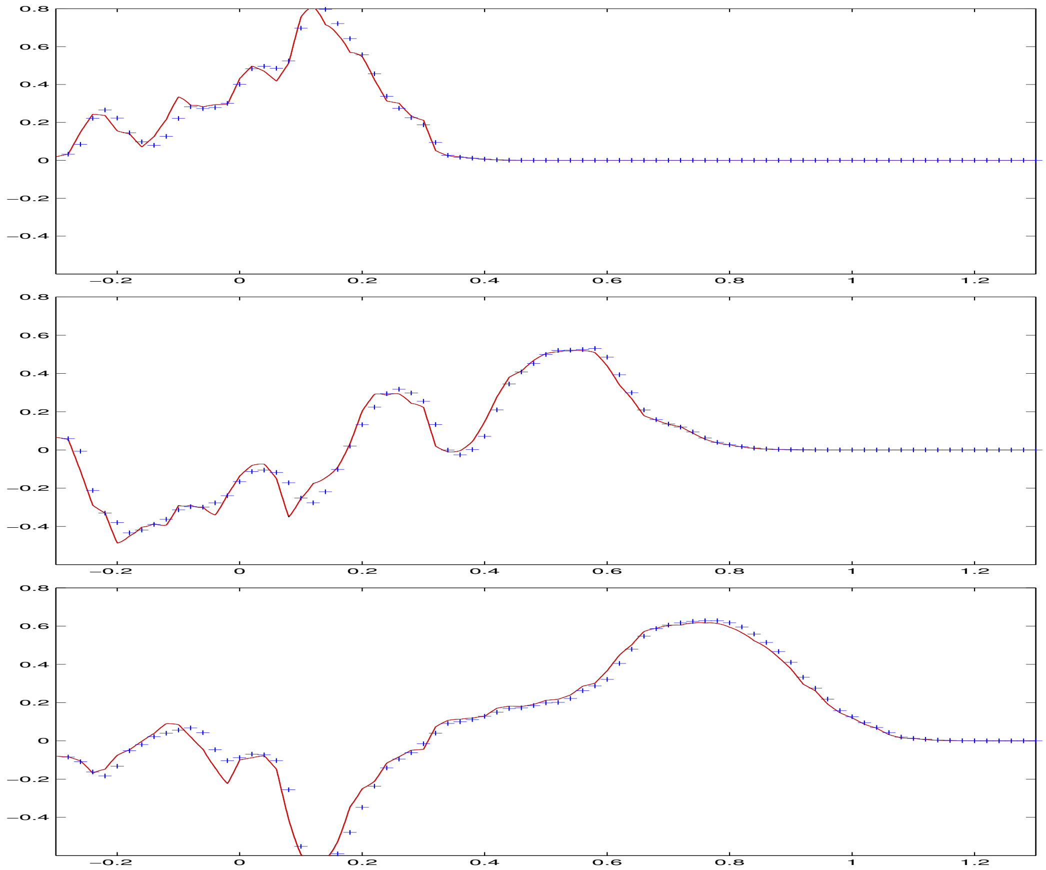

Figure 4.14: Pressure at T=.02, T=.07, and T=1, for acoustics in a random medium with $\rho = k$ as shown in Figure 4.13. The exact and numerical solutions are shown for N=6400 as solid lines which lie on top of one another to plotting accuracy. The numerical solution for N=100 is also shown as + symbols.

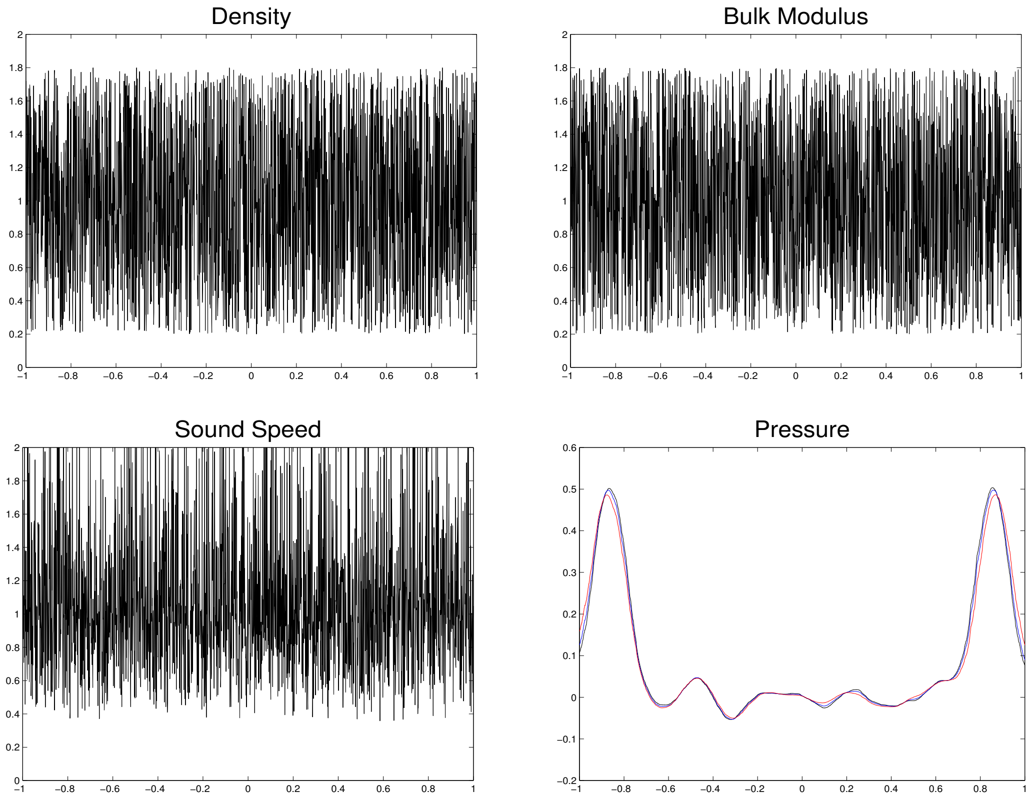

Figure 4.15: Profiles of density (upper left), bulk modulus (upper right), sound speed (lower left), and the pressure at $T = 1.0$. Three resolutions are shown in the bottom right: N=2000, N=4000, and N=8000.

Chapter 5

NUMERICS OF TWO DIMENSIONAL ACOUSTICS AND ELASTICITY

In this chapter we give a brief description of the 2D numerics and Riemann solutions for heterogeneous linear acoustics and elasticity. As in 1D, CLAWPACK uses waves found via Riemann solutions to compute cell averaged updates. Previously we showed that the 1D update formula used limited waves in conjunction with a first-order Godunov scheme and second-order correction terms to define a cell-averaged solution at the next time step. Here we will show how the 2D update formula is a straight forward extension of of what was done in 1D. To compute the 2D update, we must solve Riemann problems in both the x and y directions. Left and right going waves in the x direction are generated as well as up and down going waves in the y direction. An added complication that arises in 2D comes from the fact that, in general, waves do not propagate orthogonal to cell interfaces. Extra correction terms that must be solved for to properly account for this **transverse propagation**. See [34] for a very thorough discussion of the multi-dimensional algorithm.

5.1 Two Dimensional Riemann Solutions

5.1.1 Two Dimensional Acoustic Riemann Solution

Recall that the 2D heterogeneous acoustic system for a the ith cell is given as

$$q_t + A_i q_x + B_i q_y = 0. \tag{5.1}$$

Here q and A_i are given as

$$q = \begin{bmatrix} p \\ v_1 \\ v_2 \end{bmatrix}, \quad A = \begin{bmatrix} 0 & k_i & 0 \\ 1/\rho_i & 0 & 0 \\ 0 & 0 & 0 \end{bmatrix}, \tag{5.2}$$

Here B_i has a similar form to A_i and the eigenvalues of A_i are

$$\lambda^1 = -c_{pi}, \quad \lambda^2 = c_{pi}, \quad \lambda^3 = 0. \tag{5.3}$$

Recall that $c_{pi} = \sqrt{\frac{\lambda_i + 2\mu_i}{\rho_i}}$ is the sound speed of the compression waves and that the P-wave eigenvectors take the form

$$r^1 = \begin{bmatrix} -c_{pi} \\ 1/\rho_i \\ 0 \end{bmatrix}, r^2 = \begin{bmatrix} c_{pi} \\ 1/\rho_i \\ 0 \end{bmatrix}, r^3 = \begin{bmatrix} 0 \\ 1 \\ 0 \end{bmatrix}. \tag{5.4}$$

To solve the heterogeneous linear 2D acoustic Riemann problem we follow the same procedure that was used in the 1D case. We must find the waves that emanate into neighboring cells from each cell interface. In 2D we must compute waves in both the x and y directions. Here we show how to compute the solution to the Riemann problem in the x direction. The y direction solution uses the same technique and is nearly identical.

As shown above, the 2D acoustic system has two non-zero eigenvalues corresponding to two pressure waves. As with the 1D acoustic case, the solution of the Riemann problem in the x direction is found by setting the jump in the state variables q that exists between two neighboring cells equal to the sum of the two pressure waves that emanate from the interface dividing the cells. For example, the Riemann problem at the $(i-1/2)$ interface is found by solving for the amplitudes of the waves defined in the following:

$$q_i - q_{i-1} = \mathcal{W}^1 + \mathcal{W}^2. \tag{5.5}$$

Recall that these waves must be eigenvectors with some unknown amplitude α^1 and α^2. Here the two waves are defined as

$$\mathcal{W}^1_{i-1/2} = \alpha^1_{i-1/2} \begin{bmatrix} -c_{pi-1} \\ 1/\rho_{i-1} \\ 0 \end{bmatrix} \equiv \alpha^1_{i-1/2} r^1_{i-1} \tag{5.6}$$

$$\mathcal{W}^2_{i-1/2} = \alpha^2_{i-1/2} \begin{bmatrix} c_{pi} \\ 1/\rho_i \\ 0 \end{bmatrix} \equiv \alpha^2_{i-1/2} r^2_i. \tag{5.7}$$

This leads to the following 2×2 system to solve for $\alpha^1_{i-1/2}$ and $\alpha^2_{i-1/2}$:

$$\begin{bmatrix} p_i - p_{i-1} \\ v_{1i} - v_{1i-1} \end{bmatrix} = \begin{bmatrix} -c_{pi-1} & c_{pi} \\ 1/\rho_{i-1} & 1/\rho_i \end{bmatrix} \begin{bmatrix} \alpha^1_{i-1/2} \\ \alpha^2_{i-1/2} \end{bmatrix} \tag{5.8}$$

Solving for $\alpha^1_{i-1/2}$ and $\alpha^2_{i-1/2}$ solves the Riemann problem and defines the waves $\mathcal{W}^1 + \mathcal{W}^2$. These waves, along with the similar waves defined by the B matrix for the y direction are used in the update formula shown below to give the cell update at the next time step.

5.1.2 Two Dimensional Elastic Riemann Solution

Here for completeness we show the details of the heterogeneous linear elastic Riemann solution. Note that the solution procedure is identical to that shown above. Just as with the 2D acoustic system, the cell wise 2D elastic system is governed by the following:

$$q_t + A_i q_x + B_i q_y = 0. \tag{5.9}$$

Here the state variable q has five components: three stress and two velocity. The cell-wise coefficient matrix A_i and q are given as

$$q = \begin{bmatrix} \sigma_{11} \\ \sigma_{12} \\ \sigma_{22} \\ v_1 \\ v_2 \end{bmatrix}, \quad A = - \begin{bmatrix} 0 & 0 & 0 & (\lambda_i + 2\mu_i) & 0 \\ 0 & 0 & 0 & 0 & \mu_i \\ 0 & 0 & 0 & \lambda_i & 0 \\ 1/\rho_i & 0 & 0 & 0 & 0 \\ 0 & 1/\rho_i & 0 & 0 & 0 \end{bmatrix}. \tag{5.10}$$

As we showed in a previous section, the linear elastic system has four nonzero eigenvalues associated with two pressure waves and two shear waves. The eigenvalues of A_i are given as

$$\lambda^1 = -c_{pi}, \quad \lambda^2 = c_{pi}, \quad \lambda^3 = -c_{si}, \quad \lambda^4 = c_{si}, \quad \lambda^5 = 0. \tag{5.11}$$

The P-wave eigenvectors r^1 and r^2 take the form

$$r^1 = \begin{bmatrix} \lambda_i + 2\mu_i \\ \lambda_i \\ 0 \\ c_{pi} \\ 0 \end{bmatrix}, \quad r^2 = \begin{bmatrix} \lambda_i + 2\mu_i \\ \lambda_i \\ 0 \\ -c_{pi} \\ 0 \end{bmatrix}, \tag{5.12}$$

and the S-wave eigenvectors r^3 and r^4 are given as

$$r^3 = \begin{bmatrix} 0 \\ 0 \\ \mu_i \\ 0 \\ c_{si} \end{bmatrix}, \quad r^4 = \begin{bmatrix} 0 \\ 0 \\ \mu_i \\ 0 \\ -c_{si} \end{bmatrix}. \tag{5.13}$$

As with the 2D acoustic case shown above, the solution of the elastic Riemann problem in the x direction is found by setting the jump in q equal to the sum of waves. In this case, the Riemann problem at the $(i-1/2)$ interface consists of four waves. To solve the Riemann problem we must find the amplitudes of the two P-waves and two S-waves given in the following:

$$q_i - q_{i-1} = \mathcal{W}^1 + \mathcal{W}^2 + \mathcal{W}^3 + \mathcal{W}^4. \tag{5.14}$$

As above, these waves must be eigenvectors with unknown amplitudes α^1, α^2, α^3, and α^4. Here the two P-waves are defined as

$$\mathcal{W}^1_{i-1/2} = \alpha^1_{i-1/2} \begin{bmatrix} \lambda_{i-1} + 2\mu_{i-1} \\ \lambda_{i-1} \\ 0 \\ c_{pi-1} \\ 0 \end{bmatrix} \equiv \alpha^1_{i-1/2} r^1_{i-1}, \quad \mathcal{W}^2_{i-1/2} = \alpha^2_{i-1/2} \begin{bmatrix} \lambda_i + 2\mu_i \\ \lambda_i \\ 0 \\ -c_{pi} \\ 0 \end{bmatrix} \equiv \alpha^2_{i-1/2} r^2_i, \tag{5.15}$$

and the two S-waves are given as

$$\mathcal{W}^3_{i-1/2} = \alpha^3_{i-1/2} \begin{bmatrix} 0 \\ 0 \\ \mu_{i-1} \\ 0 \\ c_{si-1} \end{bmatrix} \equiv \alpha^3_{i-1/2} r^3_{i-1}, \quad \mathcal{W}^4_{i-1/2} = \alpha^4_{i-1/2} \begin{bmatrix} 0 \\ 0 \\ \mu_i \\ 0 \\ -c_{si} \end{bmatrix} \equiv \alpha^4_{i-1/2} r^4_i. \tag{5.16}$$

This leads to two 2×2 systems to solve for the amplitudes of the four waves. The amplitudes of the two P-waves are found by solving the following:

$$\begin{bmatrix} \sigma_{11i} - \sigma_{11i-1} \\ v_{1i} - v_{1i-1} \end{bmatrix} = \begin{bmatrix} \lambda_{i-1} + 2\mu_{i-1} & \lambda_i + 2\mu_i \\ c_{pi-1} & c_{pi} \end{bmatrix} \begin{bmatrix} \alpha^1_{i-1/2} \\ \alpha^2_{i-1/2} \end{bmatrix}. \tag{5.17}$$

Similarly the amplitudes of the two S-waves are found by solving

$$\begin{bmatrix} \sigma_{12i} - \sigma_{12i-1} \\ v_{2i} - v_{2i-1} \end{bmatrix} = \begin{bmatrix} \mu_{i-1} & \mu_i \\ c_{si-1} & c_{si} \end{bmatrix} \begin{bmatrix} \alpha^3_{i-1/2} \\ \alpha^4_{i-1/2} \end{bmatrix}. \tag{5.18}$$

The B matrix can be used to find similar waves for the y direction with the same procedure.

5.2 *Two Dimensional Numerics via* CLAWPACK

5.2.1 Wave Propagation in Two Dimensions

Recall that in 1D the cell-update formula was given as

$$q_i^{n+1} = q_i^n - \frac{\triangle t}{\triangle x}(\lambda^2_{i-1/2}\mathcal{W}^2_{i-1/2} + \lambda^1_{i+1/2}\mathcal{W}^1_{i+1/2}) - \frac{\triangle t}{\triangle x}(\tilde{F}_{i+1/2} - \tilde{F}_{i-1/2}), \tag{5.19}$$

where the second order correction terms have the form

$$\tilde{F}_{i-1/2} = \frac{1}{2}\sum_{p=1}^{2} |\lambda^p_{i-1/2}| \left(1 - \frac{\triangle t}{\triangle x}|\lambda^p_{i-1/2}|\right) \mathcal{W}^p_{i-1/2}. \tag{5.20}$$

In 2D we must account for left and right going (x direction) waves and up and down going (y direction) waves. Also, as mentioned above, all such waves will typically propagate at some angle to the grid leading to transverse propagation.

For example without taking transverse propagation into account, the 2D acoustic system update formula is given as

$$\begin{aligned} q_{ij}^{n+1} = q_{ij}^n &- \frac{\triangle t}{\triangle x}(\lambda^2_{i-1/2,j}\mathcal{W}^2_{i-1/2,j} + \lambda^1_{i+1/2,j}\mathcal{W}^1_{i+1/2,j}) \\ &- \frac{\triangle t}{\triangle y}(\lambda^2_{i,j-1/2}\mathcal{W}^2_{i,j-1/2} + \lambda^1_{i,j+1/2}\mathcal{W}^1_{i,j+1/2}) \\ - \frac{\triangle t}{\triangle x}(\tilde{F}_{i+1/2,j} - \tilde{F}_{i-1/2,j}) &- \frac{\triangle t}{\triangle y}(\tilde{G}_{i,j+1/2} - \tilde{G}_{i,j-1/2}). \end{aligned} \tag{5.21}$$

Here it should be clear that the waves $\mathcal{W}^2_{i-1/2,j}$ and $\mathcal{W}^1_{i+1/2,j}$ are found by solving Riemann problems in the x direction at the $(i-1/2, j)$ and $(i+1/2, j)$ interfaces. Similarly the waves $\mathcal{W}^2_{i,j-1/2}$ and $\mathcal{W}^1_{i,j+1/2}$ are found by solving Riemann problems in the y direction at the $(i, j-1/2)$ and $(i, j+1/2)$ interfaces. Also in 2D, the terms $\tilde{G}_{i,j+1/2}$ and $\tilde{G}_{i,j-1/2}$ give the second-order correction terms for waves propagating in the y direction and are defined in the same manner as the x direction second-order correction terms shown above.

For systems with more waves, such as the elastic system, we use a more general notation. The general (2D) update formulas in CLAWPACK are defined in terms of fluctuations: $\mathcal{A}^{\pm}\triangle q$ and $\mathcal{B}^{\pm} \triangle q$. For example, the linear elastic system has four waves and the left-going fluctuation at the $(i+1/2, j)$ interface is defined as

$$\mathcal{A}^- \triangle q_{i+1/2,j} = (\lambda^1_{i+1/2,j}\mathcal{W}^1_{i+1/2,j} + \lambda^3_{i+1/2,j}\mathcal{W}^3_{i+1/2,j}). \tag{5.22}$$

Similarly the right-going fluctuation at the $(i-1/2,j)$ interface is defined as

$$\mathcal{A}^+ \triangle q_{i-1/2,j} = (\lambda^2_{i-1/2,j}\mathcal{W}^2_{i-1/2,j} + \lambda^4_{i-1/2,j}\mathcal{W}^4_{i-1/2,j}). \tag{5.23}$$

With this notation, the general 2D update formula is given as

$$q^{n+1}_{ij} = q^n_{ij} - \triangle^{UP}_{ij} - \frac{\Delta t}{\Delta x}(\tilde{F}_{i+1/2,j} - \tilde{F}_{i-1/2,j}) - \frac{\Delta t}{\Delta y}(\tilde{G}_{i,j+1/2} - \tilde{G}_{i,j-1/2}). \tag{5.24}$$

Here $\triangle^{UP}_{ij}$ is the properly weighted sum of the first-order upwind terms given as

$$\triangle^{UP}_{ij} = -\frac{\Delta t}{\Delta x}(\mathcal{A}^- \triangle q_{i+1/2,j} + \mathcal{A}^+ \triangle q_{i-1/2,j}) - \frac{\Delta t}{\Delta y}(\mathcal{B}^- \triangle q_{i,j+1/2} + \mathcal{B}^+ \triangle q_{i,j-1/2}). \tag{5.25}$$

Recall that in 1D (for the constant coefficient case) the second-order correction terms are found by modeling all the terms of a second-order Taylor expansion of the governing equation $q_t + Aq_x = 0$. The same is true in 2D for the system $q_t + Aq_x + Bq_y = 0$, but here one finds the Taylor expansion has the added complication of the cross-derivative terms of q_{xy} and q_{yx}. These cross-derivative terms are exactly the terms one must account for to properly model the transverse propagation mentioned above. The complete 2D update formula used in CLAWPACK is that given above in (5.24) where the second-order correction terms $\tilde{F}$ and $\tilde{G}$ are altered to include the transverse terms. The details of the necessary modifications to $\tilde{F}$ and $\tilde{G}$ are described in great detail in [27], [34] and [35].

5.2.2 Two Dimensional Heterogeneous Acoustic Example

In this section we review an example of 2D heterogeneous wave propagation that can be found in [17]. In the previous section we showed how the wave-propagation method is extended to 2D by solving Riemann problems in both x and y and including transverse propagation terms. Consider, for example, the $(i-1/2,j)$ interface between cells $(i-1,j)$ and (i,j) and the $(i,j+1/2)$ interface between cells $(i,j+1)$ and (i,j). In the x-direction, the material properties in the cells $(i-1,j)$ and (i,j) are used to decompose the jumps in pressure and x-velocity between these cells into left-going and right-going acoustic waves. Similarly the jump in q between the cells $(i,j+1)$ and (i,j) is used to define up-going and down-going waves. The non-orthogonal components of the left and right-going waves generated at the $(i-1/2,j)$ interface are decomposed into up and down-going waves by the use of a "transverse Riemann solver". Similarly, the non-orthogonal components of the up and down-going waves generated at the $(i,j+1/2)$ interface are decomposed into left and right-going waves via the transverse Riemann solver. As shown above, these solvers take into account the material properties in the cells and automatically give the proper speeds and directions of these waves.

A numerical test is shown in [34] which consists of a plane wave hitting an interface between two materials at an oblique angle, giving rise to transmitted and reflected waves as shown in Figure 5.2(b). In this example, the bulk modulus $k=1$ and the density ρ jumps from 1 to 4 at the interface.

We repeat the example here to illustrate the ability of the algorithm to solve a 2D acoustic example with rapidly-varying media. The example is modified in [17] by adding random fluctuations to the density ρ_{ij} in each grid cell. Figure 5.2(a) shows the density function used and Figure 5.2(c) shows the computed solution with the same plane wave as used in Figure 5.2(b). The homogenized velocity in each medium is the same as in the piecewise constant case, and so we see essentially the same transmission and reflection of the plane wave as in Figure 5.2(b), as expected.

5.2.3 Two Dimensional Acoustic-Elastic Interface

In this section we show an example of a radial acoustic pulse incident on an elastic medium. Recall that an acoustic medium only supports pressure waves while an elastic media supports both pressure and shear waves. To visualize the difference between the two types of media, a pressure wave in an acoustic medium is incident on an interface between the acoustic medium and an elastic medium. When the (acoustic) pressure wave hits the elastic material both P-waves and S-waves are generated in the elastic medium.

In the acoustic medium, the P-wave propagates with the sound speed $c_p = \sqrt{k/\rho}$, while in the elastic medium the P-wave propagates with speed $c_p = \sqrt{(\lambda+2\mu)/\rho}$. Recall the elastic S-wave propagates with speed $c_s = \mu$. In this example, the material parameters are chosen specifically so that the P-wave moves through the interface between the two types of media without a change in velocity.

$$\mu = \begin{cases} \mu = 0 & y > 1 \\ \mu = 1 & y \leq 1 \end{cases}, \qquad \lambda = \begin{cases} \lambda = 3 & y > 1 \\ \lambda = 1 & y \leq 1 \end{cases}, \qquad \rho = 1. \tag{5.26}$$

Here we find the P-wave speed in the two types of media given as $c_{pA} = \sqrt{k/\rho} = \sqrt{\lambda/\rho} = \sqrt{3} = c_{pE} = \sqrt{(\lambda+2\mu)/\rho} = \sqrt{3}$, so that the speed of the P-wave is the same in both media. In this example, we expect the P-wave to move across the interface with no change in velocity. Figure 5.2.3 shows a contour plot of σ_{22}, recall that in the acoustic (upper) medium σ_{22} corresponds to the negative of the pressure. Note that the P-wave (the outer ring) has been partially transmitted with no change in velocity. Figure 5.3 shows a contour plot of the shear stress σ_{12} in the entire domain. As the acoustic medium can not support shear stress one expects that σ_{12} should remain zero above $y =$. In both figures 5.2.3 and 5.3 one can see the S-wave behind the transmitted P-wave in the elastic medium.

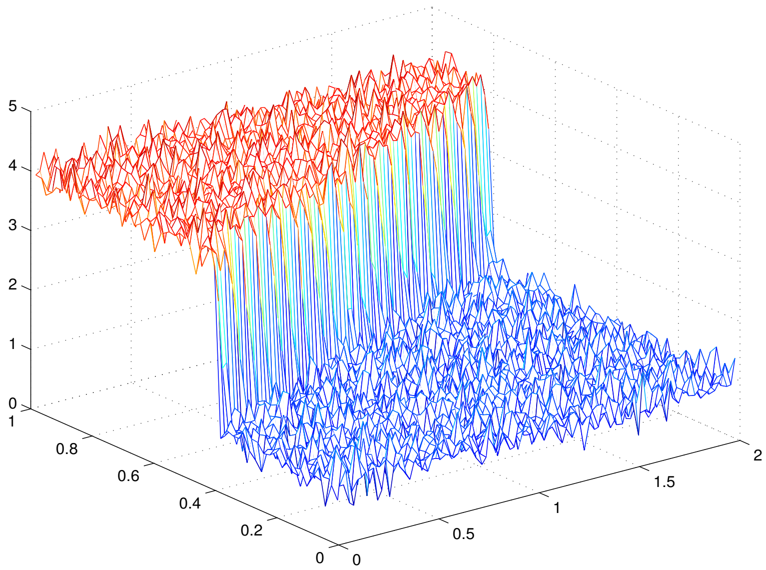

Figure 5.1: Density profile

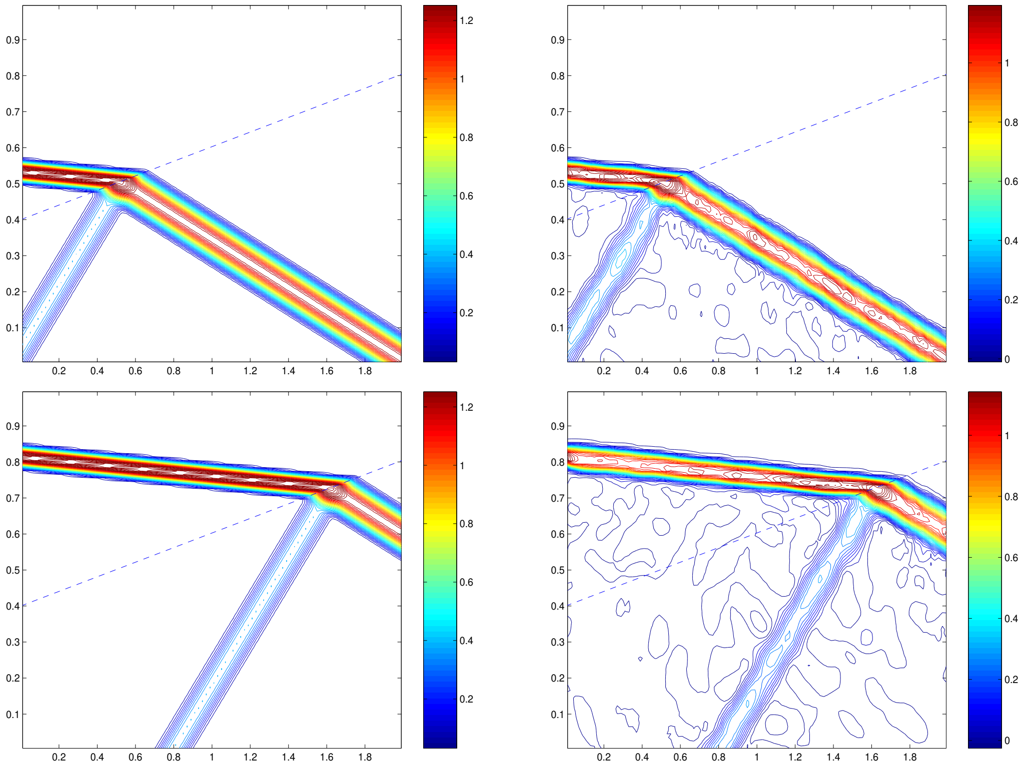

Figure 5.2: Left: Plane wave hitting an interfaces in a piecewise constant medium. (Exact Solution at two times). Right: Numerical solution for same medium with random fluctuations added as shown in Figure 5.1. Grid size N=100 x 100.

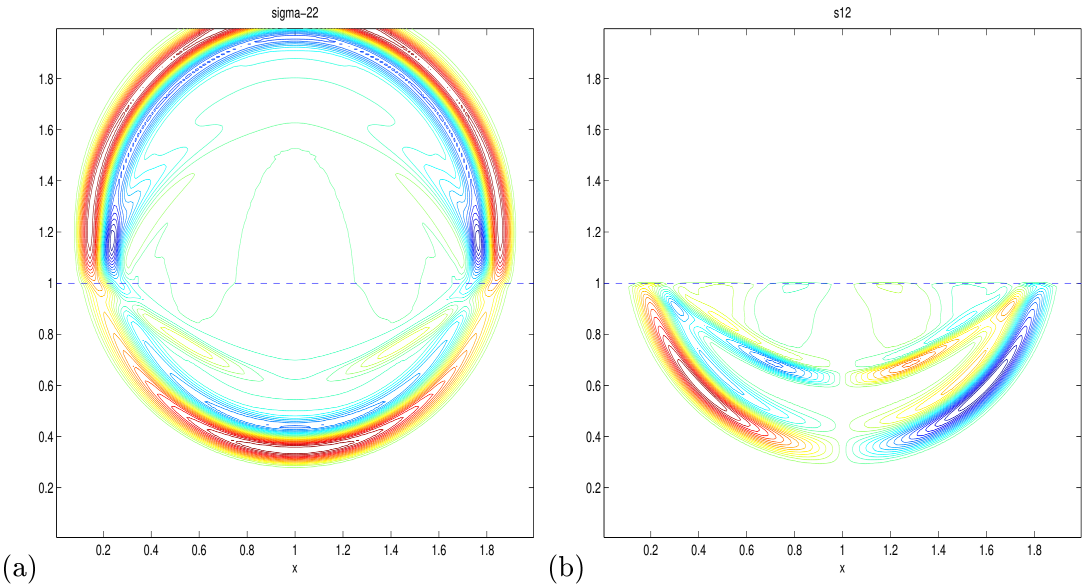

Figure 5.3: Left: Pressure disturbance, Acoustic/Elastic interface (σ_{22}) shown. Right: Shear (σ_{12}) generated by pressure disturbance.

Chapter 6

ONE DIMENSIONAL ELASTO-PLASTICITY AND DAMAGE

In this chapter we explain the difference between elastic and elastic-plastic behavior and define damage. We show how the stress-strain or constitutive relations differ when simplifying assumptions are imposed on the general nonlinear elastic-plastic constitutive relation. We introduce the Riemann solution procedure first in the context of linear elasticity. We then show how to extend the solution procedure to solve in the elastic-plastic regime under the assumption that the plastic deformation is not strong enough to cause damage. We then include damage in the model and show how to extend the solution procedure yet again to solve examples that have large enough plastic deformation to cause damage. In the last sections of the chapter we introduce an alternative solution procedure based on minimization techniques. Several examples are solved to show that both the Riemann solution method and the minimization solution method give accurate results that are in agreement.

The most general nonlinear elasto-plastic stress-strain relationship which includes damage is shown in Figure 6.1. Here we can see that the material has a nonlinear response to strain in both the elastic and plastic regimes. Note the points A, B, C, and D in Figure 6.1. As one moves from point A alphabetically to point D one can see the four important aspects of this stress-strain curve. At point A the material is at zero stress and zero strain with no plastic history. As the material is strained or loaded from point A to point B there is a nonlinear elastic response to the increased strain. The curve between points A and B is an example of a nonlinear elastic stress-strain relation for a material that has not yet been damaged or plastically deformed.

Figure 6.1 shows that loading beyond the point B or the initial yield-stress σ_{y1} causes plastic deformation. In this stress-strain curve it is assumed that there exists an initial yield-stress which separates the elastic and plastic response regions. Loading beyond the yield-stress causes the material response to strain to change from elastic to plastic. One can see that as the material is loaded beyond point B the ability of the material to support stress is greatly reduced. The portion of the curve between points B and C is an example of a nonlinear plastic stress-strain relation where the material is undergoing both plastic deformation and damage.

One can see that the primary difference between loading up to the point B and loading beyond B is that for a given increase in strain there is a much larger increase in stress in the elastic portion (up to B) than in the plastic portion of the curve (beyond B). This difference is caused by the plastic deformation of the material that occurs for loading beyond the point B. If loading stops at or before the point B and the material is unloaded from B it returns to the point A and there is no plastic strain. However if loading goes past B to the point C and the material is then unloaded it returns along a different elastic curve to the state D. One can see that at the point D the material is at a state of zero stress but the strain is non-zero. Loading along the plastic part of the curve from B to C has caused a permanent

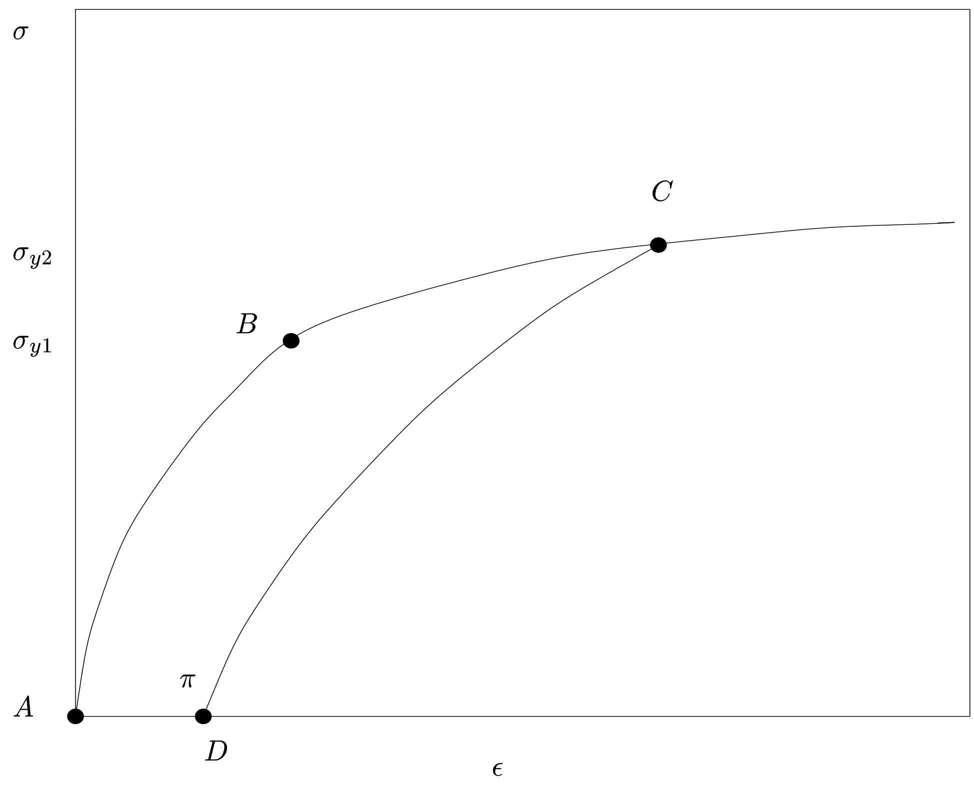

Figure 6.1: General Nonlinear Elastic-Plastic Stress-Strain Curve with Damage.

plastic strain or deformation to develop. This plastic strain is shown in Figure 6.1 as the difference in strain at zero stress between points A and D, and has a value denoted by π.

As Figure 6.1 is very general it shows three effects at once: nonlinear response, plastic deformation, and damage. The plastic deformation is shown as the difference in strain at the two zero stress states at points A and D. The damage is shown as the difference in the slope of the two elastic curves. One can see that the elastic curve between the points A and B is much steeper then the elastic curve between points C and D. The change in slope of the elastic curves is caused by damage to the material in the form of a decreased ability to support stress at a given strain value. To further clarify the ideas of nonlinear response, plastic deformation and damage we can make simplifying assumptions about the stress-strain relationship and study each effect separately.

The first assumption that is made, which is valid in many cases, is that the elastic response is linear. Throughout the rest of this work we assume that any time the loading is below yield the material response will be both linear and elastic. In Figure 6.1 this would mean that the curve between A and B would be a straight line as well as the curve between C and D. Figure 6.2 shows a stress-strain relationship with the following assumptions: the elastic and plastic response are both linear, material damage occurs for loading beyond yield. If we start at the point A in Figure 6.1 and load the material up to the point C

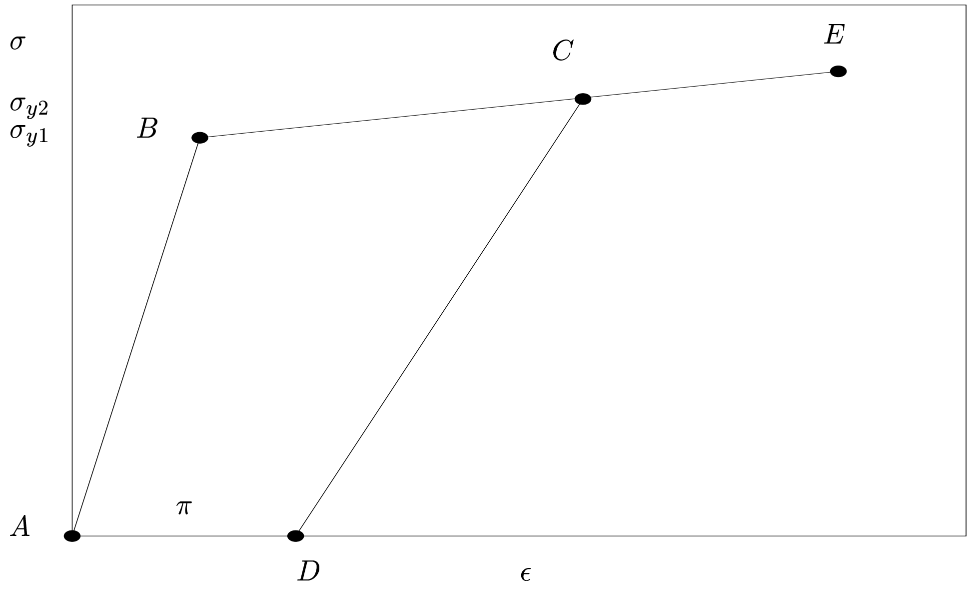

Figure 6.2: Linear Elastic and Linear Plastic Stress-Strain Curve with Damage.

and then unload back to the point D we can see three different effects. The first is that the material responds as a linear elastic solid from the point A up to the point B. Under further loading beyond the initial yield-point at B the material responds plastically out to the points C and beyond if loaded to E. Unloading from the point C back to zero stress at the point D shows that both plastic deformation and damage were caused by the plastic loading. The plastic deformation has a value of π and the damage is shown as the change in slope of the elastic curve. The basic premise is that a material that has been plastically deformed enough to cause damage will be less able to support stress than one that has not been damaged. After a material is damaged, further loading even in the elastic regime will move along a line of lesser slope to reflect that the material is weaker.

As we will show later, damage is a measure of how plastic deformation alters the future elastic behavior of a material. In Figure 6.2 it is assumed that material damage occurs even though the plastic response regime can be modeled with a straight line. The assumption that plastic response can be linear is often made (the stress-strain relation between the points B and E is a straight line) and it should be clear that damage caused by plastic deformation is a separate effect than linear or nonlinear plastic response. Figure 6.3 shows a stress-strain model with the assumption that plastic response is nonlinear and that plastic deformation is never great enough to cause damage. One can see in Figure 6.3 that if we go though the same loading and unloading for the points A though D that our assumptions are borne out by the shape of the stress-strain relation. As in the previous figure loading from A to B causes a linear elastic response. Further loading from B to C is modeled by a curve and gives a nonlinear plastic response. Unloading from C to D is again linear and elastic, and since we have assumed the deformation was too small to cause damage, the

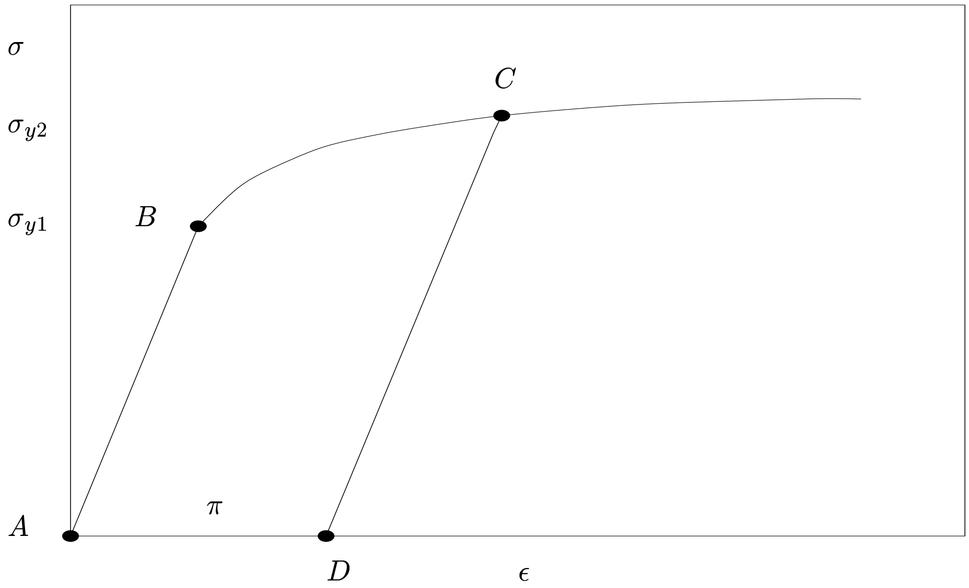

Figure 6.3: Linear Elastic and Nonlinear Plastic Stress-Strain Curve.

slope of both elastic curves is the same.

One should note that in both Figure 6.2 and Figure 6.3, as soon as loading exceeds the initial yield point the problem becomes nonlinear. It should be clear that even if the plastic response is modeled by a straight line as in Figure 6.2, one must still solve a nonlinear problem to obtain the solution for any point on the stress-strain relation beyond B. In the following sections we will explain the solution procedures used to solve examples with stress-strain relations that include elastic and plastic response as well as damage.

6.1 *Elasticity and Elasto-Plasticity*

Recall that we can reduce either the 2-D plane-strain or 2-D plane-stress equations to one-dimension. The one-dimensional reductions from plane-stress and plane-strain both lead to a system of two first-order (generally) non-linear governing equations coupled via a constitutive relation. The first equation is a relation between velocity and strain that can be thought of as the definition of strain. The time rate of change of the strain in the x-direction is equal to the differential x-velocity. The second equation is Newton's second law where force is measured by stress σ:

$$\begin{aligned} \epsilon_t - v_x \quad &= 0, \\ \rho(x)v_t - \sigma_x \quad &= 0. \end{aligned} \tag{6.1}$$

See [26] for details.

The system is closed by specifying a functional relation between the stress σ and strain

ϵ,

$$\sigma = f(\epsilon). \tag{6.2}$$

This gives a coupled non-linear system of equations where the stress-strain relation (6.2) is specific to the material and dependent on the assumptions one makes in reducing to one-dimension.

Recall that in Section 2.5 the one-dimensional reduction from linear elastic plane-strain gives the constitutive relation

$$\sigma = (\lambda + 2\mu)\epsilon. \tag{6.3}$$

In this case the 1D linearly elastic system takes the form

$$\begin{bmatrix} \sigma_{11} \\ u \end{bmatrix}_t + \begin{bmatrix} 0 & -(\lambda+2\mu) \\ -1/\rho & 0 \end{bmatrix} \begin{bmatrix} \sigma_{11} \\ u \end{bmatrix}_x = 0. \tag{6.4}$$

We will return to this system in later sections. The 1D reduction from linear elastic plane-stress assumes that all stresses other then σ_{11} are zero. This assumption gives the constitutive relation

$$\sigma = \frac{\mu(3\lambda+2\mu)}{\lambda+\mu}\epsilon. \tag{6.5}$$

As we saw in Section 2.5, the combination of (6.5) and (6.1) gives the one-dimensional linear elastic reduction from plane-stress as

$$\begin{bmatrix} \sigma_{11} \\ u \end{bmatrix}_t + \begin{bmatrix} 0 & -\frac{\mu(3\lambda+2\mu)}{\lambda+\mu} \\ -1/\rho & 0 \end{bmatrix} \begin{bmatrix} \sigma_{11} \\ u \end{bmatrix}_x = 0. \tag{6.6}$$

In the following sections we use this 1D system to introduce the tools and concepts that are necessary to simulate numerically examples in the elasto-plastic and material damage regimes. The first step is to define clearly the difference between the elastic and the elasto-plastic behavior.

6.1.1 Linear Elasticity

When material is behaving as a linearly elastic solid the stress-strain relation can be written as

$$\sigma = \beta\epsilon. \tag{6.7}$$

Here β is the elasticity tensor. In the one-dimensional reduction from plane-stress, $\beta = \frac{\mu(3\lambda+2\mu)}{\lambda+\mu}$ is just the slope of the stress-strain curve.

Figure 6.4 shows the stress-strain curve for one-dimensional linear elasticity. One can see that the system given by (6.6) has an identical eigen structure as the 1D acoustic system given in section 2.6. As in the 1D acoustic system, one can see that the solution to this system will consist of two P waves. While in the 1D acoustic system our state variables

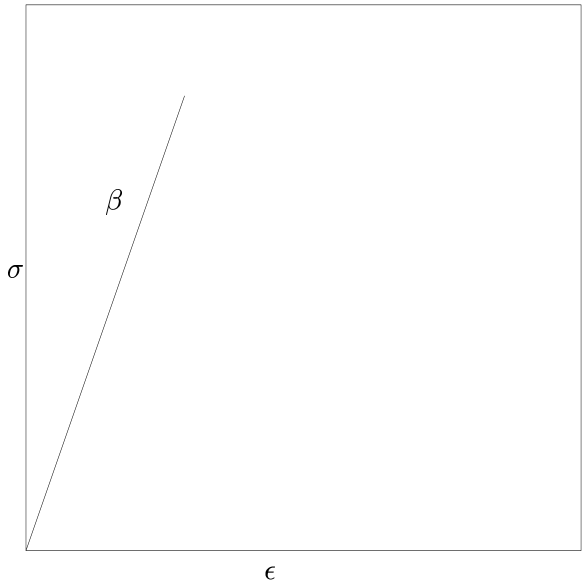

Figure 6.4: Elastic Stress-Strain Curve.

were velocity v and pressure p, in the 1D elastic system the state variables are velocity and stress σ.

Recall Figure 3.2, which shows the solution to the 1D acoustic Riemann problem in x-t space. Just as in the previous 1D linear acoustic system, the 1D linear elastic system can be solved by determining the two waves which emanate at each cell interface. Recall that in the 1D acoustic system the eigenvalues and eigenvectors in each cell are given by

$$\begin{aligned} \lambda_i^1 &= -c_i, & \lambda_i^2 &= c_i, \\ r_i^1 &= \begin{bmatrix} -\rho_i c_i \\ 1 \end{bmatrix}, & r_i^2 &= \begin{bmatrix} \rho_i c_i \\ 1 \end{bmatrix}, \end{aligned} \tag{6.8}$$

where the sound speed in the i'th cell is given by $c_i = \sqrt{\beta_i/\rho_i}$. Similarly for the 1D linear elastic system given by equation (6.6) the eigenvalues and eigenvectors in each cell are given by equation (6.8), but in this case the sound speed in each cell is given by

$$c_i = \sqrt{\frac{\mu_i(3\lambda_i + 2\mu_i)}{\rho_i(\lambda_i + \mu_i)}}. \tag{6.9}$$

One can see that while there is a quantitative difference in the eigenvalues and eigenvectors of the 1D linear acoustic and elastic systems, the solutions are qualitatively identical. As the Riemann structure is the same for both systems it follows that one can use identical solution methods on both the acoustic and elastic systems. In the next section we show how the Riemann structure of the 1D elasto-plastic system differs from that of 1D elasticity. Once this difference is clear we will show how the solution method for 1D elasticity can be extended to the plastic regime.

6.1.2 *Elasto-Plasticity*

When stress exceeds the elastic threshold of a material the nature of material behavior changes from elastic to plastic. Loading beyond the elastic threshold results in two fundamental changes in material response. Depending on the material, loading beyond the elastic threshold can cause a response which is known as **perfectly plastic** or **strain hardening**. A perfectly plastic material has a plastic response curve with zero slope. For any additional strain beyond elastic-yield, a perfectly plastic material will plastically deform without any increase in stress or initial yield-stress. A strain hardening material which is loaded beyond the initial yield-stress will also deform plastically but the stress-strain state will move along a stress-strain curve which has a slope greater then zero. Assuming that the plastic response is linear the slope β changes to a new value, $\beta_p < \beta$, so that a much smaller increase in stress results for a given increase in strain. Also the material undergoes plastic deformation π. Note that we will discuss the case where the plastic response curve is nonlinear in a later section. As stated above it is also important to note that even when the plastic response is linear one must still solve a nonlinear problem to find solutions that are plastic in nature.

In the linearly elastic regime a given change in strain corresponds to a constant multiple of the change in stress, while in the plastic regime a given change in strain results in a smaller change in stress and a plastic deformation. Figure 6.5 shows elastic and plastic

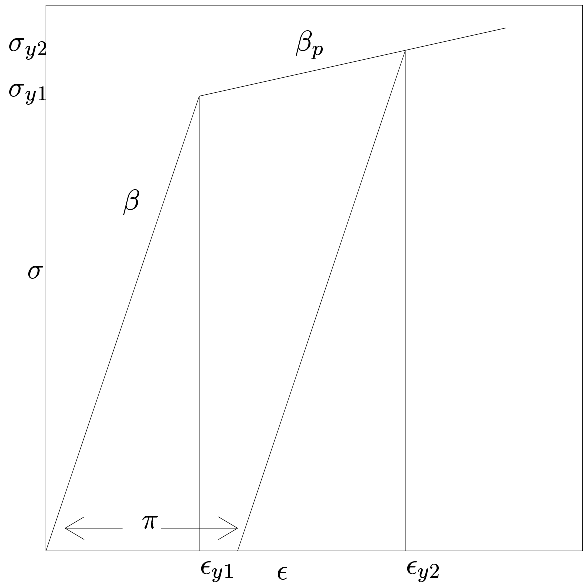

Figure 6.5: Elastic and Elasto-Plastic Stress-Strain Curve With Yield-Stress and Yield-Strain Thresholds Shown for two different loading curves. Also shown is the plastic deformation (π) caused by loading from (σ_{y1}) to (σ_{y2}).

loading curves with slopes β and $\beta_p < \beta$. Also in Figure 6.5 one can see the yield-stress thresholds σ_{y1} and σ_{y2} and yield-strain thresholds ϵ_{y1} and ϵ_{y2} for two loading curves as well as the plastic deformation π caused by loading from σ_{y1} to σ_{y2}.

It is important that Figure 6.5 be clearly understood. Suppose we start at the point of zero stress and zero strain. If the material undergoes a strain or loading then the material will behave elastically as long as the stress does not exceed the initial yield-point σ_{y1}. Once the stress exceeds σ_{y1} the material will behave plastically and an increase in strain will correspond to an increase in stress which is equal to the slope of the plastic curve times the strain, or $\beta_p(\epsilon - \epsilon_y)$. Assume that this loading continues to the point where the stress has a value of $\sigma = \sigma_{y2}$ and strain has a value of $\epsilon = \epsilon_{y2}$. Now if it is assumed that the strain is released or that the material is unloaded and that no damage occurs, then the material will behave elastically and return to a point of zero stress along a curve with slope β. However as can be seen in Figure 6.5, the material is no longer at a point of zero strain.

Figure 6.5 shows that after unloading from the point σ_{y2} to $\sigma = 0$ the material is left with a nonzero value of strain. This nonzero strain is quantified by π and is the amount of **plastic deformation** that the material has undergone. Also in Figure 6.5 one can see that if the material is loaded again it will behave elastically until the point where $\sigma = \sigma_{y2}$ before it starts to behave plastically. When the material underwent the first plastic deformation it was changed in a such a way as to "remember" that it had undergone plastic deformation. One can see that if the material is loaded in the future then the elastic or plastic response of the material is dependent on the previous loading. One of the fundamental differences between linear elasticity and elasto-plasticity is that elasto-plastic behavior is dependent on the previous plastic deformation of the material. See [23] and [19] for further details.

In the following section we discuss the Riemann solution method for the 1D elasto-plastic system. We show how moving beyond the yield point gives rise to two plastic waves in addition to the two elastic waves. One can solve for all 4 waves to develop a solution method based on that used for 1D linear acoustics.

6.2 1D Elasto-Plastic Riemann Solution

Solution techniques for the plastic and elastic regimes are very similar. Recall that if the stress exceeds the yield stress threshold then the material behaves plastically instead of elastically. In this case the solution consists of two plastic waves in addition to two elastic waves. Plastic waves move at a slower speed ($c_P = \sqrt{\beta_p/\rho}$) than elastic waves ($c_E = \sqrt{\beta/\rho}$), since $\beta_p < \beta$. While elastic waves propagate at the elastic wave speed and affect changes in stress and strain, plastic waves move at the plastic wave speed and affect changes in stress, strain, plastic dislocation, and the current value of the yield-stress threshold.

The relation between plastic movement (or plastic history) and yield-stress threshold is discussed in more detail below. Since one does not know beforehand whether a given Riemann problem will result in elastic or plastic waves, the simplest solution is to assume that both kind of waves may result in each Riemann solution. If the solution is purely elastic then the strength of the plastic waves will be found to be zero. However if there is plastic movement to the left or right of a cell interface, we may have two elastic waves and one or two non-zero strength plastic waves. Recall that the elastic Riemann solution is characterized by two waves at each cell interface. Figure 6.6 shows the elastic waves in x-t space generated by the jump in state variables at the i'th interface.

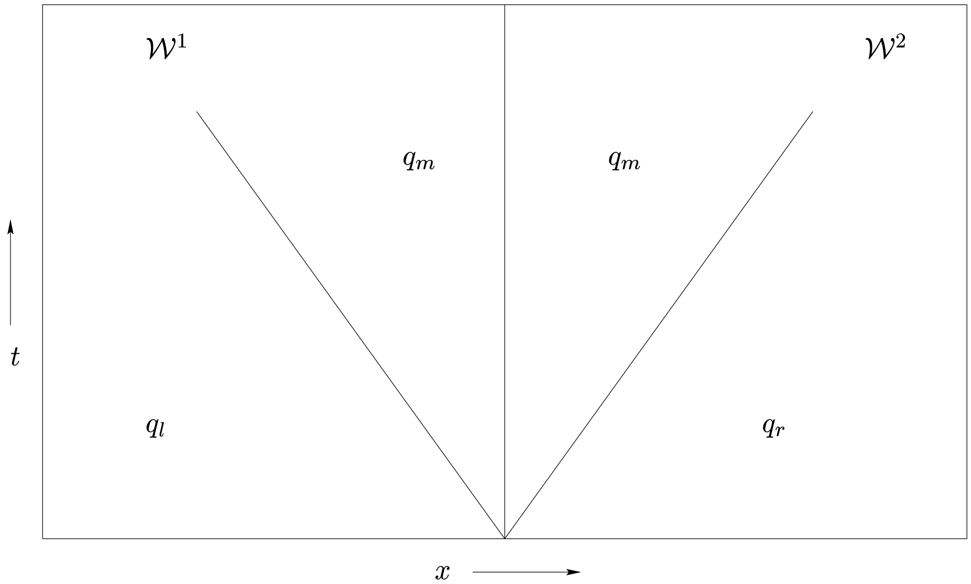

Figure 6.6: Elastic waves at the i'th interface in x-t space.

6.2.1 Elastic Riemann Solution

Just as in the acoustic case, the left and right states q_l and q_r are known along with the eigenvectors r_l^1 and r_r^2, and the jump across the interface must equal the sum of the two waves as follows:

$$q_r - q_l = \alpha^1 r_l^1 + \alpha^2 r_r^2. \tag{6.10}$$

Here r_l^1 is the 1-wave eigenvector in the cell to the left of the interface and r_r^2 is the 2-wave eigenvector in the cell to the right of the interface. As was done in the acoustic system we solve the 2×2 system (6.10) for α^1 and α^2 to uniquely determine the waves $\mathcal{W}^1$ and $\mathcal{W}^2$. The mid-state q_m can then be found via either of the following two equations:

$$q_m = q_r - \mathcal{W}^2, \tag{6.11}$$

$$q_m = q_l + \mathcal{W}^1. \tag{6.12}$$

As with the acoustic case, Figure 6.7 shows how the mid-state q_m can be seen in phase space as the interception of Hugoniot Loci for the left and right states q_l and q_r. Recall that the Hugoniot Locus for the left state is the set of all states that can be connected to q_l by a 1-wave. Similarly, for the right state the Hugoniot Locus is the set of all states that can be connected to q_r by a 2-wave.

6.2.2 Elasto-Plastic Riemann Solution

The elasto-plastic system is fundamentally different from the elastic system in that once the stress exceeds yield, the Hugoniot Loci are no longer linear. Recall that when loading

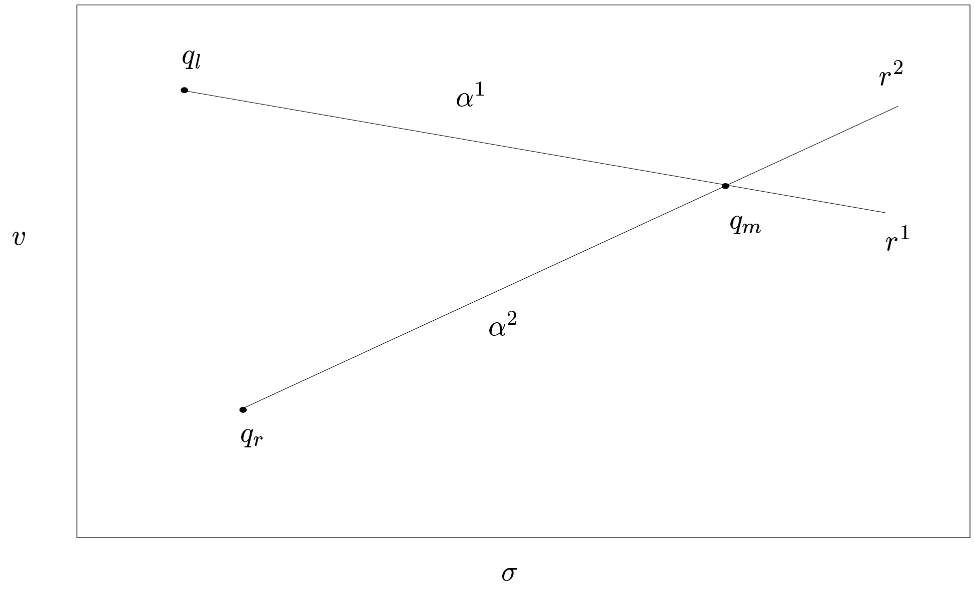

Figure 6.7: Hugoniot Loci for the 1D Linear Elastic System.

exceeds the yield-stress the material responds plastically instead of elastically. In phase space this corresponds to a change in slope at the yield point. Figure 6.8 (a) and (b) show a generalized Hugoniot Loci for left and right states. Recall that the Hugoniot locus is the set of states that can be connected to a fixed left state q_l (or fixed right state q_r) by a wave. Figure 6.8 (a) and (b) show the generalized Hugoniot loci for states q_l and q_r that include stress values that exceed the yield-stress of the left and right cells.

In Figure 6.8 (a) one can see the generalized Hugoniot locus for a state q_l. Here one can see that for any state which has a stress value less than the yield-stress (to the left of the line at σ_{yl}), the Riemann structure consists solely of an elastic 1-wave $\mathcal{W}^1$. While for any state that has a stress value greater then the yield-stress (to the right of the line at σ_{yl}), the wave structure consists of an elastic 1-wave and a plastic 3-wave. Similarly, Figure 6.8 (b) shows the generalized Hugoniot locus for a state q_r. Here, for any state which has a stress value that is less then the yield-stress (to the left of the line at σ_{rl}), the Riemann structure consists of an elastic 2-wave $\mathcal{W}^2$. Similarly, any state which has a stress value greater than the yield-stress (to the right of the line at σ_{rl}), has a wave structure that consists of an elastic 2-wave and a plastic 4-wave. Recall Figure 6.5. When the stress in any state exceeds the yield-stress, the constitutive relation (or slope of the stress-strain curve) changes from $\sigma = \beta\epsilon$ to $\sigma = \beta_p\epsilon$ where $\beta_p < \beta$. The change from elastic to plastic behavior is shown in Figure 6.8 as the change in slope of the Hugoniot locus at the yield stress.

For any given elasto-plastic Riemann problem the left and right states will have generalized Hugoniot loci of the form shown in Figure 6.8. To find the solution state (or mid state q_m) one need only overlay these two curves and find where they intersect. The intersection of any two such curves must lead to a solution that has one of the following four forms: two

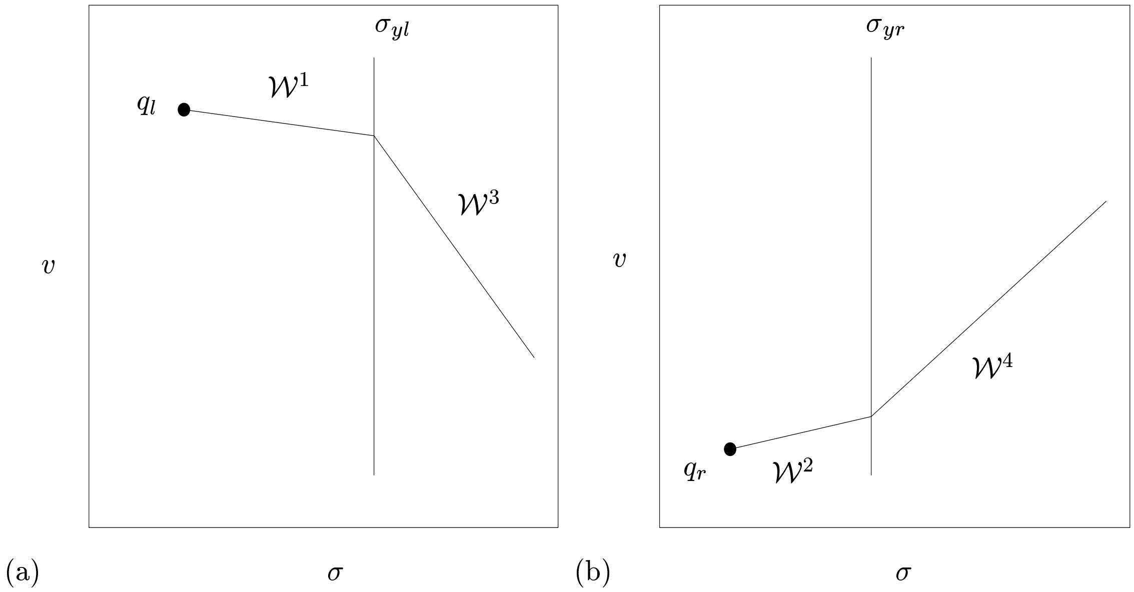

Figure 6.8: Hugoniot loci for the left (a) and right (b) states q_l and q_r.

elastic waves, two elastic waves and a left-going plastic wave, two elastic waves and a right going plastic wave, or two elastic waves and two plastic waves.

In general the yield stress for the left and right states will not be the same. Depending on whether the stress in the mid-state q_m (the point where the two loci curves intersect) is greater or less then the yield stress in the left hand cell or right hand cell or both, the Riemann solution may have any one of the four solution configurations.

Example 1. Two elastic waves. If the stress in the mid-state is less then the yield-stress in both cells the solution will consist of only two elastic waves. Figure 6.9 (a) shows an example where the solution state q_m lies to the left (less then) the yield-stress in both the left and right cells. In this example the Riemann structure consists of two elastic waves $\mathcal{W}^1$ and $\mathcal{W}^2$ which connect the left and right states to the solution state q_m. Figure 6.10 shows this same example in stress-strain space instead of stress-velocity space. Note that what is shown in this figure is the stress-strain relationship for both the left and right cells. Here we can see that the left state q_l is connected to the mid state q_m by a purely elastic wave. Similarly the right state q_r is also connected to the mid state q_m by a purely elastic wave. Here we can also see that the mid state q_m has a stress value which lies below the yield-stress values of both cells shown as σ_{yl} and σ_{yr}. Note that while the stress is continuous across the cell interface (σ_m is the same in both cells), the strain is discontinuous with a jump of $(\epsilon_{mr} - \epsilon_{ml})$.

Example 2. Two elastic waves and one plastic wave. If the stress in the mid state is greater than the yield-stress in one of the cells (to the left of the interface for example) and less than the yield-stress in the cell to the right of the interface, the solution consists of an elastic wave moving to the right and both elastic and plastic waves moving to the

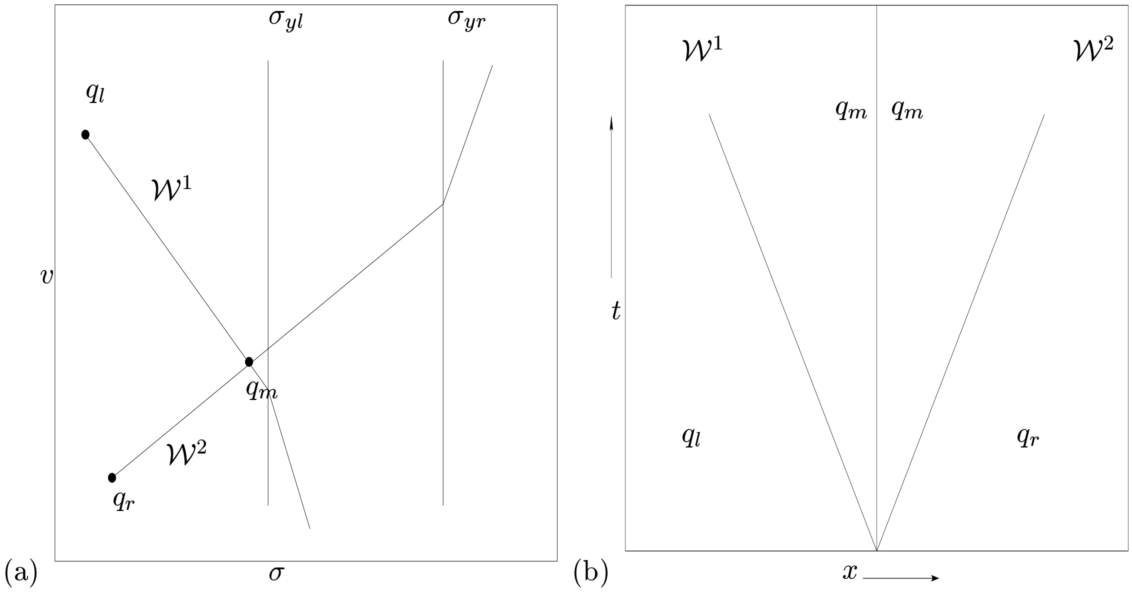

Figure 6.9: (a) Intersection of Hugoniot Loci for the left and right states q_l and q_r. Here q_m is less then the yield-stress in both the left and right cells. (b) Elastic $\mathcal{W}^1$ $\mathcal{W}^2$ and Plastic $\mathcal{W}^3$ waves for the example shown in (a). (a) shows the waves and states in phase-space (σ-v) while (b) shows the waves and states in x-t space.

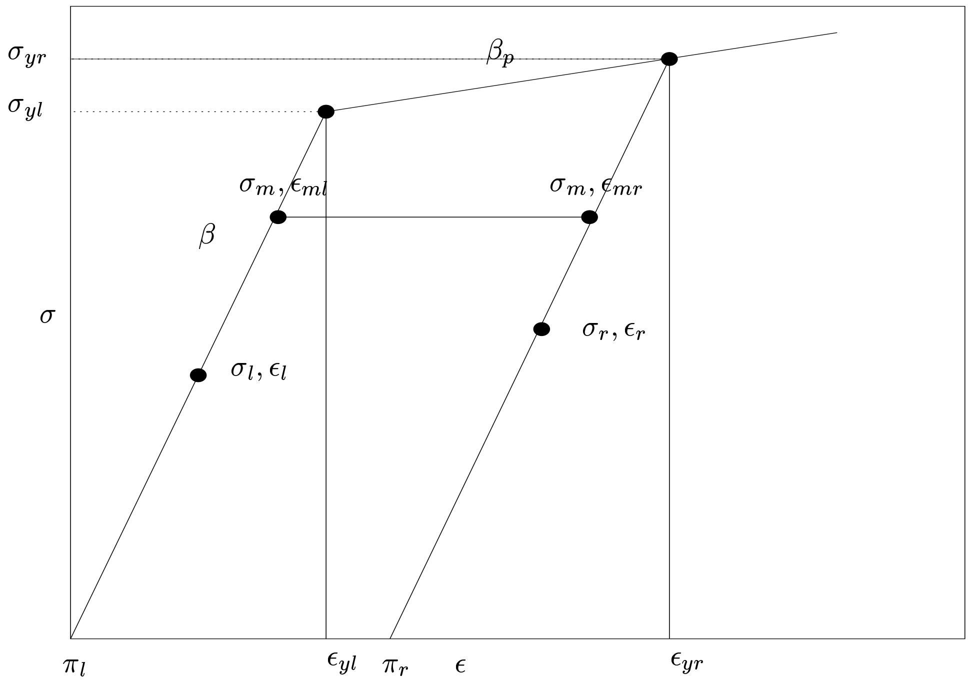

Figure 6.10: Elastic and Elasto-Plastic Stress-Strain Curve With Yield-Stress and Yield-Strain Thresholds Shown for two neighboring cells. Also shown is the plastic deformation π_r and π_l which exists initially in each cell. The solution lies at the mid-state σ_m. Note the jump in strain $(\epsilon_{mr} - \epsilon_{ml})$ and plastic deformation $(\pi_r - \pi_l)$ between the cells.

left. In Figure 6.11 (a) and (b) one can see the waves in both phase (σ-v) space and x-t space. Figure 6.11 (a) shows the left and right states q_l and q_r that exist initially in the left and right cells. Figure 6.12 shows the left, right, and mid (solution) states and where they lie on the stress-strain curves of two neighboring cells. In the left cell there is no plastic deformation initially and the left state q_l is below yield. In the right cell there is an initial plastic deformation π_r and the right state q_r is also below yield for this cell. The mid-state q_m has a stress value that exceeds the yield-stress of the left cell but not that of the right cell. In Figure 6.12 the stress-strain curves for both cells are shown so one can see where all these states lie in relation to the stress-strain curve of each cell.

Figure 6.11 (a) and (b) show how to construct the solution state q_m. Since the state variables σ and v in q_m must be continuous across the interface between the left and right cells (shown Figure 6.11 (b)), we see that in phase space (Figure 6.11 (a)) the intersection of the two Hugoniot loci will determine the solution q_m. It is important to observe that while σ and v are continuous across the interface the strain ϵ will not be continuous in general. Figure 6.11 (b) and Figure 6.12 show the stress σ_m in both the left and right cells. Figure 6.12 again shows σ_m to have the same value in both the right and left cells, but in this figure one can also see the jump in strain and plastic deformation across the interface. In the left cell there is a plastic wave across which there is a jump in both strain ϵ and plastic deformation π_l. In the right cell there is no plastic wave, however this cell had a pre-existing plastic deformation π_r. Here we can see that although the stress values σ_{ml} and σ_{mr} are the same, the strain has a jump across the cell interface from ϵ_{ml} to ϵ_{mr}. For this example the generalized Hugoniot locus for the left state q_l is shown as an elastic 1-wave and plastic 3-wave which connects q_l to q_m. Similarly the Hugoniot locus for for the right state q_r is shown as an elastic 2-wave which connects q_r to the mid-state q_m. Figure 6.11 (b) shows the same waves and states in x-t space. One can see that for this example the solution to the Riemann problem consists of three waves: a left going elastic wave, a left going plastic wave, and a right going elastic wave. As it can not be known in advance which of the possible configurations the solution will take, we must assume a general solution of all four waves.

Example 3. Two elastic waves and two plastic waves. Figure 6.13 and Figure 6.14 show case where the solution to the Riemann problem q_m lies beyond the yield-stress of both cells. Here the Riemann solution consists of four waves: two elastic and two plastic. Also in this example only the right hand cell has a previous plastic deformation. It is important to recognize that what is shown is the stress-strain curves for two different cells and that, in general, either cell may have been previously plastically deformed. Also note that the solution q_m might lie anyplace on the stress-strain curves. The example shown in Figure 6.14 is chosen to demonstrate the case when all four waves have a non-zero amplitude. While Figure 6.14 shows the left, right and solution states in σ-ϵ space, the solution procedure is much more transparent if viewed in phase space.

For the elasto-plastic Riemann solution we assume that the solution at each interface consists of 4 waves. Across each cell interface there may be a jump in stress σ, velocity v, strain ϵ, plastic deformation π, elastic constants β and β_p and yield-stress threshold σ_y. For each Riemann problem there is a left and right cell yield-stress threshold associated with the previous loading history of the cells to the left and right of each cell interface. The solution

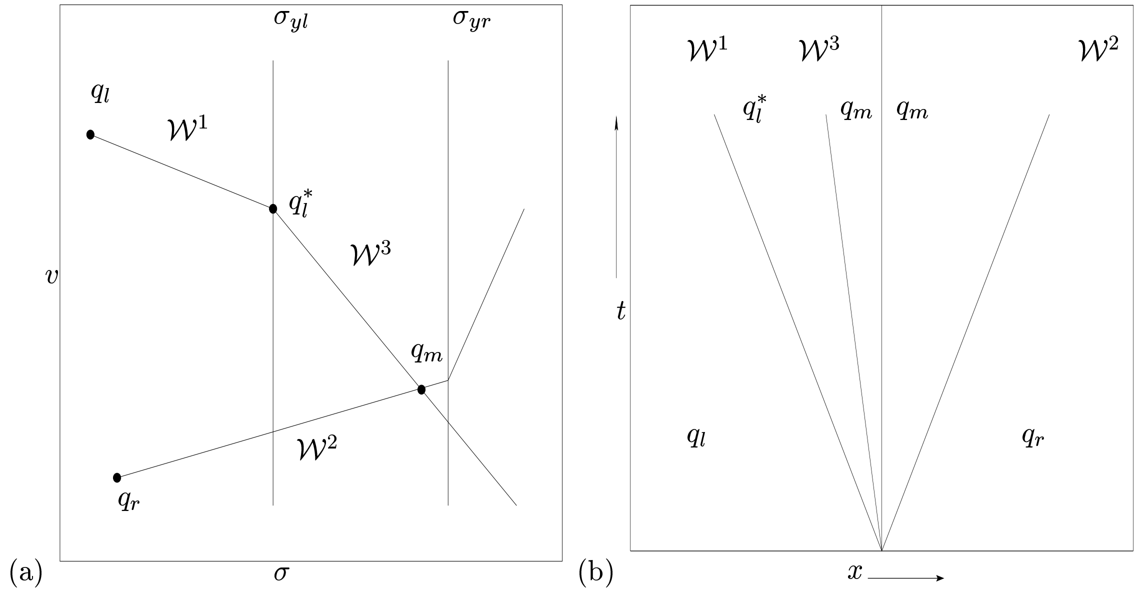

Figure 6.11: (a) Intersection of Hugoniot Loci for the left and right states q_l and q_r. Here q_m exceeds the yield-stress in the left cell but not for the right cell. (b) Elastic (W1 and W2) and Plastic (W3) waves for the example shown in (a). (a) shows the waves and states in phase-space (σ-v) while (b) shows the waves and states in x-t space.

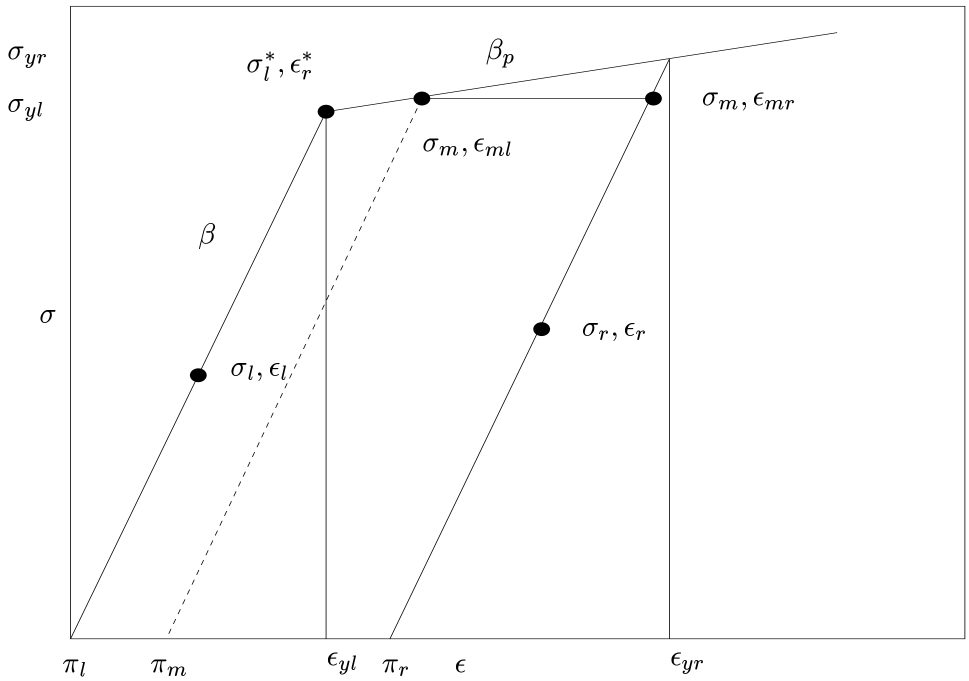

Figure 6.12: Elastic and Elasto-Plastic Stress-Strain Curve With Yield-Stress and Yield-Strain Thresholds Shown for two neighboring cells. Also shown is the plastic deformation (π_r) which exists in the right cell. The solution lies at the mid-state σ_m. The mid-state σ_m has a stress which lies beyond the yield-stress of the left cell but not the right cell. Note the jump in strain ($\epsilon_{mr} - \epsilon_{ml}$) and plastic deformation ($\pi_r - \pi_l$) between the cells.

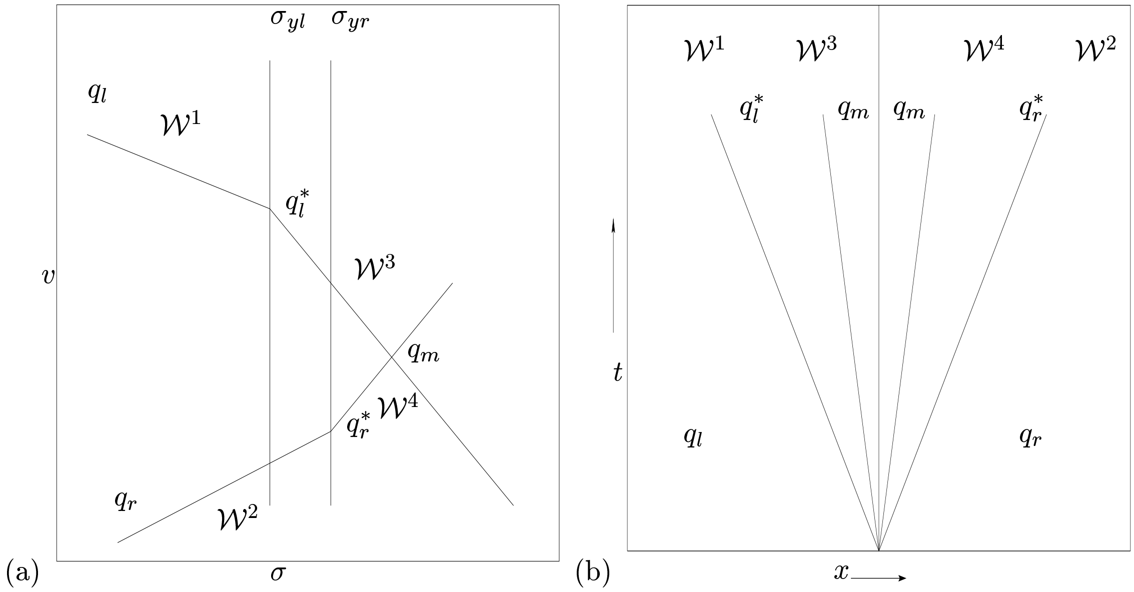

Figure 6.13: (a) Intersection of Hugoniot Loci for the left and right states q_l and q_r. (b) Elastic $\mathcal{W}^1$ $\mathcal{W}^2$, and Plastic $\mathcal{W}^3$ $\mathcal{W}^4$ waves in the general 1D Elasto-Plastic Riemann Problem.

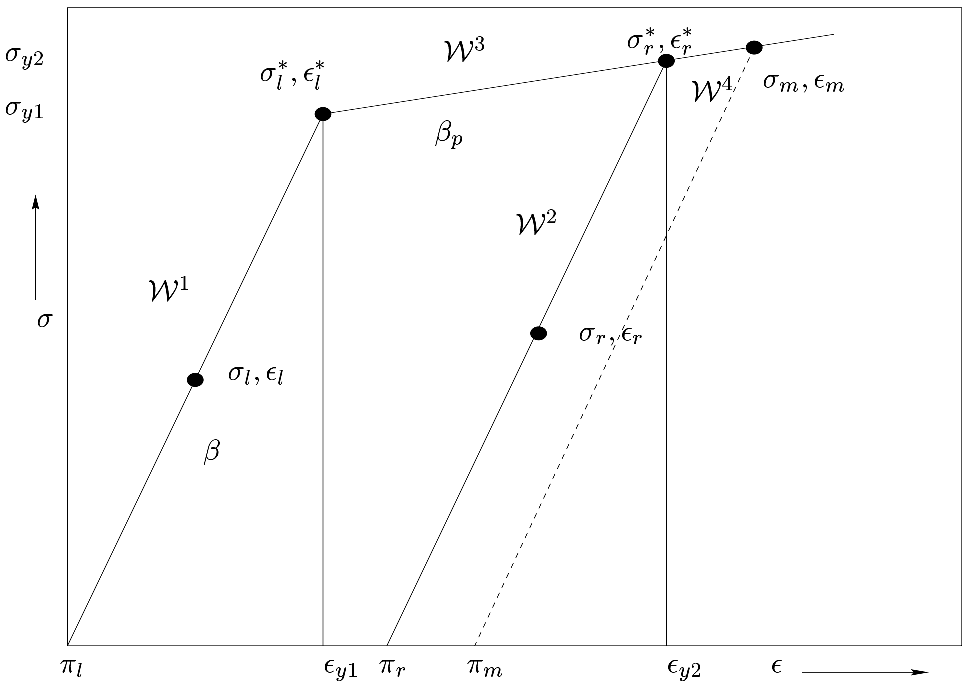

Figure 6.14: Elastic and Elasto-Plastic Stress-Strain Curve With Yield-Stress and Yield-Strain Thresholds Shown for two neighboring cells. Also shown is the initial plastic deformation π_r and π_l in the right and left cells and the final plastic deformation π_m in both cells. The solution lies at the mid-state σ_m, ϵ_m. The mid-state stress σ_m lies beyond the yield-stress of the the left and right cells.

strategy for a given Riemann problem is as follows. First calculate the two elastic waves assuming that there is no plastic deformation. The new stress in each cell is found by adding in the contributions of these two elastic waves. Comparing the new stress to the yield-stress threshold of both the left and right states determines weather or not plastic waves need to be calculated. If the solution stress in each cell is below the yield-stress threshold we are done and can move on to the next Riemann problem. Otherwise, when the new stress is greater than either the left or right yield-stress thresholds, we must calculate the left or right going plastic waves based on the difference between the left and right yield-stresses and the left and right state stresses. This order is chosen since the elastic regime is the cheapest in which to obtain a computational solution.

Figure 6.13 (a) shows the same example shown in Figure 6.14 but in σ-v space. Here we see the solution q_m in Figure 6.13 (a) as the intersection of the Hugoniot Loci for the left and right states. Recall that for this example the stress at q_m has exceeded the yield-stress in both the left and right-hand cells. One can see that since σ_{yl} and σ_{yr} are known, the amplitudes of the waves elastic waves $\mathcal{W}^1$ and $\mathcal{W}^2$ can be determined by equation (6.10) in the form

$$\sigma_{y1} - \sigma_l = \alpha^1 r_l^1, \tag{6.13}$$

$$\sigma_r - \sigma_{y2} = \alpha^2 r_r^2. \tag{6.14}$$

Once the elastic waves are known, equation (6.18) can be written as

$$q_r - q_l - \alpha^1 r_l^1 + \alpha^2 r_r^2 = \alpha^{1P} r^{1P} + \alpha^{2P} r^{2P}. \tag{6.15}$$

Here the only unknowns are the amplitudes of the plastic waves α^{1P} and α^{2P}. As with the elastic system, once the four waves are known we can solve for the mid-state by either of the following two forms of equation (6.15):

$$q_m = q_r - \mathcal{W}^2 - \mathcal{W}^{2P}, \tag{6.16}$$

$$q_m = q_l + \mathcal{W}^1 + \mathcal{W}^{1P}. \tag{6.17}$$

In Figure 6.13 (a) we can see basis for the solution procedure to find the amplitude of the four waves in phase space. Figure 6.13 (b) shows the same four waves in x-t space. Here we see the wave structure for the general 1D elasto-plastic Riemann problem and how those waves will affect the solution in the next time step. Recall that the jump between q_l and q_r must be given by the sum of these four waves as

$$q_r - q_l = \alpha^1 r_l^1 + \alpha^2 r_r^2 + \alpha^{1P} r^{1P} + \alpha^{2P} r^{2P} \tag{6.18}$$

Here the superscript P represents the plastic waves. On the left and right are the known states q_l and q_r. Across the elastic waves $\mathcal{W}^1$ and $\mathcal{W}^2$ there can be jumps in stress, strain and velocity. Since the left and right yield-stress thresholds are known we can calculate the solutions q_l^* and q_r^* via (6.10) above. We then calculate the jumps in stress and velocity across waves $\mathcal{W}^3$ and $\mathcal{W}^4$ via (6.18). Once the jumps in stress and velocity across all four waves have been calculated the jumps in strain and plastic-deformation across waves $\mathcal{W}^3$ and $\mathcal{W}^4$ can be calculated. Given the jumps in stress, strain, and velocity across $\mathcal{W}^3$ and $\mathcal{W}^4$ the plastic deformation in regions 3 and 4 can be found to complete the solution.

Once the proper stress and velocity in each cell is determined we can use them to find the strain and plastic deformation π_i. Given the initial plastic-deformation π_i, yield-stress σ_{yi} and elastic constant K_i, the strain at yield ϵ_{yi} in each cell can be determined by

$$\sigma_{yi} = \beta_i(\epsilon_{iy} - \pi_i) \implies \epsilon_{iy} = \pi_i + \sigma_{iy}/K_i. \tag{6.19}$$

See Figure 6.14. If the stress is greater then the yield-stress than the strain is determined by

$$\sigma = \sigma_y + \beta_p(\epsilon - \epsilon_y) \implies \epsilon = \epsilon_y + (1/\beta_p)(\sigma - \sigma_y). \tag{6.20}$$

Here β_p is the coefficient of plastic deformation. Once the new strain is known the new plastic deformation (across the plastic wave) is given as

$$\sigma = \beta(\epsilon - \pi) \implies \pi = \epsilon - \sigma/K. \tag{6.21}$$

Recall the solution procedure for the i'th Riemann problem. Given Q_{i-1} on the left and Q_i on the right we can solve for the two elastic waves as

$$\mathcal{W}^1_{i-1/2} = \alpha^1_{i-1/2}\begin{bmatrix} \rho_{i-1}K_{i-1} \\ 1 \end{bmatrix} \equiv \alpha^1_{i-1/2}r^1_{i-1}, \quad \text{and} \tag{6.22}$$

$$\mathcal{W}^2_{i-1/2} = \alpha^2_{i-1/2}\begin{bmatrix} -\rho_i K_i \\ 1 \end{bmatrix} \equiv \alpha^2_{i-1/2}r^2_i. \tag{6.23}$$

New values of Q_i are found by adding in the contributions of these waves as

$$Q_m = Q_{i-1} + \mathcal{W}^1_{i-1/2} \quad \text{or} \quad Q_m = Q_i - \mathcal{W}^2_{i-1/2}. \tag{6.24}$$

The new value of σ_{mi} in each cell is compared to the yield-stress threshold σ_{yi} in each cell. If $\sigma_{mi} < \sigma_{yi}$ then the solution is purely elastic and we can move to the next cell. However, if $\sigma_{mi} > \sigma_{yi}$ then the solution contains plastic behavior and we must compute plastic waves. Recall that the plastic waves are found by solving for the intersection of Hugoniot loci of the points q_r and q_l as shown in Figure 6.13 (a). In the elastic system all that was needed to define the waves for the Riemann solution was to find the eigenvalues and magnitudes of the eigenvectors of the matrix

$$A_i = \begin{bmatrix} 0 & \beta_i \\ 1/\rho_i & 0 \end{bmatrix}.$$

Now to define the waves for the elasto-plastic Riemann solution one needs to find the eigenvalues and magnitudes of the eigenvectors of following:

$$A_i = \begin{bmatrix} 0 & \beta_i \\ 1/\rho_i & 0 \end{bmatrix}, \quad \text{if} \quad \sigma_i < \sigma_{yi}$$

$$A_i = \begin{bmatrix} 0 & \beta_{p,i} \\ 1/\rho_i & 0 \end{bmatrix}, \quad \text{if} \quad \sigma \geq \sigma_{yi}.$$

To solve this we use the procedure described above to find the elastic waves $\mathcal{W}^1_{i-1/2}$ and $\mathcal{W}^2_{i-1/2}$. Figure 6.13 (a) shows $\mathcal{W}^1_{i-1/2}$ as the line between the left state q_l, and the yield-stress threshold for the left state at q_l^*. Similarly $\mathcal{W}^2_{i-1/2}$ is shown as the line between the right state q_r, and the yield-stress threshold for the right state at q_r^*.

6.2.3 Example of 1D Elasto-Plastic Riemann Solution

In order to test the solution procedure we set up an initial-value problem that gives rise to two elastic and two plastic waves. Wave speeds of the elastic waves are given by $\pm\sqrt{\beta/\rho}$ while wave speeds of the plastic waves are given by $\pm\sqrt{\beta_p/\rho}$. We set $\beta = 100$, $\beta_p = 1$, and $\rho = 1$. For these values of material constants we expect to have the elastic waves move at speed ± 10 and plastic waves to move at speed ± 1. The initial yield-stress threshold is set at $\sigma_y = 20$ so that there will be plastic waves at any point where we have a stress $\sigma > \sigma_y = 20$. In this example the domain is divided into two regions by an initial velocity that is positive on the right half and negative on the left half. Stress and strain are initialized at $\sigma = \epsilon = 0$. For a time of $t = .1$ the elastic waves move a distance of $d = 1.0$ and the plastic waves move a distance of $d = 0.1$. See Figure 6.15 for stress, velocity and strain at $t = 0.1$. Note that the elastic and plastic waves move at the appropriate speeds and that the elastic stress does not exceed the initial yield-stress threshold.

In Figure 6.15 one can see that across the elastic wave there is a small jump in strain while across the plastic wave there is a relatively large jump in the strain associated with a relatively small jump in the stress. Recall that in the region of plastic deformation the stress-strain relation changes from $\sigma = \beta\epsilon$ to $\sigma = \beta_p\epsilon$ where $\beta_p < \beta$. Once the strain forces the stress to exceed the yield-stress threshold, most of the remaining strain energy causes plastic deformation. In this example the initial velocity was set so that the plastic waves would cause a jump in π from the initial value of $\pi = 0$ to a value near $\pi = 8$.

One should also note the clear distinction between linear elastic behavior and linear elasto-plastic behavior. Each time the stress exceeds the current value of the elastic yield-stress threshold, the material response changes from elastic to plastic. As shown in Figure 6.14, each time there is a jump from elastic to plastic behavior there is a corresponding jump from one slope β to the next β_p. As described above, solution values in the elastic and elasto-plastic regimes that have small enough amplitude plastic deformation do not cause damage. However, if the plastic deformation exceeds a certain critical value, the material begins to undergo permanent irreversible damage. The inclusion of damage mechanics into the model will force a change in the solution procedure as damage affects the future elastic behavior.

6.3 Non-Linear Elasto-plasticity and Damage

While loading beyond the elastic yield-stress threshold causes plastic deformation, further loading beyond the damage yield-stress threshold σ_{yD} gives rise to damage. Damage can be thought of as a measure of the permanent debonding of the material from the level of atoms to the level of crack formation. While plastic deformation is a measure of molecular level slips within the material, and therefore reversible, damage is a measure of permanent debonding and is irreversible. If a material is damaged enough it will fail. At failure the material has been damaged as much as possible and we define $D = 1$ at failure. Assuming an undamaged material $D = 0$, loading beyond the damage yield-stress threshold causes an increase in both plastic deformation π and damage D until the point of failure at $D = 1$. In each grid cell we define $D(\pi)$ where $0 \leq D(\pi) \leq 1$. The relation between plastic movement and damage as well as solution procedures for this regime are discussed below.

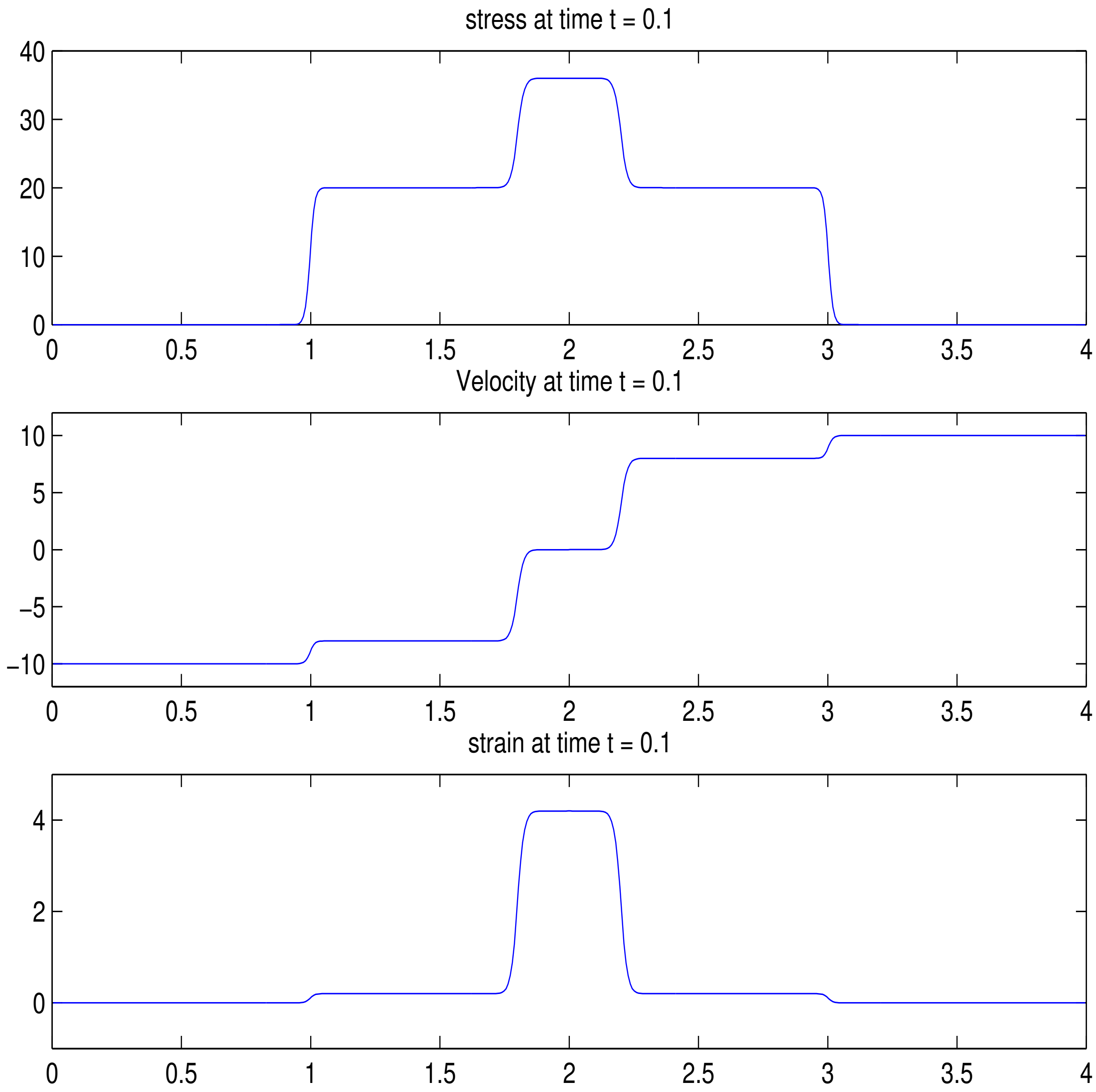

Figure 6.15: Stress Velocity and Strain at N=4000.

It is very important to note that in the following discussion we add two independent concepts to the previous model and develop a solution procedure that can solve examples that contain either or both of these ideas. As we discussed in the opening section of this chapter, one can consider adding both damage and non-linear plasticity to our elastic-plastic model. Figure 6.2 shows the elastic-plastic stress-strain relation with the inclusion of damage. One can see that increasing values of plastic deformation cause a decrease in the slope of the elastic response. This change in the elastic response is separate from the phenomenon of non-linear plasticity and can be considered separately. Figure 6.3 shows the elastic-plastic stress-strain curve with the inclusion of non-linear plasticity but no damage. Here one can see that once the stress exceeds the yield-stress, the relation between stress and strain is no longer linear. Rather then attack these added complication separately, in the remainder of this chapter we outline a solution procedure that can handle both of these additions to our previous elastic-plastic model.

As mentioned above, once the plastic deformation is large enough to cause damage the elastic stress-strain curve is reduced in slope to reflect the weakening of the material. Recall (6.1) and (6.2) as

$$\begin{aligned} \epsilon_t - v_x &= 0, \\ \rho(x)v_t - \sigma_x &= 0, \end{aligned} \tag{6.25}$$

where we have

$$\sigma = f(\epsilon). \tag{6.26}$$

When the solution is assumed to be linearly elastic or linearly elastic-plastic the constitutive relation (6.26) is defined as a linear or bilinear relationship,

$$\sigma = f(\epsilon) = \beta\epsilon \quad \text{or} \quad \beta_p\epsilon. \tag{6.27}$$

In previous sections we showed how to solve examples where a linear elasto-plastic stress-strain relationship was assumed. Throughout this section we assume that the elasto-plastic stress-strain relationship is non-linear and that damage occurs. Once the stress exceeds the yield-stress threshold, a linear relationship between stress σ and strain ϵ can no longer be specified. Also as a material is damaged, the damage changes how the material behaves under further loading. Since a damaged material can not withstand the same strains as an undamaged material the elastic and plastic stiffnesses of the material, β and β_p, must decrease with increased damage. Note that in this case π and $D(\pi)$ must be solved for simultaneously.

Damage is defined as a scalar-valued quantity such that $0 \leq D(\pi) \leq 1$, where D is determined by the current value of π as

$$D(\pi) = \frac{\pi - \pi_D}{\pi_r - \pi_D}. \tag{6.28}$$

Here π_r and π_D are material constants that must be determined. The value of plastic deformation where damage starts to occur is defined as π_D and the value of plastic deformation where failure occurs is defined as π_r. Figure (6.16) shows the relation between the onset of damage and the failure of the material at $\pi = \pi_r$, or $D(\pi) = 1$. See [24], and [32] for further details. For a damaged material, loading below the damage yield-stress threshold is given by the following relation:

$$(1 - D(\pi))\beta = \frac{\sigma}{(\epsilon - \pi)}. \tag{6.29}$$

Note that this is just the definition of the slope of the line between σ_{y2} and π_y shown in Figure (6.17). Loading above the damage yield-stress threshold is determined by the differential relation

$$\frac{d\sigma}{d\epsilon} = (1 - D(\pi))\beta_p. \tag{6.30}$$

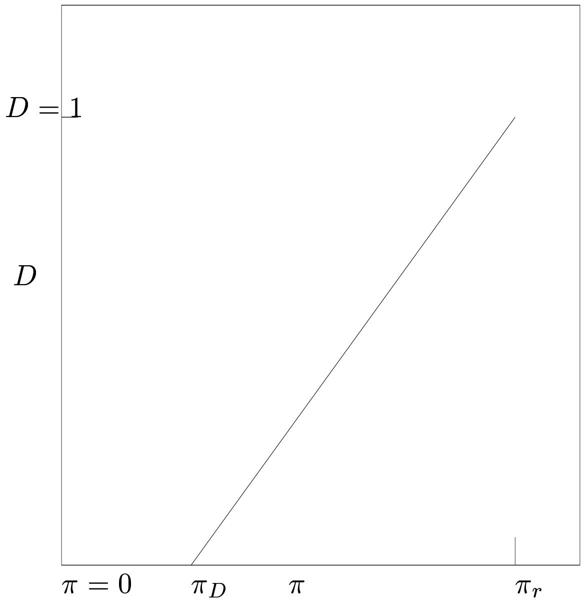

Figure 6.16: Relation between plastic dislocation, damage, and failure.

Figure (6.17) shows that for stress below the damage yield-stress threshold σ_D no damage occurs and the solution method above can be used for the system (6.1). If the stress exceeds σ_D then damage must be included and we solve the following system:

$$\begin{aligned} \epsilon_t - v_x \quad &= 0, \\ \rho(x)v_t - \sigma_x \quad &= 0. \end{aligned} \tag{6.31}$$

The system is closed by the following relations between the stress σ, strain ϵ, plastic movement π, and damage D as

$$(1 - D(\pi)) = \frac{\sigma}{\beta(\epsilon - \pi)}, \quad \sigma < \sigma_D, \tag{6.32}$$

$$\frac{d\sigma}{d\epsilon} = (1 - D(\pi))\beta_p, \quad \sigma > \sigma_D, \tag{6.33}$$

$$D(\pi) = \frac{\pi - \pi_D}{\pi_r - \pi_D}, \quad \pi > \pi_D. \tag{6.34}$$

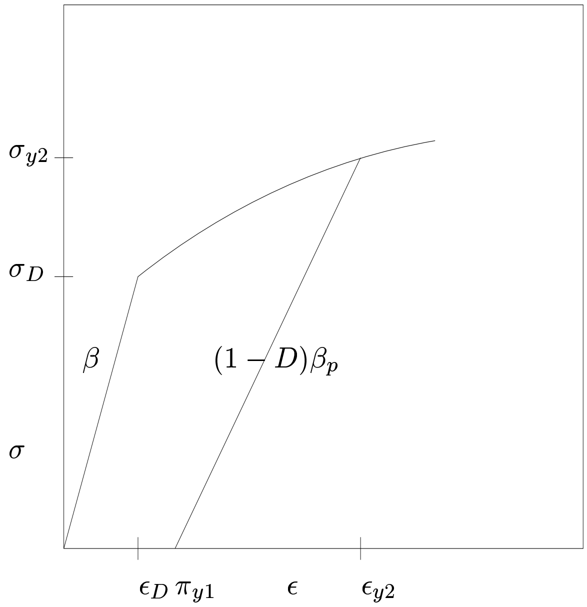

Figure 6.17: Elastic and Elasto-Plastic with Damage stress-stain curve. Note the change in Elastic Response slope after the material has been damaged by loading beyond σ_{y1}.

Here π_r, π_D, K, K_1, and ρ are known physical constants and σ, ϵ, v, π, and D are the five unknowns which must be solved for.

Although we have five equations and five unknowns, a solution procedure is not readily apparent from looking at equations (6.31)-(6.34). The equations (6.32)-(6.33) can be rewritten as

$$\sigma = (1 - D(\pi))\beta(\epsilon - \pi), \quad \text{for} \quad \sigma < \sigma_D \tag{6.35}$$

$$\frac{d\sigma}{d\epsilon} = (1 - D(\pi))\beta_p, \quad \text{for} \quad \sigma > \sigma_D. \tag{6.36}$$

In this form one can see that the elastic and plastic moduli are now dependent on the damage.

Equations (6.35) and (6.36) show that as the material is damaged the wave speeds are decreased. As waves causing damage move through the material, the information carried by the waves affects the material in such a way as to change the speed of the waves. While the linear (elastic) and bi-linear (elasto-plastic) Riemann solutions have predetermined wave speeds, the non-linear wave speeds are unknowns. To determine the wave speeds we use the Rankine-Hugoniot jump condition to write the wave speeds in terms of other solution variables.

The Rankine-Hugoniot jump condition applied to (6.31) with $\rho = 1$ give

$$s(v_r - v_l) = \sigma(\epsilon_r, \pi_r) - \sigma(\epsilon_l, \pi_l), \tag{6.37}$$

$$s(\epsilon_r - \epsilon_l) = (v_r - v_l). \tag{6.38}$$

We can solve (6.37) and (6.38) for the wave speeds $\pm s$ to find

$$s = \pm\sqrt{\frac{\sigma(\epsilon_l, \pi_l) - \sigma(\epsilon_r, \pi_r)}{\epsilon_r - \epsilon_l}}. \tag{6.39}$$

See [58] for details. Substitution of equation (6.39) into (6.38) gives the velocity to the right of a left-going shock as

$$v = v_l + \sqrt{(\sigma - \sigma_l)(\epsilon - \epsilon_l)}. \tag{6.40}$$

Similarly the velocity to the left of a right-going shock is found as

$$v = v_r - \sqrt{(\sigma_r - \sigma)(\epsilon_r - \epsilon)}. \tag{6.41}$$

Here v_r and v_l are the known velocities at the left and right states q_l^* and q_r^*. We can combine (6.40) and (6.41) with (6.34), (6.35), and (6.36), to get the following system of five equations and five unknowns:

$$\frac{d\sigma}{d\epsilon} = (1 - D)\beta_p, \quad \sigma > \sigma_D, \tag{6.42}$$

$$D = A\pi + B, \tag{6.43}$$

$$\sigma = (1 - D)\beta(\epsilon - \pi), \quad \sigma < \sigma_D, \tag{6.44}$$

$$v = v_l + \sqrt{(\sigma - \sigma_l)(\epsilon - \epsilon_l)}, \tag{6.45}$$

$$v = v_r - \sqrt{(\sigma_r - \sigma)(\epsilon_r - \epsilon)}. \tag{6.46}$$

Equation (6.42) defines the stress-strain relation for all stress such that $\sigma > \sigma_D$. We can solve (6.42), with (6.43) and initial condition $D(\pi = \pi_D) = 0$, via Newton's method to find a one-to-one relation between σ, ϵ, D, and π. If a material is deformed plastically such that $\pi > \pi_D$, then stress-strain values will move out along the curve defined by the solution of (6.42) and (6.43). Since the values of σ, ϵ, D, and π determined by solving system (6.42)-(6.43) are one-to-one and do not change over time, once (6.42)-(6.43) is solved it can be stored and need never be computed again (for a given material).

Figure (6.18) shows the transition from elastic behavior to elasto-plastic behavior with damage across the left and right yield-stress thresholds. To the left of both thresholds one can see the elastic waves of known strength. Recall that the elastic waves are found using the jump condition (3.7). The intersection of the two plastic waves q_m is found by solving the system (6.45)-(6.46). Note that once we have solved the system (6.42)-(6.43) then v_l, v_r, σ_l, σ_r, ϵ_l, and ϵ_r are all known at any point on the stress-strain curve shown in Figure

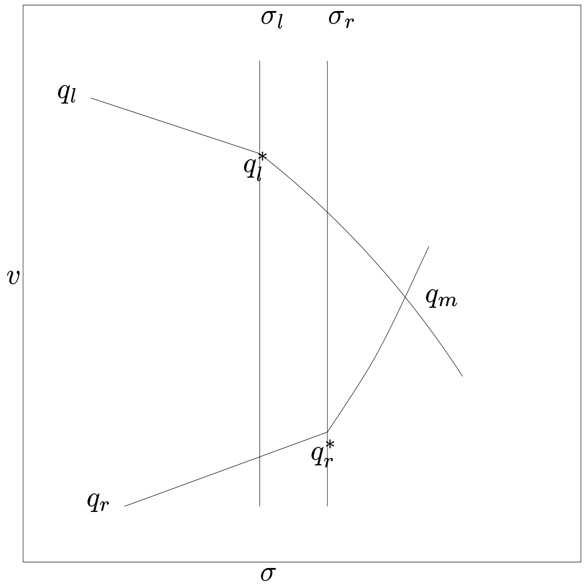

Figure 6.18: Example of Riemann Solution Structure for nonlinear elasto-plastic stress-strain relation in σ-v space.

(6.17). In particular these quantities are all known at the yield-stress threshold lines shown in Figure (6.18). One can eliminate v from the system (6.45)-(6.46) and use a root finding method to solve for σ and ϵ at q_m.

Once the values of σ, ϵ, and v are known at the solution state q_m, the differences between the values of these quantities at q_m and at the yield-stress thresholds can be used to determine the jumps across the plastic waves. Given the jumps in σ, ϵ, and v across the plastic waves we can determine the jumps in π and D via (6.43) and (6.44). One should note that this solution method is based on an approximate Riemann solution. We use the Rankine-Hugoniot jump condition to solve for rarefaction waves even though this condition is only strictly valid for shocks. As we will see in the next example, plastic waves resulting from a nonlinear stress-strain elasto-plastic relation turn out to be rarefactions.

Figure 6.19 shows the stress-strain relation used in the next example. We assume that initially the entire material has been pre-strained beyond its initial yield-point σ_{y1} up to the point σ_{y2}. Loading between σ_{y1} and σ_{y2} caused plastic deformation π and damage D at all points in the material. The material was then unloaded back to a state of zero stress along the curve shown with slope $(1-D)\beta$. This means that any further loading in the material must start from the point shown as A.

Figure 6.20 shows the initial values for stress, velocity, and strain for the example discussed above. The stress-strain relation and nonzero initial values of plastic deformation and damage for all cells in the material are shown in Figure 6.19. As shown in Figure 6.20, while the stress and strain are initially zero there is a jump in velocity at the center of the medium. Also Figure 6.21 shows that there exists a uniform nonzero plastic strain and a

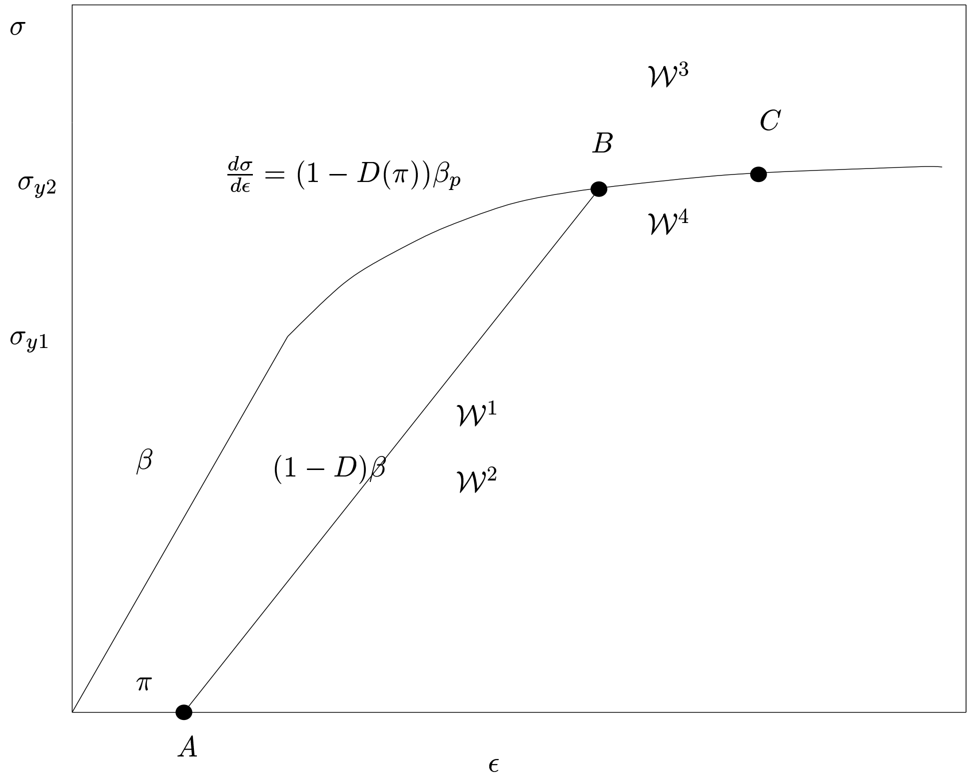

Figure 6.19: Linear Elastic and Nonlinear Elasto-Plastic Stress-Strain Curves for two neighboring cells with nonzero initial Plastic Deformation and Damage.

small amount of damage everywhere in the material. Initially all states q in this example project to the point A in Figure 6.19. The velocity difference is chosen to be large enough that both elastic and plastic waves will form and the mid-state q_m will lie at the point C in Figure 6.19. The jump in velocity shown in Figure 6.21 will cause an elastic response up to the point B followed by a plastic response with damage up to the point C in Figure 6.19. The two elastic and two plastic waves are shown in stress-strain space in Figure 6.19.

Figure 6.3 shows how these four waves evolve after a short time. As expected the two elastic waves are jump discontinuities that travel at the speed $c_E = \sqrt{(1-D)\beta/\rho}$. The two plastic waves are rarefactions that move at the speed $c_P = \sqrt{(1-D)\beta_p/\rho}$. All four waves are also shown in Figure 6.19. Here one can see that the sound-speed of any given elastic wave is a constant since D does not change during elastic response. Conversely the sound-speed of a plastic wave decreases while moving from point B to point C since the value of D increases across a plastic wave, leading to a rarefaction wave.

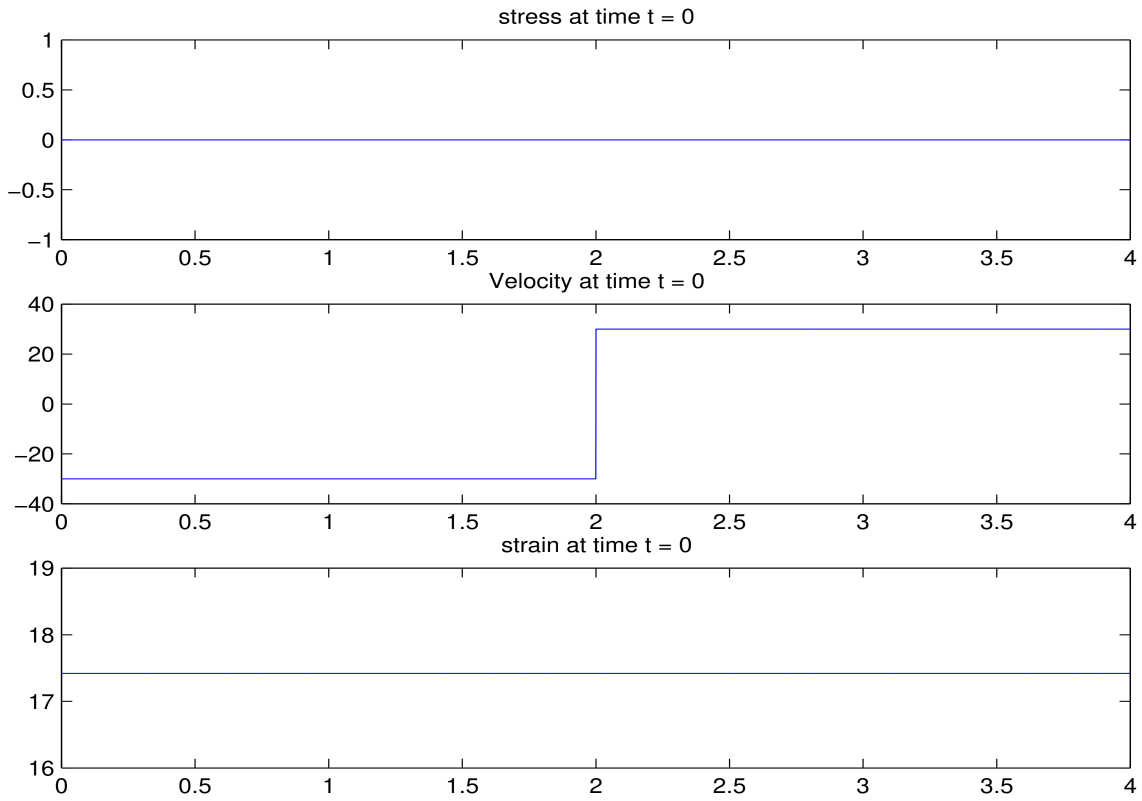

Figure 6.20: Initial Stress, Velocity, and Strain N=4000.

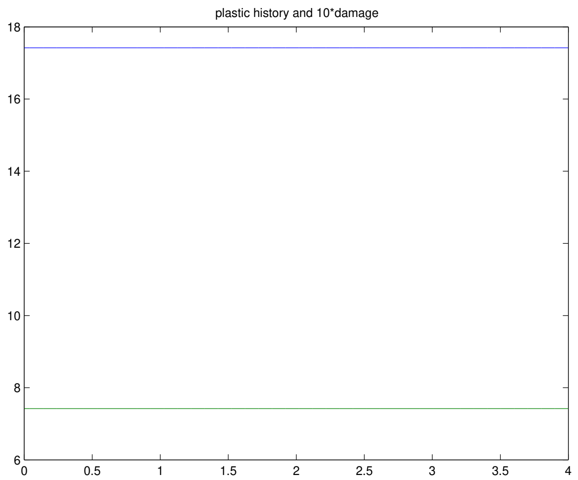

Figure 6.21: Top: 10×Damage. Bottom: Plastic Deformation, N=4000.

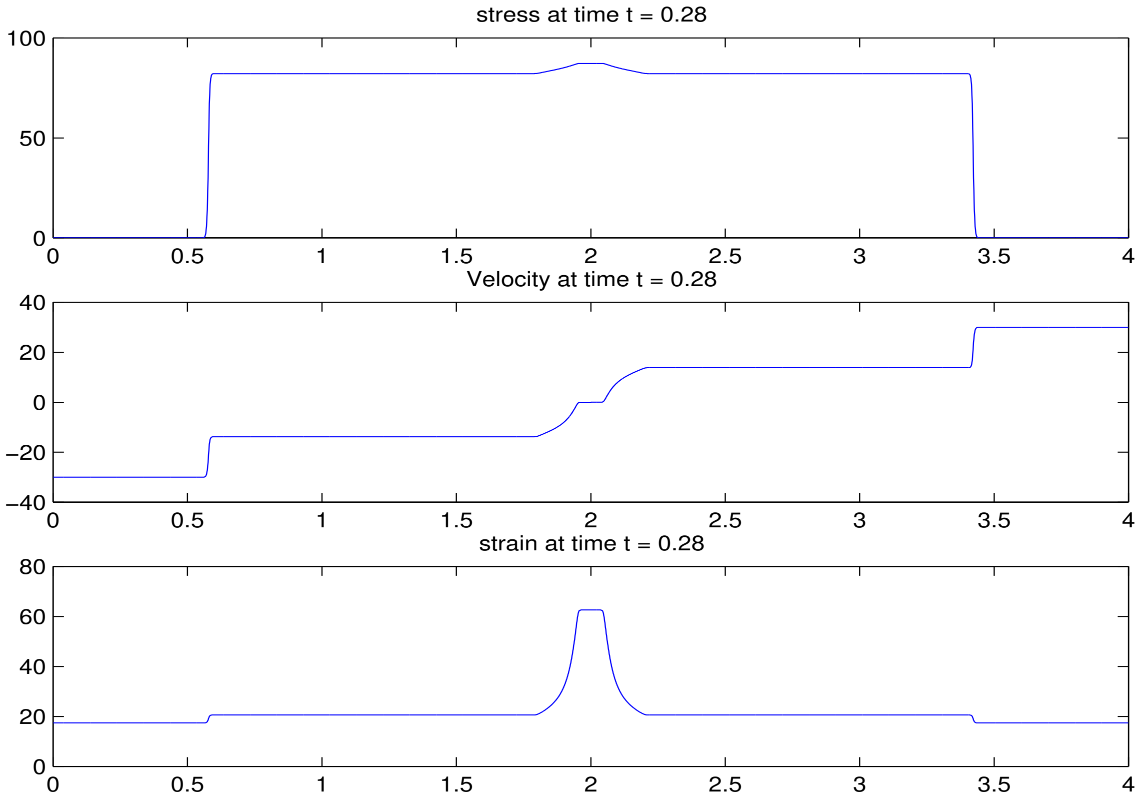

Figure 6.22: Stress, Velocity, and Strain N=4000 at t=0.28.

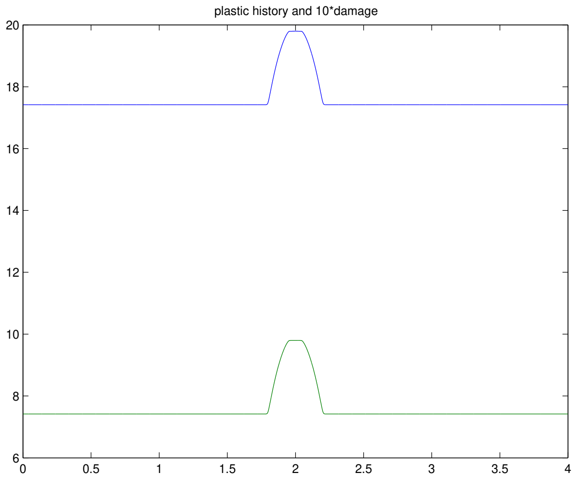

Figure 6.23: Top: 10×Damage. Bottom: Plastic Deformation, N=4000.

6.4 Solution via Minimization

In the previous sections we have shown that the 1D problem is straight forward enough to solve exactly via a Riemann solution approach. Two (and three) dimensions is where the real problems of interest lie and extension of the above techniques to 2D and higher is unclear at best. Instead of attempting to derive a 2D elasto-plastic Riemann solution we use minimization techniques to solve for the solution outside of the elastic range. In one dimension, we know that the solutions obtained via the Riemann formulation are correct and and can be used as a check to make sure that solutions obtained by minimization are also correct. While extension of the Riemann solution method to 2D is unclear, extension of minimization techniques from 1D to 2D and even 3D should not prove as difficult.

In 2D elasto-plasticity the boundary between elastic and plastic response is a 3D yield-surface defined in stress space. Updating the state variables by solving the elastic system via standard Riemann solution techniques gives new stress values. A yield condition is then used to check whether the new stress values are inside or outside of the current yield surface. If the new stress is within the yield surface then the elastic update is correct and no more needs to be done. If the stress is outside the yield surface then the elastic update is incorrect and we must solve for the proper state variables and the new yield surface.

In the following sections we will introduce the two main tools needed to formulate a solution via minimization: the **yield criterion** and the **energy function**. We will show how to derive the yield criterion and the energy function for the three dimensional case as well as the 2D plane-strain and plane-stress cases and their 1D reductions. We then use the 1D plane-stress system given by (6.6) to illustrate the connection between the solutions obtained via minimization and those obtained via our Riemann solution. We end the chapter with several examples of 1D elasto-plastic behavior in different types of heterogeneous material.

In one dimension the point at which material response to strain changes from elastic to plastic is the yield point. In two or three dimensions the set of points at which material response to strain changes from elastic to plastic is described by a yield surface in σ space. Recall that in the 1D linear elastic systems given by (2.33) and (2.35), the stress is represented as a scaler while in two or three dimensions the stress is represented as a tensor. Figure 6.5 shows that a material with zero initial plastic strain the yield criterion is the initial yield point σ_y. For positive values of stress, Figure 6.5 shows that initially the yield criterion is

$$F(\sigma, \pi) = \sigma - \sigma_y = 0 \quad \text{where} \quad \pi = 0. \tag{6.47}$$

Here a material with zero plastic deformation will respond elastically so long as $F(\sigma, \pi) < 0$ while the material will respond plastically for values of stress such that $F(\sigma, \pi) \geq 0$. Note that $F(\sigma, \pi) > 0$ can never happen. As soon as the stress is large enough so that $F(\sigma, \pi) = 0$, two things happen: plastic deformation starts to occur, and σ and π change in such a way so that that $F(\sigma, \pi) = 0$ is always maintained.

Recall Figure 6.5. Here we see that the first value of stress for which $F(\sigma) = 0$ is at $\sigma = \sigma_{y1}$. As the stress continues to grow beyond σ_{y1} we move up along the plastic part of the stress-strain relation while simultaneously defining new yield-stress and plastic deformation values. The new values of yield-stress and plastic deformation are incorporated into $F(\sigma)$

so that any time the material is deforming plastically (or at yield) $F(\sigma) = 0$ is always satisfied. Figure 6.5 also shows that after the material has been plastically deformed the point at which material response changes from elastic to plastic is dependent on the amount of plastic dislocation π. This means that for loading beyond σ_y the yield criterion must be written as

$$F(\sigma) = \sigma - (\sigma_y + E_1\pi) = 0. \tag{6.48}$$

Here we can see that (6.47) is the special case of (6.48) where $\pi = 0$. In the following section we show how this one-dimensional yield condition is a special case of the general 3-D Maxwell-Huber-von Mises criterion. See [23], [9], and [10] for details.

6.4.1 Yield Criterion

Recall that in three dimensions stress is represented by six independent components. Any stress state in the six-dimensional stress-space can be represented by a combination of these six stress components. Stress space is divided into two parts by the yield surface. States that lie in the elastic region of stress space are in the interior of the yield surface while states at the yield-surface undergo plastic deformation while re-defining the yield surface. It may help to consider an inflated balloon where the surface of the balloon represents the yield-surface in stress space. All stress states which are the result of elastic response lie inside the balloon without touching the (interior) surface. States which are the result of plastic response lie on or outside the surface of the balloon. However, in moving from the elastic to the plastic region the stress state can not pass through the surface of balloon. Consider an object inside the balloon which tries to move outside. The balloon will stretch to some new configuration. Hence plastic response moves the initial surface to some exterior position while at the same time stretching or re-defining the surface configuration of the balloon. With this in mind, the stress response to strain must be either elastic and interior to the yield-surface or plastic and at yield. Recall that this is just an extension of the 1D example. In 1D the elastic response to strain moves up the elastic curve until the initial yield-point, after which the response to strain moves out along the plastic curve while at the same time re-defining the (new) yield-strain.

In three dimensions the Cauchy stress tensor σ is given as

$$\sigma = \begin{bmatrix} \sigma_{11} & \sigma_{12} & \sigma_{13} \\ \sigma_{21} & \sigma_{22} & \sigma_{23} \\ \sigma_{31} & \sigma_{32} & \sigma_{33} \end{bmatrix}. \tag{6.49}$$

For metallic materials one can assume that the hydrostatic pressure has no effect on plastic yielding and can be removed from any yield criterion. In this work we have assumed that the yield criterion is independent of the hydrostatic pressure and only dependent on the deviatoric stress tensor S. We decompose the Cauchy stress tensor into two parts,

$$\sigma_{ij} = p\delta_{ij} + S_{ij}. \tag{6.50}$$

Here p is the hydrostatic stress (pressure), given as

$$p = \frac{1}{3}(\sigma_{11} + \sigma_{22} + \sigma_{33}), \tag{6.51}$$

and S_{ij} is the 3-D deviatoric stress tensor, given as

$$S_{ij} = \sigma_{ij} - p\delta_{ij}. \tag{6.52}$$

$$\mathbf{S_3} = \begin{bmatrix} \sigma_{11} - \frac{1}{3}(\sigma_{11} + \sigma_{22} + \sigma_{33}) & \sigma_{12} & \sigma_{13} \\ \sigma_{21} & \sigma_{22} - \frac{1}{3}(\sigma_{11} + \sigma_{22} + \sigma_{33}) & \sigma_{23} \\ \sigma_{31} & \sigma_{32} & \sigma_{33} - \frac{1}{3}(\sigma_{11} + \sigma_{22} + \sigma_{33}) \end{bmatrix}. \tag{6.53}$$

To determine if a material is behaving elastically or plastically we need a Yield criterion. The basic assumption in plasticity is that for any point in the material that has a stress-state which satisfies the yield criterion, the material will deform plastically; otherwise the material deforms elastically. If we ignore thermal effects we can write the yield function as

$$F(\sigma_{ij}) = 0. \tag{6.54}$$

with

$$F(\sigma_{ij}) < 0 \qquad \text{for elastic deformation domain} \tag{6.55}$$

$$F(\sigma_{ij}) = 0 \qquad \text{on the yield surface.} \tag{6.56}$$

Recall that we have assumed plastic yielding is only related to the deviatoric stress tensor S and that hydrostatic pressure has no effect on plastic yielding. The Maxwell-Huber-von Mises Criterion assumes that plastic yielding will only occur when the second invariant of the deviatoric stress tensor reaches a critical value which is a material property. In 3-D the yield criterion takes the form

$$\frac{3}{2}S_{ij}S_{ij} = \sigma_{11}^2 - \sigma_{11}\sigma_{22} - \sigma_{11}\sigma_{33} + \sigma_{22}^2 - \sigma_{22}\sigma_{33} + \sigma_{33}^2 + 3\sigma_{12}^2 + 3\sigma_{23}^2 + 3\sigma_{13}^2 = \alpha^2 \tag{6.57}$$

Assuming that α^2 can be measured for a given material the yield function is given as

$$F(\sigma_{ij}) = \sigma_{11}^2 - \sigma_{11}\sigma_{22} - \sigma_{11}\sigma_{33} + \sigma_{22}^2 - \sigma_{22}\sigma_{33} + \sigma_{33}^2 + 3\sigma_{12}^2 + 3\sigma_{23}^2 + 3\sigma_{13}^2 - \alpha^2. \tag{6.58}$$

Plane-Stress Yield Criterion

In two dimensions one must decide to investigate either the **plane-stress** problem or the **plane-strain** problem. First we consider plane stress which assumes that all non-zero stresses lie in the 2-D plane of interest. For the plane-stress problem this means that the 2-D deviatoric stress tensor takes the form

$$\mathbf{S_2} = \begin{bmatrix} \sigma_{11} - \frac{1}{3}(\sigma_{11} + \sigma_{22}) & \sigma_{12} & 0 \\ \sigma_{21} & \sigma_{22} - \frac{1}{3}(\sigma_{11} + \sigma_{22}) & 0 \\ 0 & 0 & -\frac{1}{3}(\sigma_{11} + \sigma_{22}) \end{bmatrix}. \tag{6.59}$$

Note that even though the stresses outside of the plane are all zero the strains and associated velocities will not be zero in general but are still outside the scope of interest in the model.

With S_2 given above, the plane-stress yield condition reduces to

$$\sigma_{11}^2 - \sigma_{11}\sigma_{22} + \sigma_{22}^2 + 3\sigma_{12}^2 = \alpha^2. \tag{6.60}$$

Here we assume that α takes the form

$$\alpha = (\sigma_y + \beta_p \pi), \tag{6.61}$$

where σ_y is the initial yield stress of the material, π is the plastic strain, and E_1 is the slope of the plastic stress-strain relationship. This gives the 2-D plane-stress plastic yield condition as

$$\sqrt{\sigma_{11}^2 - \sigma_{11}\sigma_{22} + \sigma_{22}^2 + 3\sigma_{12}^2} - (\sigma_y + \beta_p \pi) = 0. \tag{6.62}$$

where σ_y and E_1 are material constants.

If we make the reduction from plane-stress with only σ_{11} nonzero then the deviatoric stress tensor is given by

$$\mathbf{S_1} = \begin{bmatrix} \sigma_{11} - \frac{1}{3}(\sigma_{11}) & 0 & 0 \\ 0 & -\frac{1}{3}(\sigma_{11}) & 0 \\ 0 & 0 & -\frac{1}{3}(\sigma_{11}) \end{bmatrix}. \tag{6.63}$$

This gives the yield condition for the 1D system (2.35) as

$$\sqrt{\sigma_{11}^2} - (\sigma_y + \beta_p \pi) = 0. \tag{6.64}$$

Plane-Strain Yield Criterion

Recall that for the plane-strain case it is assumed that strain only exists in the plane, which gives a non-zero stress $\sigma_{33} = \frac{\lambda}{2(\lambda+\mu)}(\sigma_{11} + \sigma_{22})$. This alters the 2-D deviatoric stress tensor to

$$\mathbf{S} = \begin{bmatrix} \frac{\sigma_{11}(4\mu+3\lambda)-\sigma_{22}(2\mu+3\lambda)}{6(\mu+\lambda)} & \sigma_{12} & 0 \\ \sigma_{21} & \frac{\sigma_{22}(4\mu+3\lambda)-\sigma_{11}(2\mu+3\lambda)}{6(\mu+\lambda)} & 0 \\ 0 & 0 & -\frac{\mu(\sigma_{11}+\sigma_{22})}{3(\mu+\lambda)} \end{bmatrix}. \tag{6.65}$$

With $\mathbf{S_2}$ given above we find that the plane-strain yield condition is given as

$$\sqrt{\frac{(\sigma_{11}^2 + \sigma_{22}^2)(3\lambda^2 + 6\lambda\mu + 4\mu^2) - 2\sigma_{11}\sigma_{22}(3\lambda^2 + 6\lambda\mu + 2\mu^2) + 12\sigma_{12}^2(\lambda^2 + 2\lambda\mu + \mu^2)}{4(\lambda+\mu)^2}} \\ -(\sigma_y + \beta_p \pi) = 0. \tag{6.66}$$

Recall that the system which models the one dimensional reduction from plane-strain is given by (2.33). If we make the similar reduction on the yield criterion the stresses must satisfy $\sigma_{33} = \sigma_{22} = \frac{\lambda}{\lambda+2\mu}\sigma_{11}$, which puts $\mathbf{S}$ in the form

$$\mathbf{S} = \begin{bmatrix} \frac{4\mu\sigma_{11}}{3\lambda+2\mu} & \sigma_{12} & 0 \\ \sigma_{12} & -\frac{2\mu\sigma_{11}}{3\lambda+2\mu} & 0 \\ 0 & 0 & -\frac{2\mu\sigma_{11}}{3\lambda+2\mu}. \end{bmatrix}. \tag{6.67}$$

This gives the yield condition for the 1D system given in (2.33) as

$$\sqrt{\frac{4\mu^2\sigma_{11}^2}{(\lambda+2\mu)^2}} - (\sigma_y + \beta_p \pi) = 0. \tag{6.68}$$

6.4.2 Energy Function

To solve elasto-plasticity via minimization techniques we need to minimize the energy subject to the constraint functions (yield criterion) described above. The energy function we want to minimize takes the form,

$$\xi(\sigma,\pi)=\frac{1}{2}(\sigma-\sigma^T)(\epsilon-\epsilon^T)+\frac{1}{2}\beta_p(\pi-\pi^T)^2. \tag{6.69}$$

See [19] for details. Here σ^T, ϵ^T, and π^T are trial guesses at the solution values. Recall that the constitutive relation is given as

$$\begin{bmatrix}\sigma_{11}\\\sigma_{22}\\\sigma_{33}\\\sigma_{12}\\\sigma_{23}\\\sigma_{13}\end{bmatrix}=\begin{bmatrix}\lambda+2\mu & \lambda & \lambda & 0 & 0 & 0\\ \lambda & \lambda+2\mu & \lambda & 0 & 0 & 0\\ \lambda & \lambda & \lambda+2\mu & 0 & 0 & 0\\ 0 & 0 & 0 & 2\mu & 0 & 0\\ 0 & 0 & 0 & 0 & 2\mu & 0\\ 0 & 0 & 0 & 0 & 0 & 2\mu\end{bmatrix}\begin{bmatrix}\epsilon_{11}\\\epsilon_{22}\\\epsilon_{33}\\\epsilon_{12}\\\epsilon_{23}\\\epsilon_{13}\end{bmatrix}. \tag{6.70}$$

If we define Σ_3 as the vector of stresses, Ψ_3 as the vector of strains, and C_3 as the matrix of elastic constants, then (6.70) can be written as

$$\Sigma_3=C_3\Psi_3. \tag{6.71}$$

Equation (6.71) can be inverted to give

$$\Psi_3=C_3^{-1}\Sigma_3. \tag{6.72}$$

Here we write the strain in terms of the stress to find the inverse matrix and we find that

$$\begin{bmatrix}\epsilon_{11}\\\epsilon_{22}\\\epsilon_{33}\\\epsilon_{12}\\\epsilon_{23}\\\epsilon_{13}\end{bmatrix}=\begin{bmatrix}\frac{\lambda+\mu}{\mu(3\lambda+2\mu)} & \frac{-\lambda}{2\mu(3\lambda+2\mu)} & \frac{-\lambda}{2\mu(3\lambda+2\mu)} & 0 & 0 & 0\\ \frac{-\lambda}{2\mu(3\lambda+2\mu)} & \frac{\lambda+\mu}{\mu(3\lambda+2\mu)} & \frac{-\lambda}{2\mu(3\lambda+2\mu)} & 0 & 0 & 0\\ \frac{-\lambda}{2\mu(3\lambda+2\mu)} & \frac{-\lambda}{2\mu(3\lambda+2\mu)} & \frac{\lambda+\mu}{\mu(3\lambda+2\mu)} & 0 & 0 & 0\\ 0 & 0 & 0 & \frac{1}{2\mu} & 0 & 0\\ 0 & 0 & 0 & 0 & \frac{1}{2\mu} & 0\\ 0 & 0 & 0 & 0 & 0 & \frac{1}{2\mu}\end{bmatrix}\begin{bmatrix}\sigma_{11}\\\sigma_{22}\\\sigma_{33}\\\sigma_{12}\\\sigma_{23}\\\sigma_{13}\end{bmatrix}. \tag{6.73}$$

Rather then write out the 3-D energy function completely, we write out the necessary matrices and how they are combined. See Section 6.5 for a detailed explanation of trial functions.

The vector of six stress components Σ_3 and their associated trial functions is given by

$$\Sigma_{3T}=\begin{bmatrix}(\sigma_{11}-\sigma_{11}^T)\\(\sigma_{22}-\sigma_{22}^T)\\(\sigma_{33}-\sigma_{33}^T)\\(\sigma_{12}-\sigma_{12}^T)\\(\sigma_{23}-\sigma_{23}^T)\\(\sigma_{13}-\sigma_{13}^T)\end{bmatrix}. \tag{6.74}$$

With this notation the 3-D energy function takes the form

$$\xi(\sigma,\pi) = \frac{1}{2}\Sigma_{3T}^t C_3^{-1}\Sigma_{3T} + \frac{1}{2}\beta_p(\pi-\pi^T)^2. \tag{6.75}$$

Note that T signifies the trial value and t means matrix or vector transpose.

Plane-Stress Energy Function

Recall that in the 2-D plane-stress problem all stresses that have a subscript 3 are zero, so we can write equation (6.75) as

$$\xi(\sigma,\pi) = \frac{1}{2}\Sigma_{2T}^t C_2^{-1}\Sigma_{2T} + \frac{1}{2}\beta_p(\pi-\pi^T)^2. \tag{6.76}$$

Here Σ_{2T}^t takes the form

$$\Sigma_{2T}^t = \left[\ (\sigma_{11}-\sigma_{11}^T) \quad (\sigma_{22}-\sigma_{22}^T) \quad 0 \quad (\sigma_{12}-\sigma_{12}^T)\ \right] \tag{6.77}$$

Similarly C_2^{-1} is written as

$$C_2^{-1} = \begin{bmatrix} \frac{\lambda+\mu}{\mu(3\lambda+2\mu)} & \frac{-\lambda}{2\mu(3\lambda+2\mu)} & \frac{-\lambda}{2\mu(3\lambda+2\mu)} & 0 \\ \frac{-\lambda}{2\mu(3\lambda+2\mu)} & \frac{\lambda+\mu}{\mu(3\lambda+2\mu)} & \frac{-\lambda}{2\mu(3\lambda+2\mu)} & 0 \\ \frac{-\lambda}{2\mu(3\lambda+2\mu)} & \frac{-\lambda}{2\mu(3\lambda+2\mu)} & \frac{\lambda+\mu}{\mu(3\lambda+2\mu)} & 0 \\ 0 & 0 & 0 & \frac{1}{2\mu} \end{bmatrix} \tag{6.78}$$

Equation (6.76) can be simplified to find

$$\begin{aligned} \xi(\sigma,\pi) = {} & [2(\lambda+\mu)(\sigma_{11}-\sigma_{11}^T)^2 - 2\lambda(\sigma_{11}-\sigma_{11}^T)(\sigma_{22}-\sigma_{22}^T) + 2(\lambda+\mu)(\sigma_{22}-\sigma_{22}^T)^2 \\ & + (3\lambda+2\mu)(\sigma_{12}-\sigma_{12}^T)^2]/4\mu(3\lambda+2\mu) + \frac{1}{2}\beta_p(\pi-\pi^T)^2. \end{aligned} \tag{6.79}$$

We combine equations (6.62) and (6.79) to get the 2-D plane-stress minimization problem. Here the energy function (6.79) must be minimized subject to the yield criteria constraint

$$\sqrt{\sigma_{11}^2 - \sigma_{11}\sigma_{22} + \sigma_{22}^2 + 3\sigma_{12}^2} - (\sigma_y + E_1\pi) = 0. \tag{6.80}$$

This is a nonlinear minimization problem of four variables with a nonlinear constraint.

We reduce the plane-stress energy function to 1D by the further assumption that all stresses with subscript 2 in equation (6.79) are zero. This gives the 1D energy function for the system given by (2.35) as

$$\xi(\sigma,\pi) = \frac{(\lambda+\mu)(\sigma_{11}-\sigma_{11}^T)^2}{2\mu(3\lambda+2\mu)} + \frac{1}{2}\beta_p(\pi-\pi^T)^2. \tag{6.81}$$

Similarly we can combine equations (6.64) and (6.81) to find the 1D minimization problem for the system given in (2.35). Here we find a nonlinear minimization problem of two variables

$$\xi(\sigma,\pi) = \frac{(\lambda+\mu)(\sigma_{11}-\sigma_{11}^T)^2}{\mu(3\lambda+2\mu)} + \frac{1}{2}\beta_p(\pi-\pi^T)^2, \tag{6.82}$$

where the 1D energy function above must be minimized subject to the constraint given by the 1D yield criterion

$$\sqrt{\sigma_{11}^2} - (\sigma_y + E_1\pi) = 0. \tag{6.83}$$

Plane-Strain Energy Function

As with the plane-stress energy function we start with the energy function that needs to be minimized, which is

$$\xi(\sigma,\pi) = \frac{1}{2}\Sigma_{2T}^t C_2^{-1}\Sigma_{2T} + \frac{1}{2}E_1(\pi - \pi^T)^2. \tag{6.84}$$

In the case of plain-strain it is no longer true that $\sigma_{33} = 0$. Instead Σ_{2T}^t takes the form

$$\Sigma_{2T}^t = \left[\ (\sigma_{11} - \sigma_{11}^T) \quad (\sigma_{22} - \sigma_{22}^T) \quad (\sigma_{33} - \sigma_{33}^T) \quad (\sigma_{12} - \sigma_{12}^T)\ \right] \tag{6.85}$$

Recall that in the case of plane-strain $\sigma_{33} = \frac{\lambda}{2(\lambda+\mu)}(\sigma_{11} + \sigma_{22})$. C_2^{-1} remains unchanged and is written as

$$C_2^{-1} = \begin{bmatrix} \frac{\lambda+\mu}{\mu(3\lambda+2\mu)} & \frac{-\lambda}{2\mu(3\lambda+2\mu)} & \frac{-\lambda}{2\mu(3\lambda+2\mu)} & 0 \\ \frac{-\lambda}{2\mu(3\lambda+2\mu)} & \frac{\lambda+\mu}{\mu(3\lambda+2\mu)} & \frac{-\lambda}{2\mu(3\lambda+2\mu)} & 0 \\ \frac{-\lambda}{2\mu(3\lambda+2\mu)} & \frac{-\lambda}{2\mu(3\lambda+2\mu)} & \frac{\lambda+\mu}{\mu(3\lambda+2\mu)} & 0 \\ 0 & 0 & 0 & \frac{1}{2\mu} \end{bmatrix} \tag{6.86}$$

This leads to a simplified 2-D plane-strain energy function in the form

$$\begin{aligned}\xi(\sigma,\pi) = [(\lambda+2\mu)((\sigma_{11} - \sigma_{11}^T)^2 + (\sigma_{22} - \sigma_{22}^T)^2) - 2\lambda(\sigma_{11} - \sigma_{11}^T)(\sigma_{22} - \sigma_{22}^T) \\ +2(\lambda+\mu)(\sigma_{12} - \sigma_{12}^T)^2]/8\mu(\lambda+\mu) + \frac{1}{2}\beta_p(\pi - \pi^T)^2.\end{aligned} \tag{6.87}$$

As in the plane-stress case we must minimize (6.87) subject to the plane-strain yield condition

$$\sqrt{\frac{(\sigma_{11}^2 + \sigma_{22}^2)(3\lambda^2 + 6\lambda\mu + 4\mu^2) - 2\sigma_{11}\sigma_{22}(3\lambda^2 + 6\lambda\mu + 2\mu^2) + 12\sigma_{12}^2(\lambda^2 + 2\lambda\mu + \mu^2)}{4(\lambda+\mu)^2}} \\ -(\sigma_y + \beta_p\pi) = 0. \tag{6.88}$$

The plane-strain yield condition can be reduced to one dimension with the assumption that $\sigma_{22} = \sigma_{33} = \frac{\lambda}{\lambda+2\mu}\sigma_{11}$. This gives the 1D energy function for the system given by (2.33) as

$$\xi(\sigma,\pi) = \frac{(\sigma_{11} - \sigma_{11}^T)^2}{2(\lambda+2\mu)} + \frac{1}{2}\beta_p(\pi - \pi^T)^2. \tag{6.89}$$

As in the previous example, (6.89) must be minimized subject to the yield condition

$$\sqrt{\frac{4\mu^2\sigma_{11}^2}{(\lambda+2\mu)^2}} - (\sigma_y + \beta_p\pi) = 0. \tag{6.90}$$

Above we have explained how to computationally solve elasto-plastic problems via minimization techniques. Previously, in Section 6.2 we explained how to solve the same problems via Riemann solution techniques. In the following section we show how these two approaches are related and how they differ from each other both conceptually and algorithmically.

6.5 Connection between Riemann Solution and Minimization

In previous sections we have shown how to numerically solve 1D elasto-plastic problems via Riemann solution and minimization techniques. We now show in 1D why the two methods give nearly identical results and how they are related. Recall that in the Riemann solution approach the basic cell-wise algorithm has the following two steps: solve elasto-plastic Riemann problems at the left and right edges to find the elastic and plastic waves which will be used to update the cell, update the state variables by averaging the old cell value with the values found by solving the elasto-plastic Riemann problems at cell edges. Solving via minimization is a way to implement numerically what are known as projection or return mapping methods. The basic premise of projection methods is that the final plastic solution can be found by the following series of steps: solve elastic Riemann problems at the left and right edges to find the purely elastic waves ignoring the possibility of plasticity. These waves are used to update the cell and find a trial state. We then check this trial state against the cell's yield condition. If the stress is not above yield we are done. If trial state stress exceeds the yield condition then we must project back to a final state which satisfies the (new) yield condition while minimizing the free energy. Recall that the 1d reduction from plane-stress has an energy function given by

$$\xi(\sigma,\pi) = \frac{(\lambda+\mu)(\sigma_{11}-\sigma_{11}^T)^2}{\mu(3\lambda+2\mu)} + \frac{1}{2}\beta_p(\pi-\pi^T)^2. \tag{6.91}$$

Here the energy function must be minimized subject to the yield-criterion constraint given as

$$\sqrt{\sigma_{11}^2} - (\sigma_y + E_1\pi) = 0. \tag{6.92}$$

Note that Figure 6.26 and Figure 6.27 are drawn in both x-t space to show elastic and plastic wave propagation and σ-t space to show stress values associated with Riemann problems.

The numerical solution to the minimization problem is implemented by first solving purely elastic Riemann problems between each cell and then using a black-box solver to ensure that the cell-averaged stress updates to the cells are either below or at yield. Once these Riemann problems have been solved and the cell-wise averages computed, the new values are checked against the yield-criterion given above. If the yield-criterion is violated then the cell-wise values of stress and plastic deformation are sent as trial functions to a minimization package capable of solving problems which are non-linear and have non-linear constraints. As our wave propagation solver is in Fortran we currently we use NAG routines to facilitate the minimization.

As we will show below, the primary difference between these two methods is that the Riemann solution approach finds the plastic and elastic jumps at each interface and then averages these states to find a final state which is either below or at plastic yield. Unlike the Riemann approach, projection methods only find the elastic jumps at each interface to find a new cell averaged value which is may be below, at, or above the plastic yield. If the new value is above the yield then a procedure is used to "project" back to find a final solution that is at the plastic yield. To illustrate exactly how these methods differ we must first recall exactly how the Riemann solution method works and then compare it with how the projection solution method works.

Figure 6.24 shows how to compute the solution of a given elastic-plastic Riemann problem. Recall that the left state q_l is connected to the state q_l^* via an elastic 1-wave $\mathcal{W}^1$ while the right state q_r is connected to the state q_r^* via an elastic 2-wave $\mathcal{W}^2$. Also recall that since the yield-stresses σ_{yl} and σ_{yr} are known, the states q_l^* and q_r^* can be found and then used as the new starting left and right states in the plastic Riemann problem with solution q_m. The solution state q_m is connected to the state q_l^* via the plastic wave $\mathcal{W}^3$ and connected to the state q_r^* via the plastic wave $\mathcal{W}^4$. Figure 6.26 shows all these states and waves for the elasto-plastic Riemann problems at both the left and right cell edges of the i'th cell. Here one can see the initial stress values in the states q_{i-1}^n, q_i^n, and q_{i+1}^n along with the elastic and plastic waves at each cell interface.

In the example shown in Figure 6.26, the Riemann solution shown at the left $(i-1/2)$ interface has two elastic and two plastic waves while the Riemann solution shown at the right $(i+1/2)$ interface has two elastic and one plastic wave. The pair of states q_{i-1}^n and q_i^n in Figure 6.26 correspond to the states q_l and q_r in Figure 6.24. Across the elastic waves one can see the states $q_{l,i-1/2}^*$ and $q_{r,i-1/2}^*$ which have stress values at current value of the yield-stress $\sigma_{i-1,y}$ and $\sigma_{i,y}$. Note that $\sigma_{i-1,y}$ and $\sigma_{i,y}$ are the dotted lines to the left and right of the $(i-1)$ interface. Also note that the stress state in $q_{r,i-1/2}^*$ for the Riemann problem at the left cell edge and the stress state in $q_{l,i+1/2}^*$ (the inner two most triangular regions) for the Riemann problem at the right cell edge must have the same stress value as both of these elastic stress states are at the current value of the cell's yield $\sigma_{i,y}$. Figure 6.26 also shows that across the plastic waves one can see plastic stress values (darker triangular regions) in the states $q_{m,i-1/2}$ and $q_{m,i+1/2}$. Here $q_{m,i-1/2}$ could correspond to q_m shown in Figure 6.24 while $q_{m,i+1/2}$ could correspond to $q_{m,Riemann}$ shown in Figure 6.28. Note that while velocity v and stress σ must be continuous across the cell edges (before updating the cell averaged values) yield stress s_y and strain ϵ do not need to be continuous.

Figure 6.26 shows how the states found in the elasto-plastic Riemann solution are used to find the new cell averaged values q_i^{n+1}. For the i'th cell, the Riemann solution approach consists of first solving the two Riemann problems shown at the left and right cell edges and then averaging the states $q_{m,i-1/2}$, $q_{r,i-1/2}^*$, q_i^n, $q_{l,i+1/2}^*$, and $q_{m,i+1/2}$ to find the new cell averaged states given by q_i^{n+1}. Recall that the wave-speeds must be known in order to do a weighted average of these 5 states. Figure 6.26 shows that these weights correspond to the fraction of the cell, clearly dependent on the elastic and plastic wave speeds, occupied by the five states at the time t^{n+1}. While projection methods also start with an elastic update followed by a cell-wise check on the yield condition, projection methods must construct (plastic) solutions based on information that is strictly available in a single cell.

Figure 6.27 shows the first step in the cell-wise projection algorithm described above: solve elastic Riemann problems at the left and right edges to find the elastic waves used to update the cell and find a trial state. Unlike the elasto-plastic Riemann solution, the projection method does not explicitly define plastic waves nor solve Riemann problems which can have mid-states in the plastic regime. Similarly to Figure 6.26, Figure 6.27 shows the two elastic Riemann problems solved at either edge of the i'th cell. These Riemann problems are solved using only the elastic system with no consideration for plastic behavior. Note that Figure 6.27 shows the three stress states used to update the i'th cell: the stress value shown as $q_{m,i-1/2}$ on the left, the stress value shown as q_i^n, and that given by $q_{m,i+1/2}$ on the right. Here one can see that while the value of stress in the state $q_{m,i-1/2}$ is above yield in both the $(i-1)$'th and i'th cells, the value of stress in the state $q_{m,i+1/2}$ is above yield in the i'th cell (and therefore plastic wave should exist here) and below yield in the $(i+1)$'th cell. Keep in mind that the information about whether the stress values associated with $q_{m,i-1/2}$ and $q_{m,i+1/2}$ are above or below the current yield-stress is lost when these states are averaged along with q_i^n to find the new state $q_{i,Trial}^{n+1}$. Also note that, as in Figure 6.26, the Figure 6.27 is shown in both x-t space and σ-t space.

Now recall the second step in the projection algorithm: check the trial state vs the cell's yield condition. Figure 6.27 shows the updated "trial" stress state in the i'th cell $q_{i,Trial}^{n+1}$. Here we can see that the value of stress in the state $q_{i,Trial}^{n+1}$ is the weighted average of the three states $q_{m,i-1/2}$, q_i^n, and $q_{m,i+1/2}$. If $q_{i,Trial}^{n+1}$ lies below the yield value then we are done. Note however that when the value of stress in the state $q_{i,Trial}^{n+1}$ is compared to the cell's yield condition we find that the trial stress state has exceeded the yield condition and we must complete the final step in the algorithm: if the trial state exceeds the yield condition then we must project back to a final state which satisfies the (new) yield condition while minimizing the free energy. Figure 6.29 shows diagrammatically how this projection or minimization step takes place. See [49] for more details.

The stress states shown in Figure 6.27 as q_i^n, $q_{m,i+1/2}$, and $q_{i,Trial}^{n+1}$ are all shown in Figure 6.29 as σ_i^n, $\sigma_{m,i+1/2}$, and $\sigma_{i,Trial}^{n+1}$. Figure 6.29 shows the initial stress value in the i'th cell as σ_i^n. Here one can see that this value is connected via an elastic wave $\mathcal{W}^1$ to the mid-state stress found in the solution to the Riemann problem at the right cell edge $\sigma_{m,i+1/2}$. The three stress values σ_i^n, $\sigma_{m,i-1/2}$ and $\sigma_{m,i+1/2}$ in the states q_i^n, $q_{m,i-1/2}$, and $q_{m,i+1/2}$ are all averaged to find the new stress value $\sigma_{i,trial}^{n+1}$ associated with the state $q_{i,Trial}^{n+1}$. Note that the value of stress $\sigma_{i,trial}^{n+1}$ is shown in both Figure 6.29 and Figure 6.27.

Figure 6.29 shows how to project back from the trial value given as $\sigma_{i,trial}^{n+1}$ to the minimum energy value shown as $\sigma_i^{n+1} = \sigma_{yfinal}$. Recall that the elasto-plastic Riemann solution would have split the state $q_{m,i+1/2}$ in Figure 6.27 into the two neighboring states shown in Figure 6.26 as $q_{l,i+1/2}^*$ and $q_{m,i+1/2}$. The projection algorithm does not solve for this plastic wave, shown in Figure 6.28 as $\mathcal{W}^3$. Instead, only the elastic waves are solved for and we find a trial state which overshoots the correct plastic solution and must be projected back down or minimized. Recall Section 6.4 described the numerical procedure for minimizing the total elastic and plastic energy subject to the constraint that the solution satisfies some new yield condition. Figure 6.29 shows this process in 1D. Here we see the trial state as $\sigma_{i,trial}^{n+1}$. This trial state exceeds the yield condition, shown as the line with slope β_p in Figure 6.29. To minimize the energy we must find a new stress state which lies on this line and gives the smallest value of π. Figure 6.29 shows this "minimized" stress state as the intersection of three lines which gives a final stress, plastic deformation, and strain values as $\sigma_i^{n+1} = \sigma_{yfinal}$, π_{final}, and ϵ_{final}. Note that by projecting the trial stress value back along a line of constant strain we have increased the value of plastic deformation from the trial value π_{trial} out to the final value π_{final} while decreasing the stress value from $\sigma_{i,trial}^{n+1}$ down to $\sigma_i^{n+1} = \sigma_{yfinal}$. This procedure gives stress σ and plastic deformation π values which both minimize the energy function and satisfy the new yield criterion defined by the new yield-stress value σ_{yfinal}. In the following section we investigate three elasto-plastic examples and solve via both our solution methods.

6.6 One Dimensional Elasto-Plastic Examples

In this section we explore three examples and compare the solutions generated by our two different solution methods. In the first example we send two elastic waves in from the left and right boundaries. When these waves collide they constructively interfere so that their amplitude becomes greater than the yield condition. The second example is very similar except that the medium through which the waves are moving is periodically heterogeneous. The Young's modulus E and the density ρ are chosen so that while the sound speed is one everywhere there is an impedance jump between layers. In the third example the material constants are homogeneous throughout but the yield stress is heterogeneous.

6.6.1 Two Elastic Pulses that Plastically Interfere

Figure 6.30 shows two incoming elastic pulses in a homogeneous material. From top to bottom the state variables shown are the stress, velocity, strain, and plastic deformation. The solution shown is computed via both the Riemann solution procedure and the minimization procedure.

Figure 6.30 shows a wave on the left moving to the right and a wave on the right moving to the left. Note that the amplitude of both waves is below the yield stress so that they are purely elastic in nature. Figure 6.31 shows the two wave constructively interfering with an amplitude above the initial yield-stress. Here one can see the increase in plastic deformation in the region of interference.

In Figure 6.32 we can see the two waves moving apart after they have interacted. Here the pulse on the left is moving to the left and the pulse on the right is moving to the right. Note that since the plastic wave-speed is much slower then the elastic wave-speed, the pulses are distorted. Since only the higher amplitude parts of each pulse interact plastically the lower amplitude part of each pulse "pulls ahead" of the larger amplitude part. As Figure 6.32 shows, each of the pulses gets distorted in such a way that the higher amplitude gets slowed down during the plastic interaction. Figure 6.31 and Figure 6.32 both also show the permanent plastic strain and isotropic hardening of the material. In both figures Figure 6.31 and Figure 6.32 one can see that in the region of interference the material is strained at a state of zero stress. Also in this region the yield-curve is elevated in the area that underwent plastic deformation. In each cell that experienced plastic yield, i.e. $F(\sigma, \pi) = 0$, the yield function $F(\sigma, \pi)$ was redefined to include the current cell values of σ_y and π. In this sense the yield curve shows the plastic state of the material.

6.6.2 Two Elastic Pulses Plastically Interfere in a Medium with Periodic Heterogeneous Young's Modulus E

As in the previous example, Figure 6.33 shows two incoming elastic pulses. However in this example the material is made up of layers across which there is an impedance jump. Each layer is ten cells thick and in every cell the moduli are chosen so that the sound speed is

10. For this example the sound speed is given by $c = \sqrt{\frac{\mu(3\lambda+2\mu)}{\rho(\lambda+\mu)}}$ where we have chosen the following (values rounded for brevity):

$$\rho(x) = \begin{cases} \rho_1 = 1.87, & \text{for } 0 < x < 2\pi\theta\gamma \\ \rho_2 = 1, & \text{for } \ 2\pi\theta\gamma < x < 2\pi\gamma \end{cases}$$
$$\lambda(x) = \begin{cases} \lambda_1 = 60, & \text{for } 0 < x < 2\pi\theta\gamma \\ \lambda_2 = 60, & \text{for } \ 2\pi\theta\gamma < x < 2\pi\gamma \end{cases} \tag{6.93}$$
$$\mu(x) = \begin{cases} \mu_1 = 76.62, & \text{for } 0 < x < 2\pi\theta\gamma \\ \mu_2 = 38.31, & \text{for } \ 2\pi\theta\gamma < x < 2\pi\gamma \end{cases}$$

This means that each layer satisfies a different elastic constitutive relation than its neighbor. Figure 6.33 shows that for a smooth stress function the strain is discontinuous at each layer interface. As in the previous example, the stress, velocity, strain, and plastic deformation are shown initially in Figure 6.33. Also as in the previous example, the solution shown is computed via both the Riemann solution and minimization solution procedures.

In Figure 6.33 we again see an elastic pulse on the left moving to the right and another elastic pulse on the right moving to the left with the amplitudes of both pulses are below the yield stress. Figure 6.34 shows the two pulses constructively interfering with an amplitude above the initial yield-stress. Here again one can see the increase in plastic deformation and yield-stress in the region of interference.

Figure 6.35 shows the two pulses moving apart after they have interacted. Now the pulse on the left is moving to the left and the pulse on the right is moving to the right. Note that while the media properties in Figure 6.32 and Figure 6.35 were very different, the overall plastic strain is very similar in the two examples.

6.6.3 Two Elastic Pulses Plastically Interfere in a Medium with Periodic Heterogeneous Yield Criterion

This third example is very similar to the last two. In this example we assume that the material constants are homogeneous as in the first example. For this example, as with the first example, we have (μ rounded)

$$\begin{aligned} \rho(x) &= 1, \\ \lambda(x) &= 60 \\ \mu(x) &= 38.31 \end{aligned} \tag{6.94}$$

These values give the elastic sound-speed $c = \sqrt{\frac{\mu(3\lambda+2\mu)}{\rho(\lambda+\mu)}} = 10$. However in this example, we assume that the material is a composite of layers across which the yield condition jumps. Figure 6.36 shows two incoming elastic pulses in an elastically homogeneous material. Since the material is made up of layers of differing yield-stress, plastic waves will move in a heterogeneous material. As in the last two examples we have shown the stress, velocity, strain, and plastic deformation. Also as before the solution shown is computed via both our Riemann solution and minimization procedures. The only difference between this example and that shown in Figure 6.30-Figure 6.32 is that the yield condition is periodically heterogeneous on the same scale as the example shown in Figure 6.33-Figure 6.35. In a given layer the yield condition is set to be $\sigma_y = 50$ or $\sigma_y = 200$. Until they interact the elastic pulses never go above either of these values we can see exactly what is expected in Figure 6.36. The incoming pulses shown in Figure 6.36 do not exceed the yield condition in any layer, and they each propagate elastically just as they did in Figure 6.30.

Figure 6.37 shows the two pulses during the period of plastic interference. Note that plastic deformation only occurs in alternating layers where the initial yield-stress has been exceeded. In the other layers the amplitude of the stress during constructive interference never reaches the yield-stress of 200 and therefore no plastic deformation occurs in these layers.

In Figure 6.38 we see the two pulses moving apart after they have interacted. The pulse on the left is moving to the left and the pulse on the right is moving to the right. After the pulses have separated the material is left with a permanent strain only in the layers in which plastic deformation occurred. It should be clear that this is what one expects. In the first two examples the yield-stress was exceeded at all cells where the amplitude of the interfering pulses exceeded the initial yield-stress. However in the third example the layers with a high yield-stress never undergo any plastic deformation. Since these layers of high yield-stress always respond elastically there is no mechanism to cause a permanent strain.

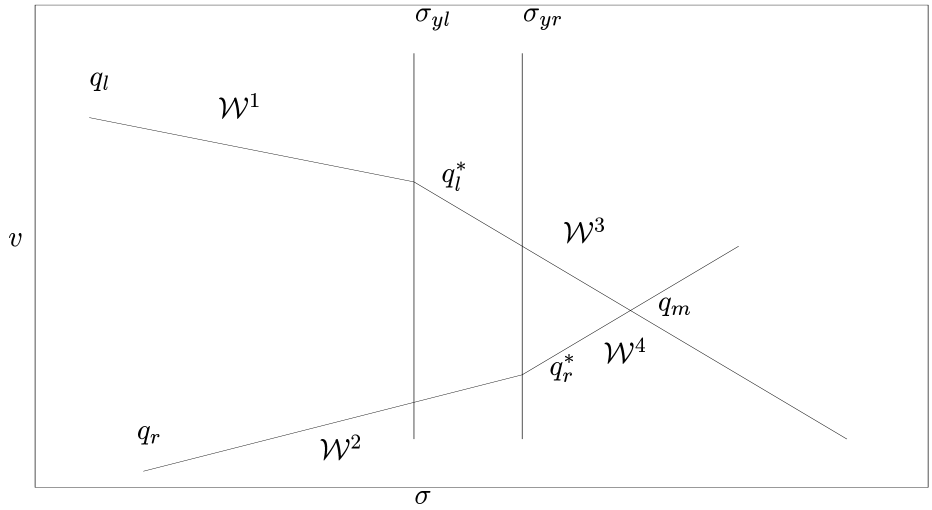

Figure 6.24: Elasto-Plastic Riemann solution. Shown are the left q_l and right q_r states on either side of a given cell interface. These states are connected via elastic waves $\mathcal{W}^1$ and $\mathcal{W}^2$ to the states q_l^* and q_r^* that have stress values equal to the yield-stress σ_{yl} in the left cell and σ_r in the right cell. The solution state q_m is found by connecting these new left and right states via the intersection of two plastic waves $\mathcal{W}^3$ and $\mathcal{W}^4$.

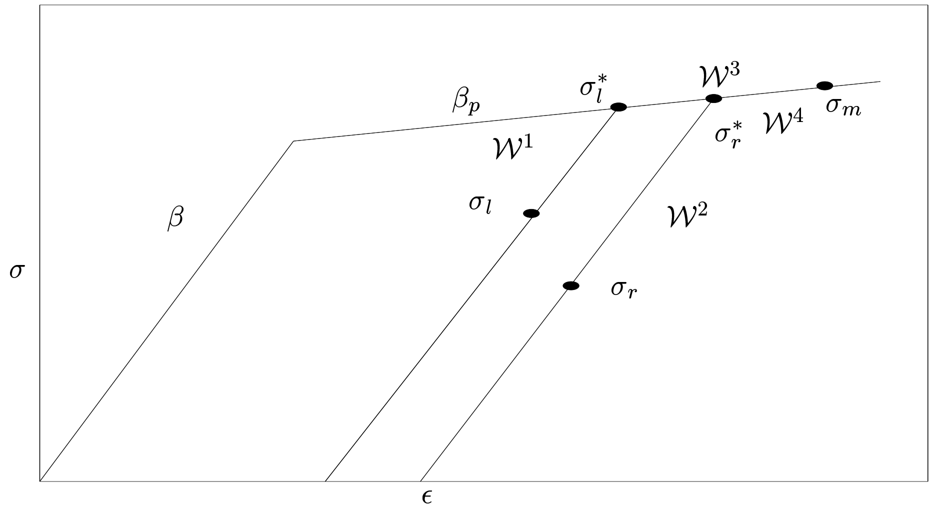

Figure 6.25: Stress-Strain relation for an Elasto-Plastic Riemann solution. Shown are the left σ_l and right σ_r stress-states on either side of a given cell interface. These states are connected via elastic waves $\mathcal{W}^1$ and $\mathcal{W}^2$ to the states-states σ_l^* and σ_r^*. The solution stress-state σ_m is found by connecting these new left and right states via the intersection of two plastic waves $\mathcal{W}^3$ and $\mathcal{W}^4$. Note that the waves and stress values shown in stress-strain space could correspond to the values shown in the previous figure in stress-velocity space. Also these states and waves are shown in the following figure for the Riemann problem at the $i-1/2$ interface .

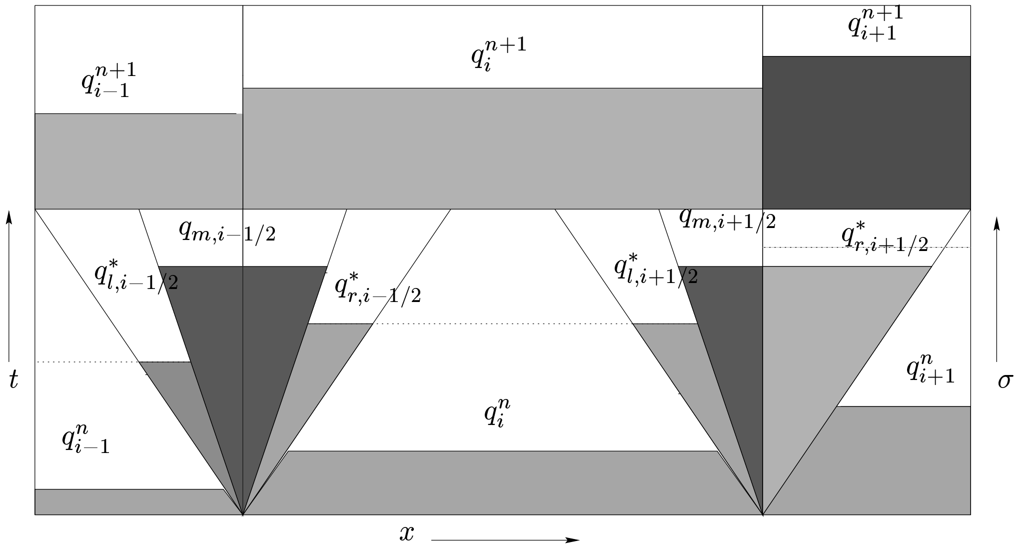

Figure 6.26: Elasto-plastic Riemann problems at both edges of the i'th cell. Note that the Riemann problem on the left consists of two elastic and two plastic waves while that on the right consists of two elastic and one plastic wave. The states $q^*_{l,i-1/2}$ and $q^*_{r,i-1/2}$ for the left Riemann problem have stress values equal to the current yield-stress of the cell while the states $q_{m,i-1/2}$ and $q_{m,i-1/2}$ have stress values in the plastic regime.

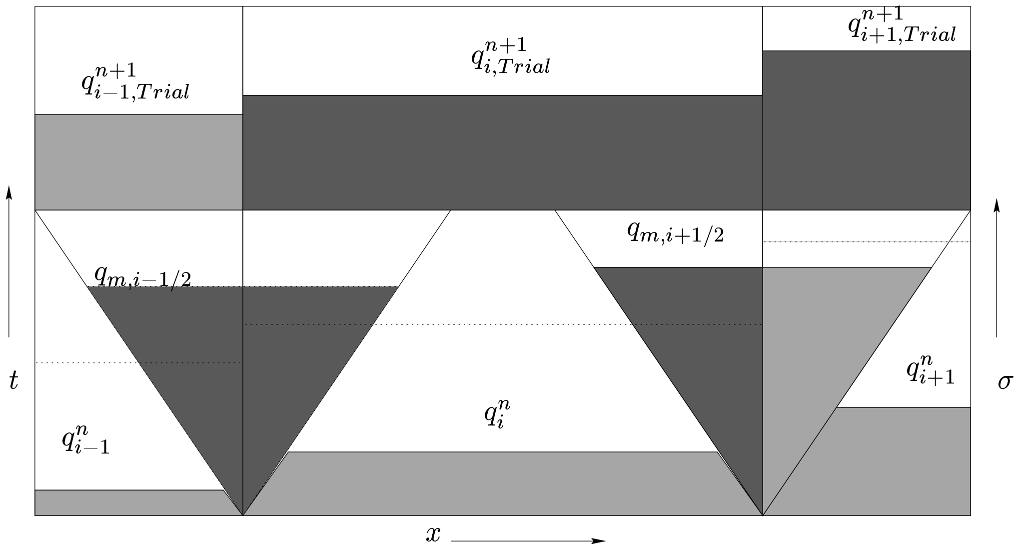

Figure 6.27: Elastic Riemann problems at both edges of the i'th cell. The state $q_{m,i-1/2}$ has a stress value which is above the current yield-stress of the $i-1$'th and i'th cell while the state $q_{m,i+1/2}$ has a stress value which is above the current yield-stress value of the i'th cell and below the current yield-stress value of the $i+1$'th cell.

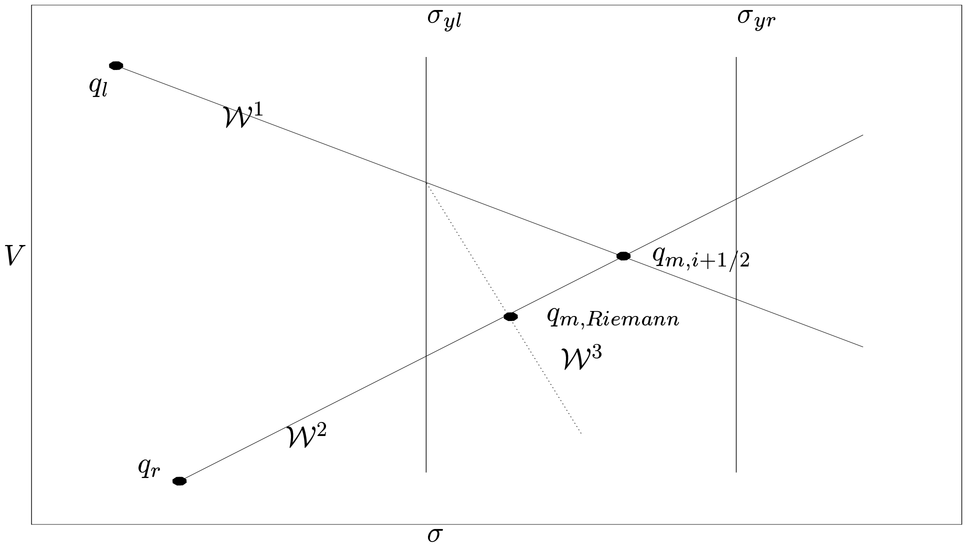

Figure 6.28: Shown are the left q_l and right q_r states on either side of the $(i+1/2)$ interface corresponding to the stresses in the states q_{i-1}^n and q_i^n in the two figures above. These states are connected via elastic waves $\mathcal{W}^1$ and $\mathcal{W}^2$ to the final state $q_{m,i+1/2}$, also shown in Figure 6.27. Note the elasto-plastic Riemann solution $q_{m,Riemann}$ for this problem contains an additional plastic wave $\mathcal{W}^3$ and is shown as $q_{m,i+1/2}$ in Figure 6.26

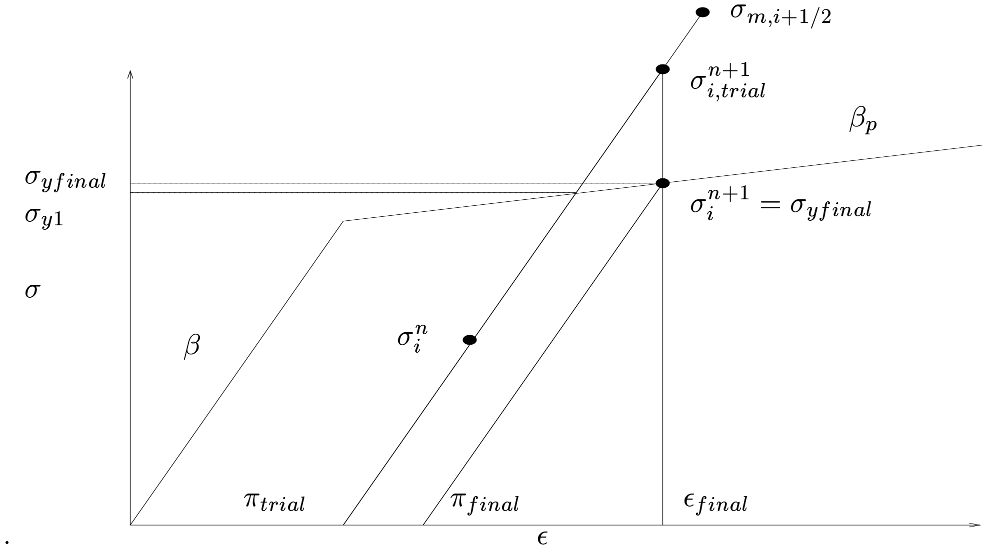

Figure 6.29: Elasto-Plastic Stress-Strain relation for the i'th cell. Here we see the initial stress value in the i'th cell σ_i^n along with the stress value $\sigma_{m,i+1/2}$ found across the elastic wave $\mathcal{W}^1$ and the cell averaged trial stress value given as $\sigma_{i,trial}^{n+1}$. The projected or minimized stress value is shown as $\sigma_i^{n+1} = \sigma_{yfinal}$.

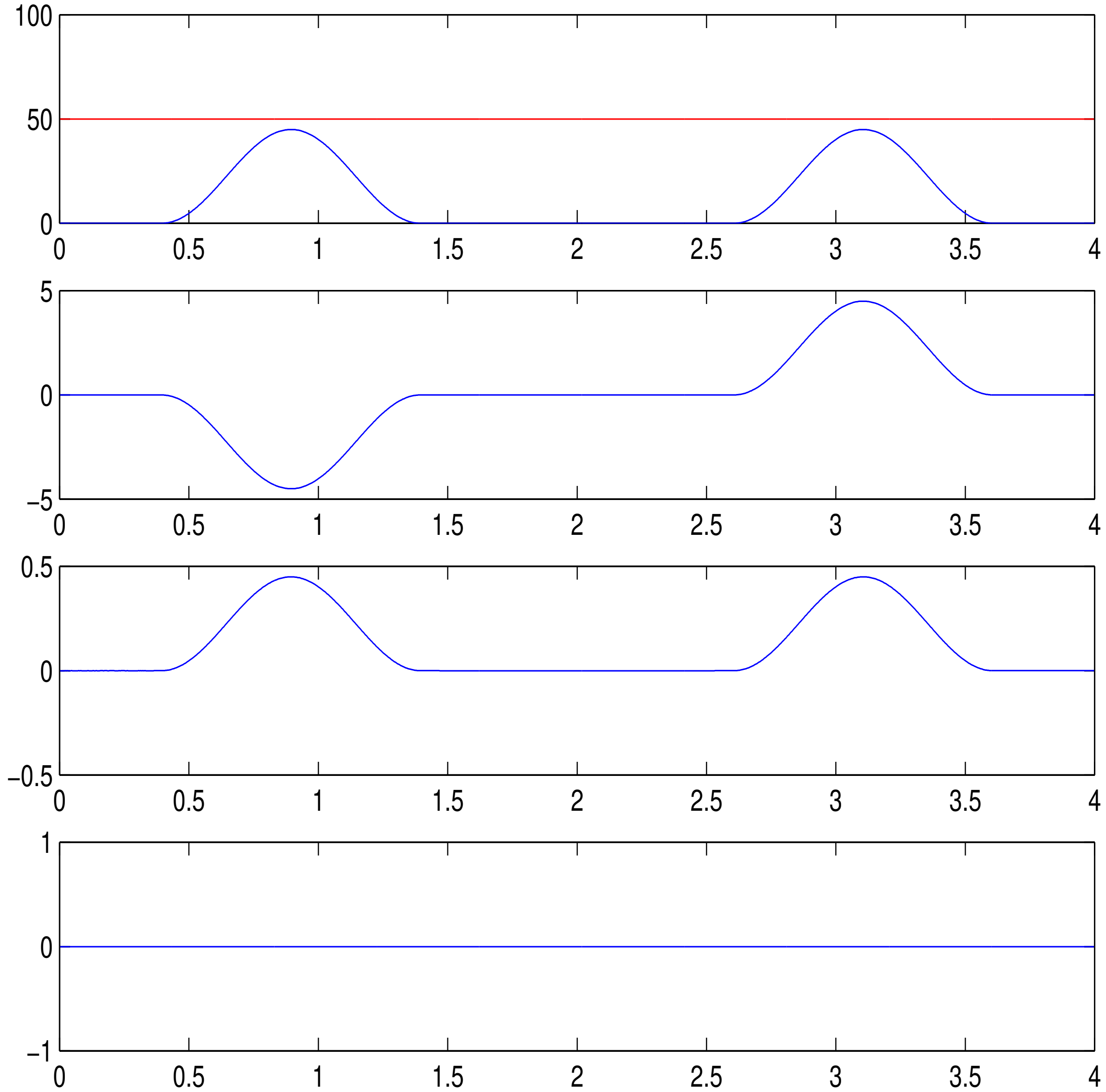

Figure 6.30: Stress, Velocity, Strain, and Plastic Deformation: Incoming waves.

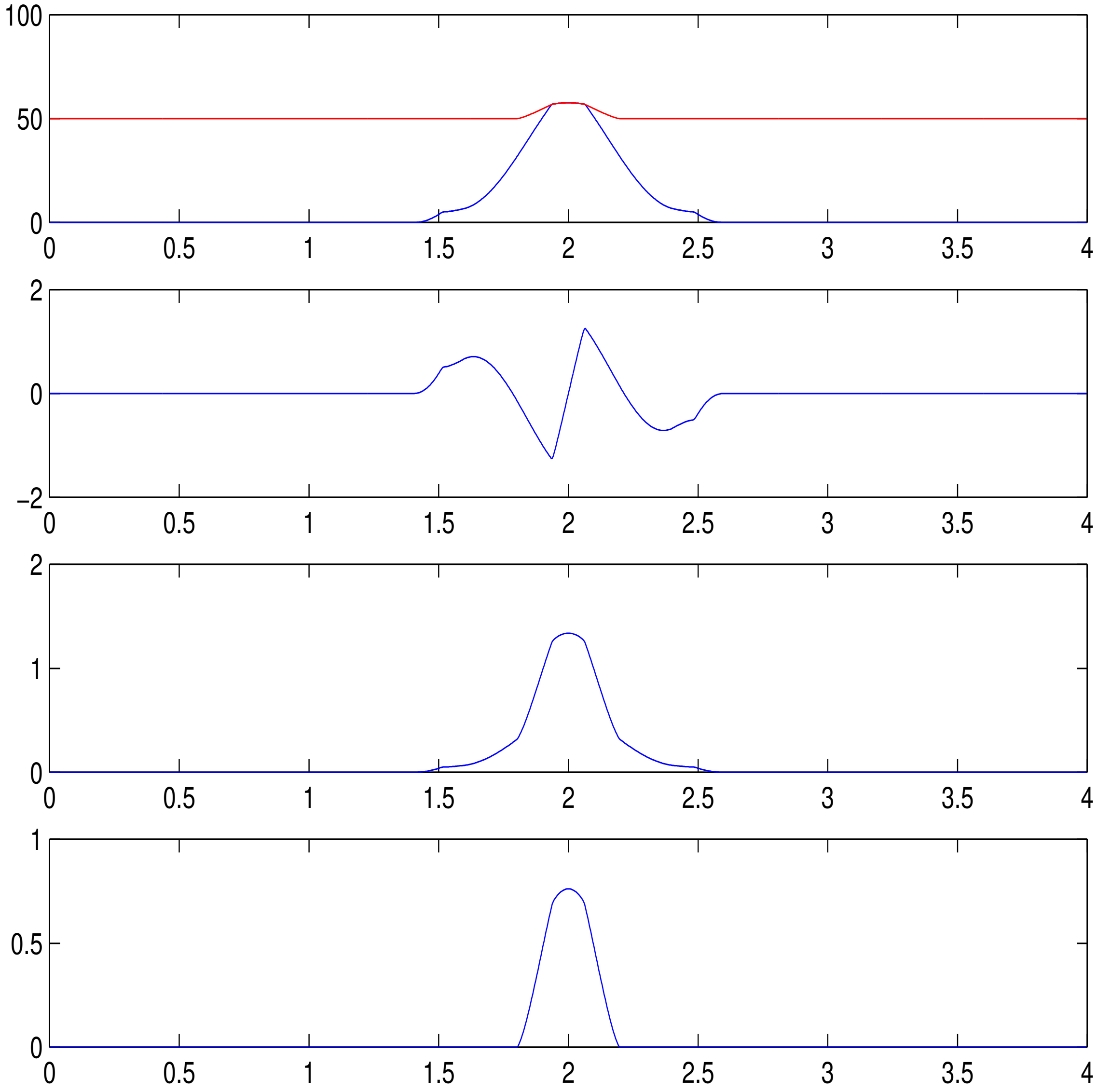

Figure 6.31: Stress, Velocity, Strain, and Plastic Deformation: Interacting waves.

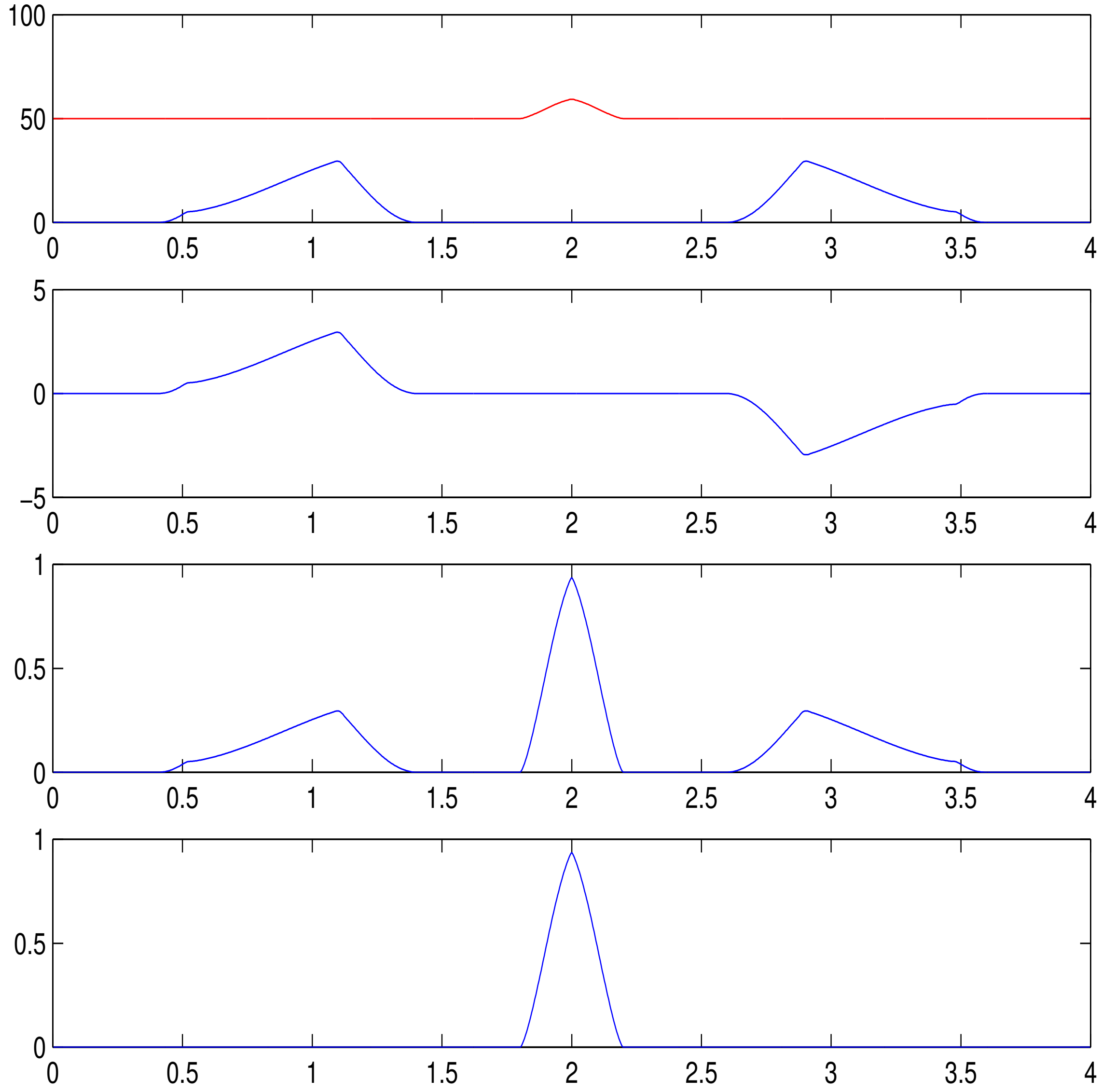

Figure 6.32: Stress, Velocity, Strain, and Plastic Deformation: Outgoing waves.

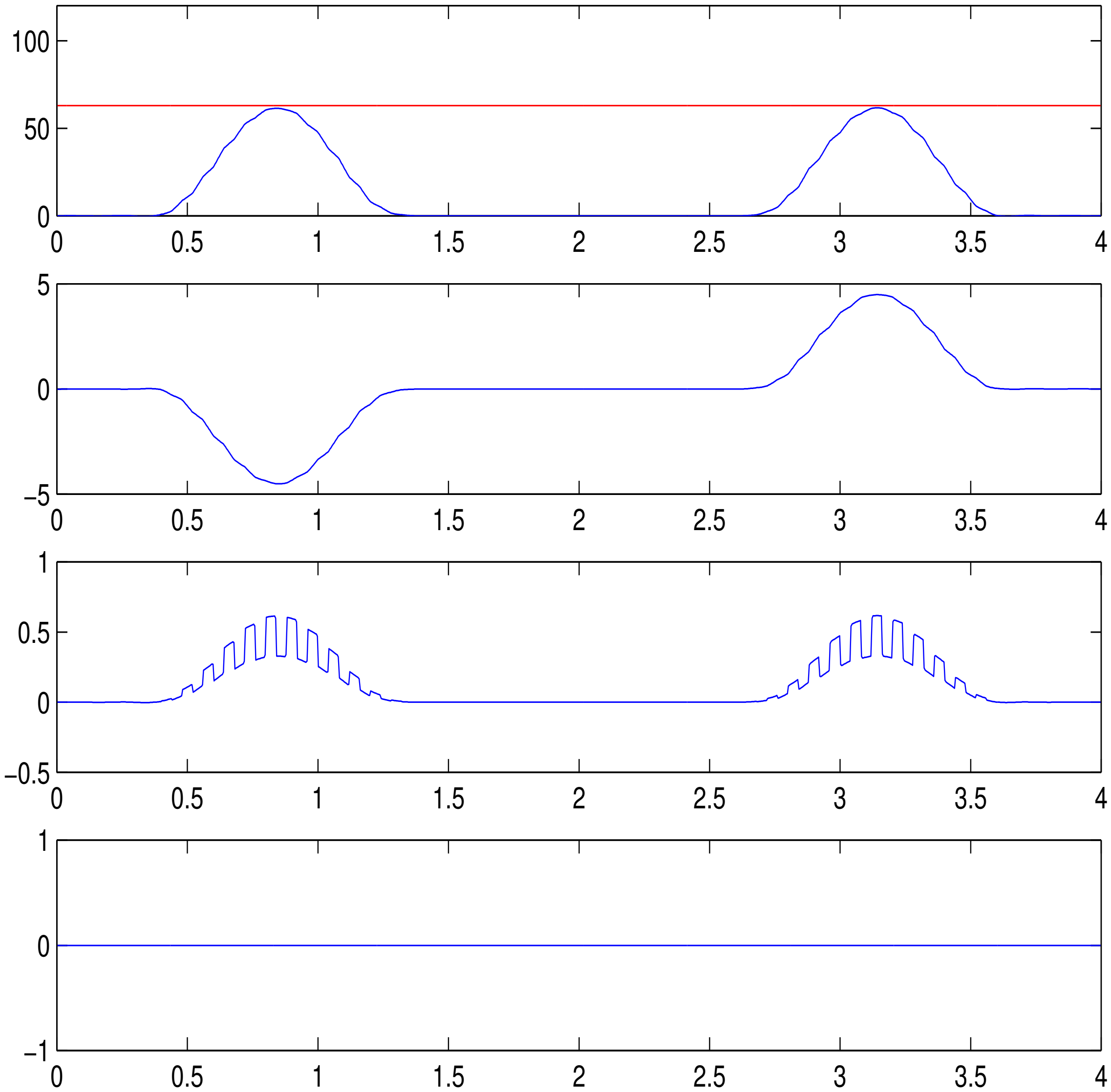

Figure 6.33: Stress, Velocity, Strain, and Plastic Deformation: Incoming waves.

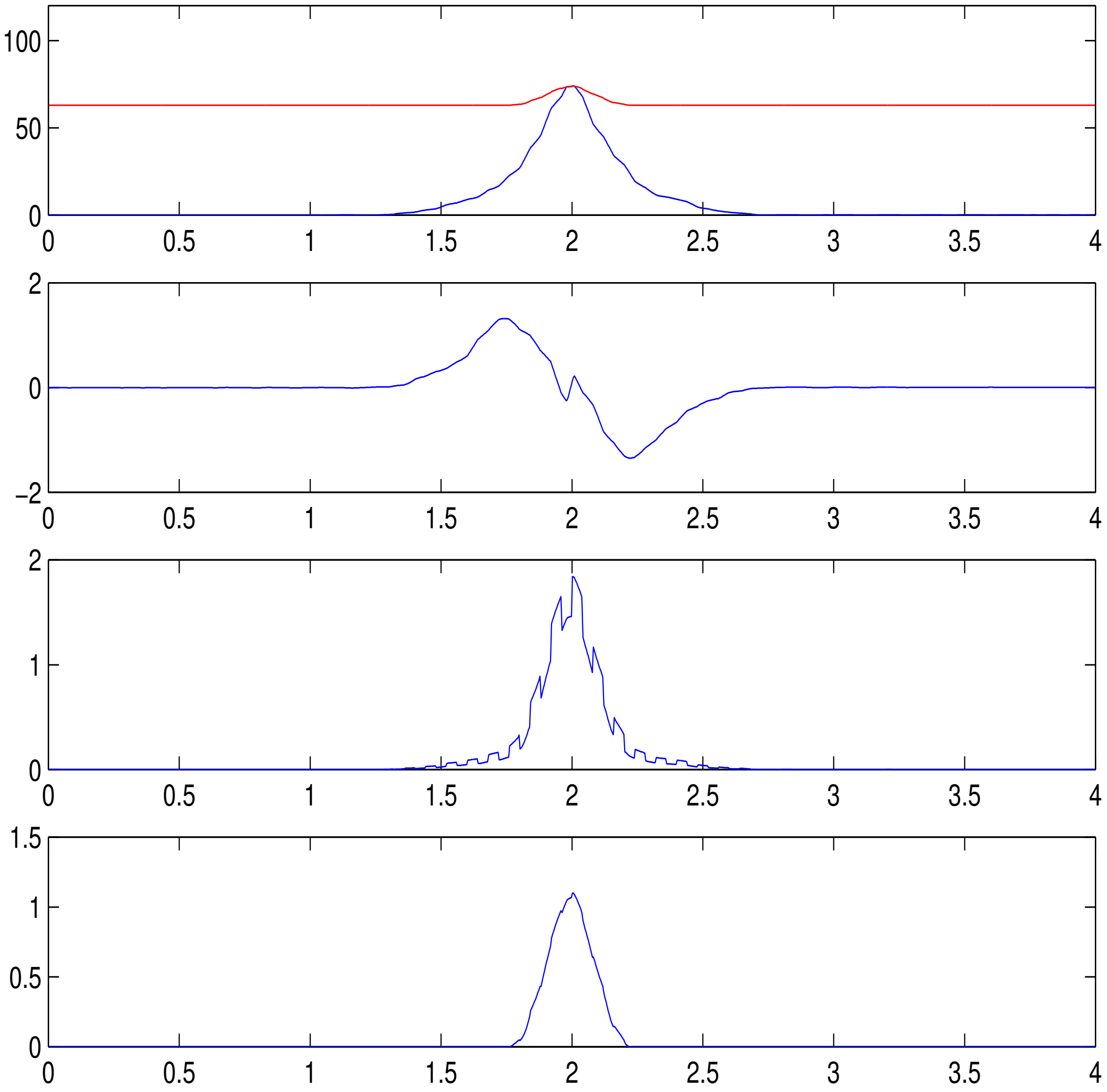

Figure 6.34: Stress, Velocity, Strain, and Plastic Deformation: Interacting waves.

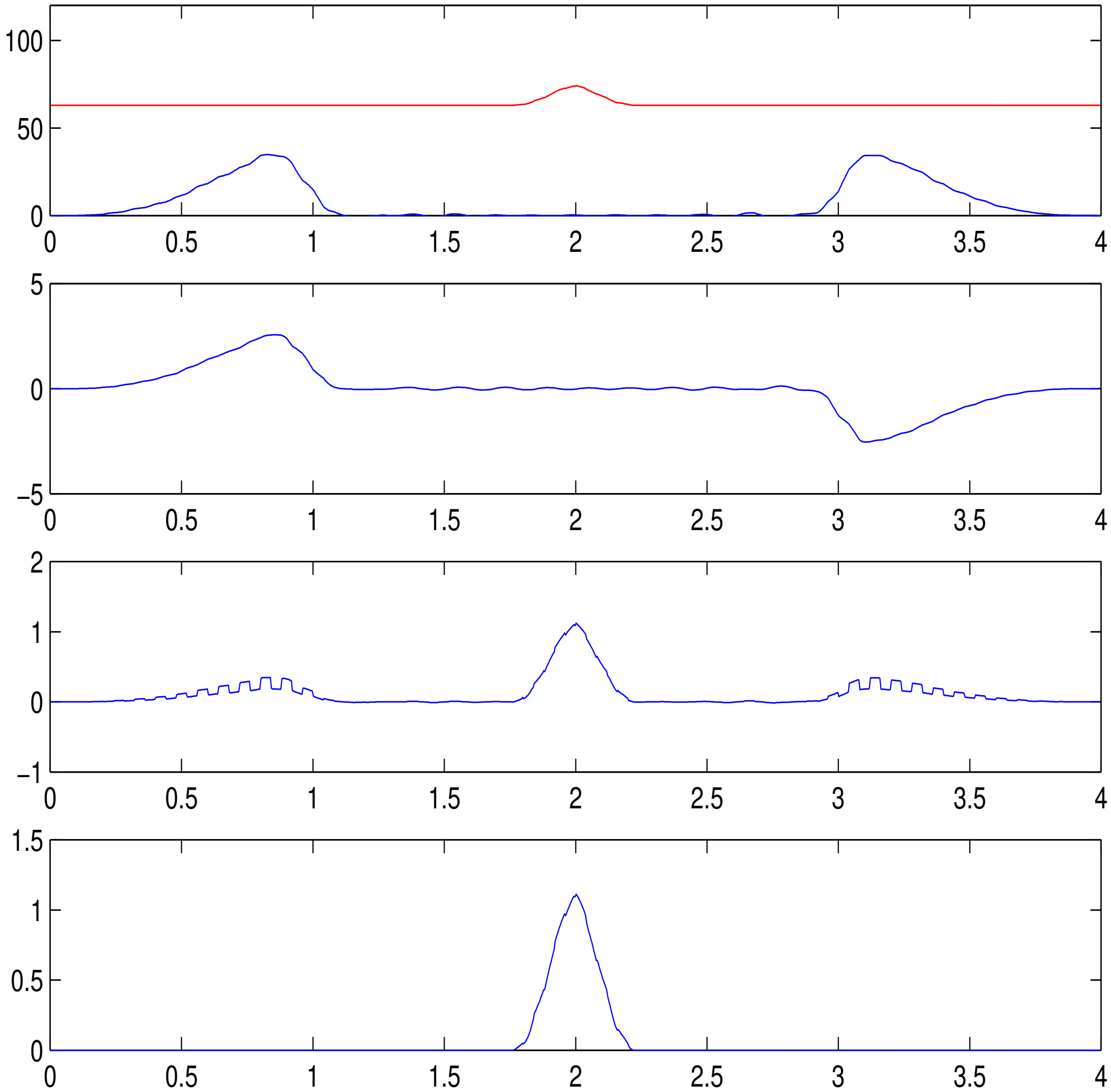

Figure 6.35: (a) Stress, Velocity, Strain, and Plastic Deformation: Outgoing waves.

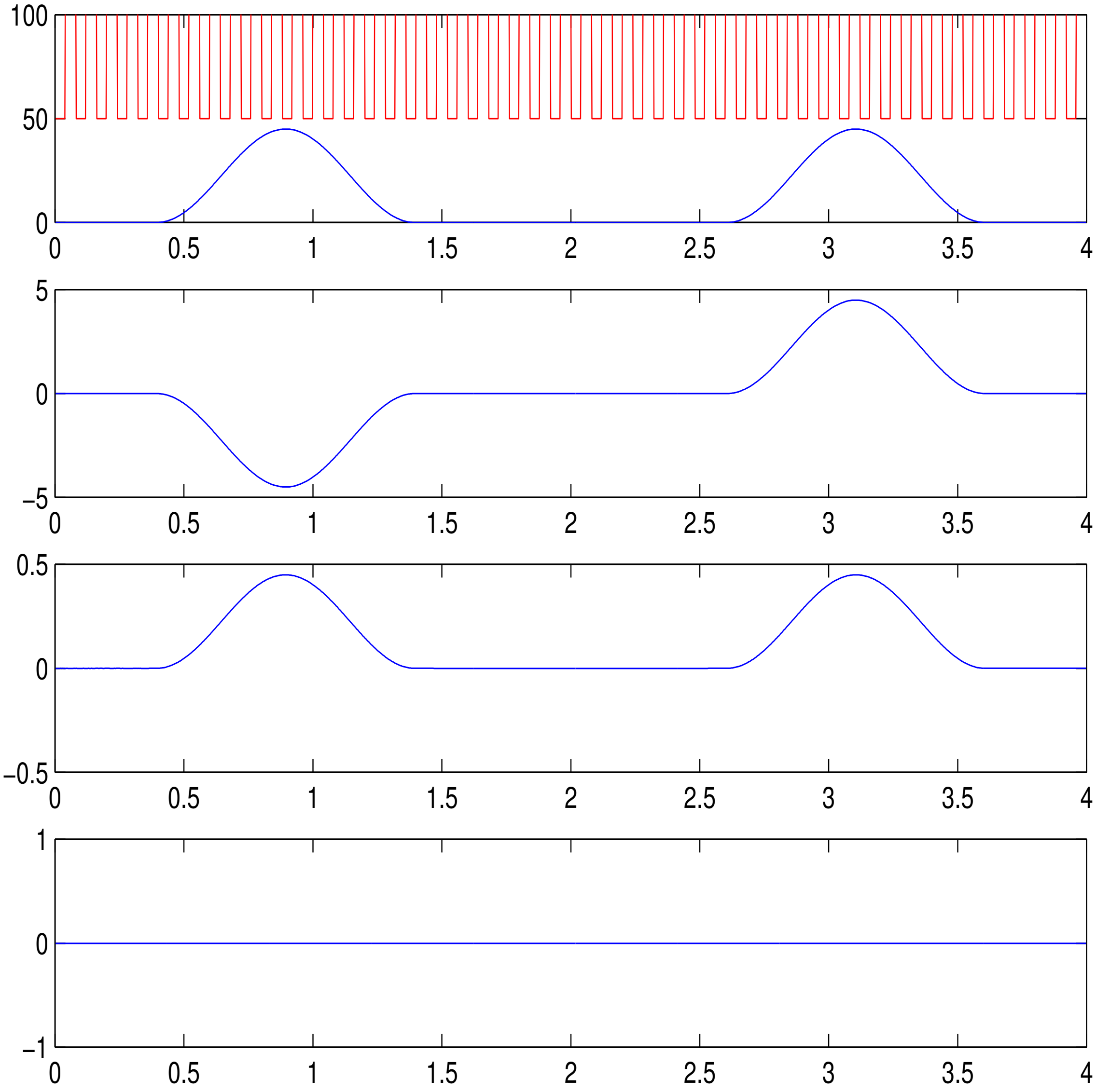

Figure 6.36: Stress, Velocity, Strain, and Plastic Deformation: Incoming waves.

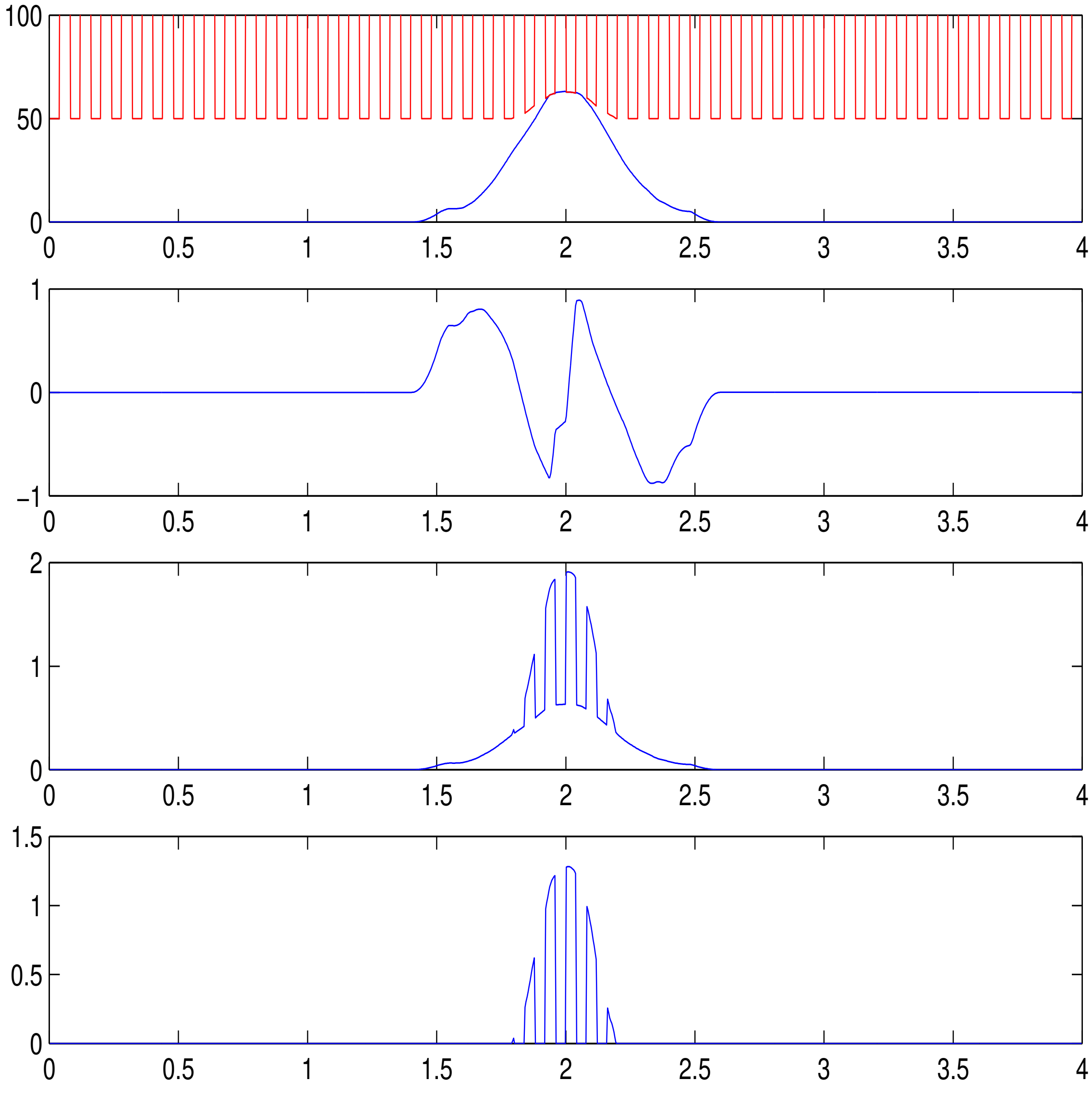

Figure 6.37: Stress, Velocity, Strain, and Plastic Deformation: Incoming waves.

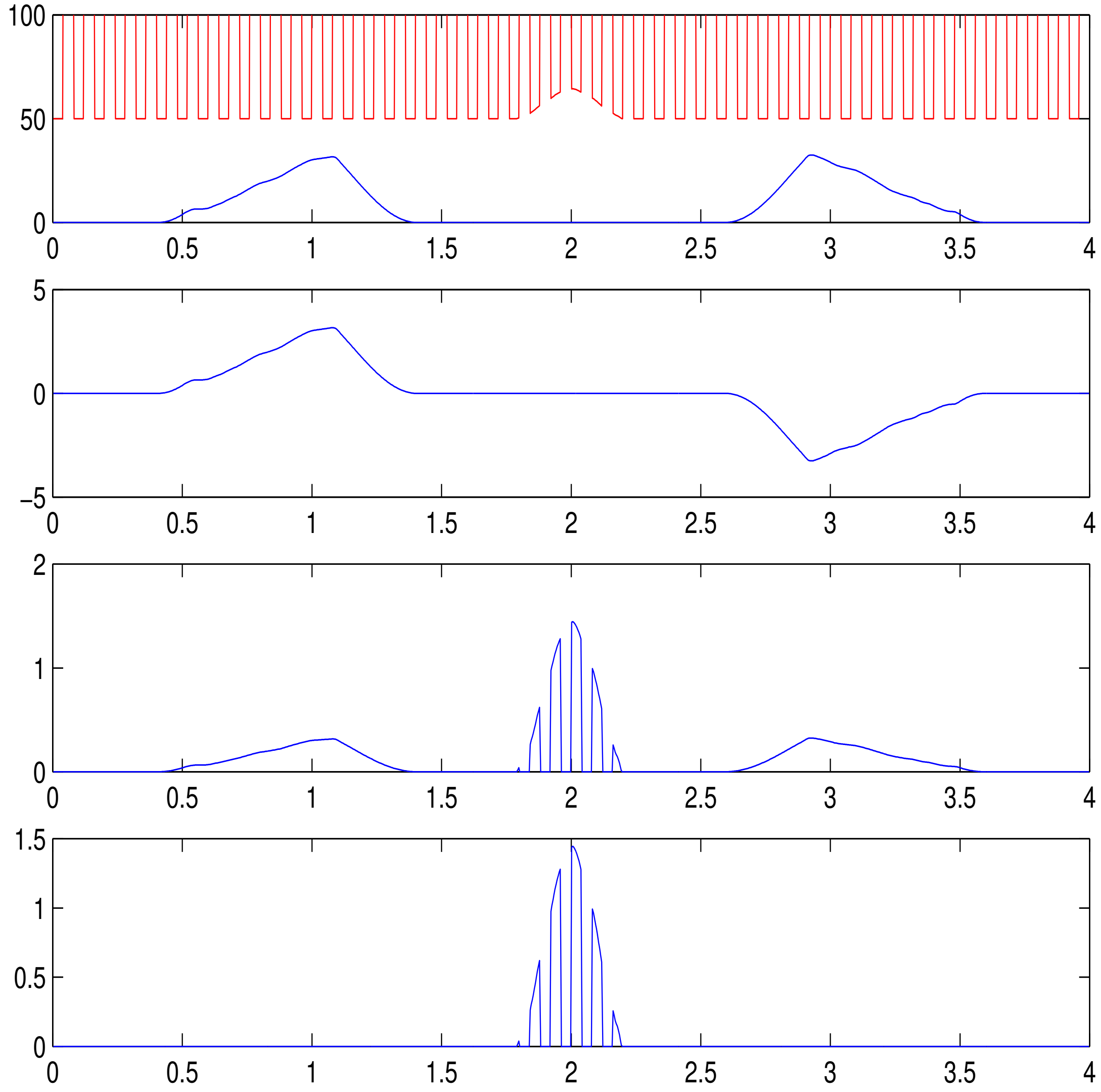

Figure 6.38: (a) Stress, Velocity, Strain, and Plastic Deformation: Incoming waves.

Chapter 7

TWO DIMENSIONAL ELASTO-PLASTICITY

In the previous chapter we explored 1D elasto-plastic examples in great detail. We explained the methods used to compute solutions first in 1D and then showed how to expand the solution procedures to problems in 2D. In this chapter we use the methods described in the previous chapter to compute solutions to several 2D problems. We begin with a plane-strain problem in 2D that only has variation in one dimension. Since the 1D solution method is assumed to give accurate results, we use this special 2D test problem to compare solutions generated by the 1D method and the 2D method. After this test case between 1D and 2D is explored, we move on to problems that are truly two-dimensional in nature. Four examples are used to illustrate different aspects 2D elasto-plastic behavior and the ability of our solution method to solve such problems.

In the first 2D example, a long thin plate (plane-strain) is pulled out on both ends. The velocity is chosen so that the waves which move inwards are elastic in nature. When these elastic waves constructively interfere in the center of the material the stress exceeds the yield stress of the material and plastic deformation occurs. In this first example the problem is constrained so that no variation occurs in the second dimension. We use this test case to compare solutions given by the 1D and 2D solution methods. The second 2D example is the same except that the constraint is removed and the material is free to act in a fully two dimensional manner. Here we will see that then the material is plastically "stretched out" lengthwise it gets "pulled in" vertically. The third 2D example is nearly identical to the second except that a layer of elastic material is in the center of the region of plastic deformation. This elastic layer is set to have a very high yield stress and is not able to be plastically deformed. In the final 2D example we look at a "disc" of 2D (plastic) material with a low yield stress embedded in a surrounding medium of (elastic) material with a very high yield-stress. A phased array boundary condition is used to generate three elastic-expansion waves (positive σ_{11}) which have a focal point at the center of the disc.

7.1 Two Dimensional Elasto-Plastic problems via Minimization

Recall the first example used to demonstrate elastic-plastic behavior, discussed in Section 6.2.3. We return to this example to test the 2D solution method by comparing solutions generated by the 1D and 2D methods. To make this comparison, a test problem is needed that exhibits the same behavior in 1D and 2D. The goal is to find an example that is essentially 1D in nature and can be computed in 2D, and then compare a "1D-slice" of this solution to its 1D analog. While it is generally true that deformation in one dimension is coupled with deformation with other dimensions, stretching in x causes compression in y for example, it is possible to compare 1D and 2D plane-strain examples if properly formulated.

The 2D plane-strain problem assumes that all non-zero strains are in the plane. Similarly the 1D reduction from plane-strain assumes that the strain is reduced to a scaler. First consider the 2D plane-strain problem as a "2D-slice" of a fully 3D problem which only has variation in the x-y plane. Then consider the 1D reduction of this problem as a "1D-strip" of that plane, the line along the x-axis for example. To properly compare such examples we must have a problem in 2D that only has variation in x. While it's true that any problem that only has variation in x is essentially a 1D problem, we can still compute the 2D test-problem using the general 2D solution method and compare the results with the 1D solution method to gain a measure of confidence about the 2D method.

7.1.1 Comparison of 1D and 2D solution methods.

In the following comparison one can think of a long rectangular table-top. If we pull on the ends of the table, then in 3D we would expect deformation in all three directions: expansion lengthwise (x direction) and compression in the width (z direction) and thickness (y direction). If we view the table "edge on" where x is the direction in which the ends are pulled, then y is the vertical direction, and z is the direction "into" the table. The 2D plane-strain assumption means that we assume the table is infinite in z and look at one slice in the x-y plane and hence we expect to see the same configuration at any two points which have the same x-y coordinates regardless of the z coordinate. Here we compare an example of a 2D plane-strain problem with a computation that is a 1D reduction from plane-strain. Recall that the 1D problem can be solved exactly and via our minimization technique as was shown in Section 6.2.3. In both 1D and 2D the two necessary ingredients which must be specified are the yield criterion and energy function.

To compare examples in 2D and 1D, one must be aware of the assumptions which are used to reduce from 2D plane-strain to 1D and adjust accordingly. In section 6.4.1 we showed that the 2D plane-strain yield criterion was given by

$$\sqrt{\frac{(\sigma_{11}^2+\sigma_{22}^2)(3\lambda^2+6\lambda\mu+4\mu^2)-2\sigma_{11}\sigma_{22}(3\lambda^2+6\lambda\mu+2\mu^2)+12\sigma_{12}^2(\lambda^2+2\lambda\mu+\mu^2)}{4(\lambda+\mu)^2}}$$
$$-(\sigma_y+\beta_p\pi)=0. \tag{7.1}$$

Similarly we showed that the yield criterion for the 1D reduction from plane-strain was given as

$$\sqrt{\frac{4\mu^2\sigma_{11}^2}{(\lambda+2\mu)^2}}-(\sigma_y+\beta_p\pi)=0. \tag{7.2}$$

Recall that to obtain the 1D criterion by reduction from the 2D criterion it is assumed that the strain tensor is reduced to a scaler given by ϵ_{11} and that the stress must satisfy the following:

$$\sigma_{33}=\sigma_{22}=\frac{\lambda}{\lambda+2\mu}\sigma_{11}. \tag{7.3}$$

With regard to the edge view of the table-top this means that in the reduction from 2D to 1D the stress is balanced in such a way that all 1D horizontal strips of the 2D solution

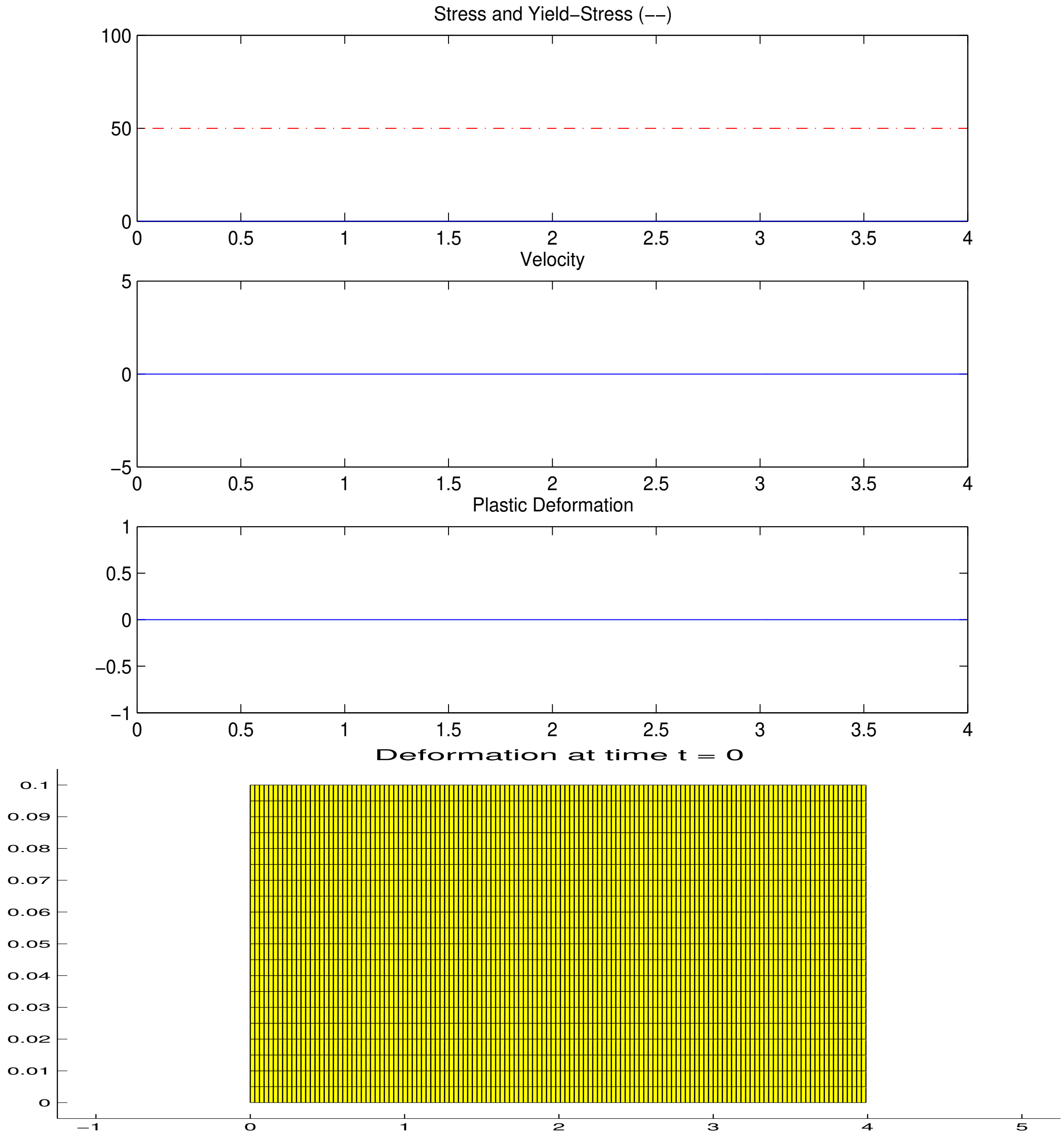

Figure 7.1: Above: Stress and Yield-Stress, Velocity, Plastic Deformation are shown in 1D and 2D (visually identical) in Lagrangian coordinates. Below: Elastic (shown by the grid) and Plastic Deformation (shown by color) in highly exaggerated Eulerian coordinates. Here one can see the initial configuration.

are the same. To make an exact comparison of a 1D and 2D example, all 1D horizontal strips in the 2D example must be identical. However it is not possible to have all such 1D

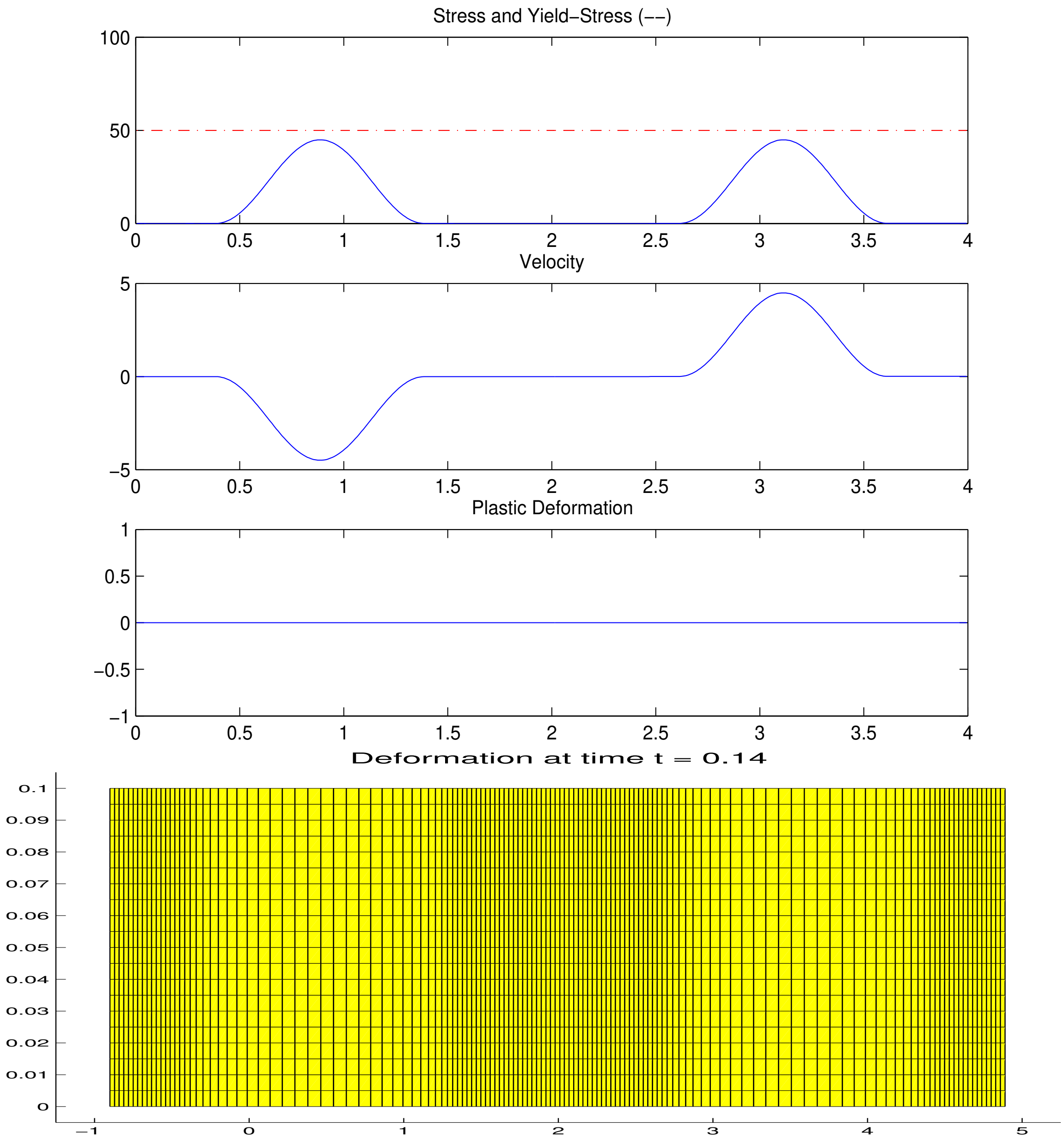

Figure 7.2: Above: Stress and Yield-Stress, Velocity, Plastic Deformation are shown in 1D and 2D (visually identical) in Lagrangian coordinates. Below: Elastic (shown by the grid) and Plastic Deformation (shown by color) in highly exaggerated Eulerian coordinates. Here one can see the incoming waves as they propagate elastically in from the edges before they start to interfere.

strips identical unless (7.3) is imposed. The only way to truly compare 1D and 2D examples

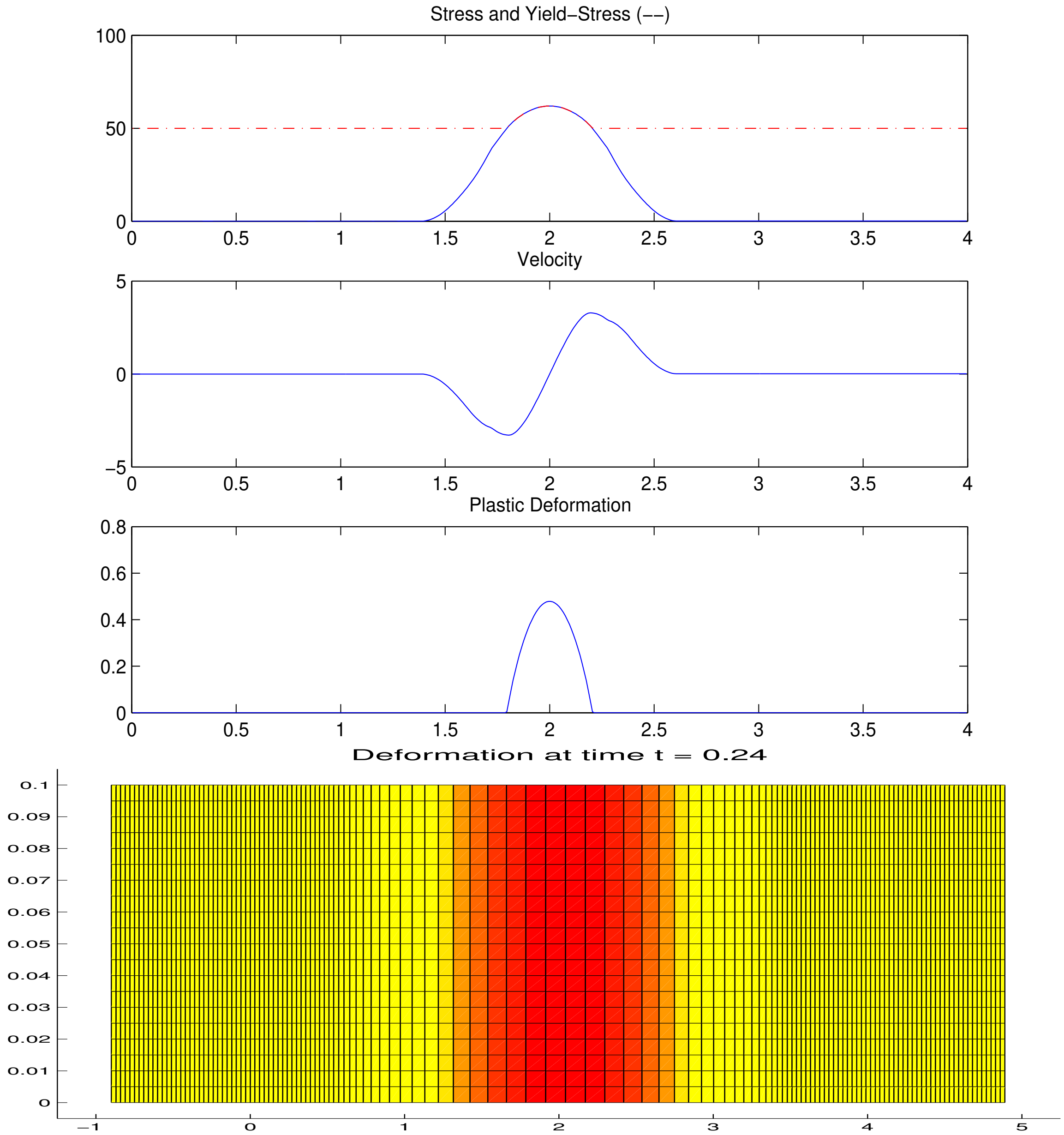

Figure 7.3: Above: Stress and Yield-Stress, Velocity, Plastic Deformation are shown in 1D and 2D (visually identical) in Lagrangian coordinates. Below: Elastic (shown by the grid) and Plastic Deformation (shown by color) in highly exaggerated Eulerian coordinates. Note that in the lower picture one can see the relative (cell wise) expansion caused by the elastic and plastic waves.

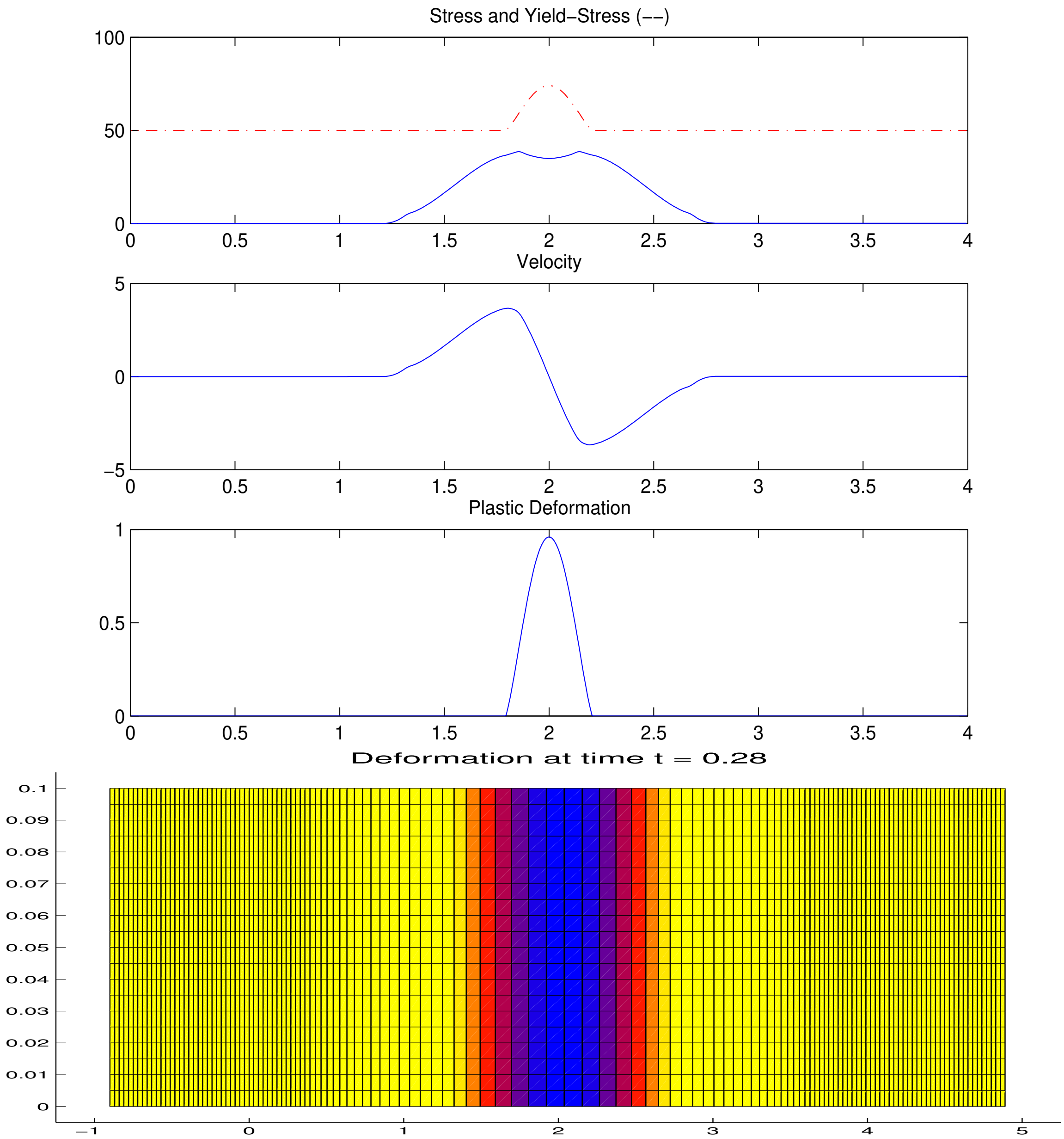

Figure 7.4: Above: Stress and Yield-Stress, Velocity, Plastic Deformation are shown in 1D and 2D (visually identical) in Lagrangian coordinates. Below: Elastic (shown by the grid) and Plastic Deformation (shown by color) in highly exaggerated Eulerian coordinates. Note how the Yield-Stress is increased via plastic expansion in the upper figure as well as the lengthening of the material in the lower (Eulerian) figure.

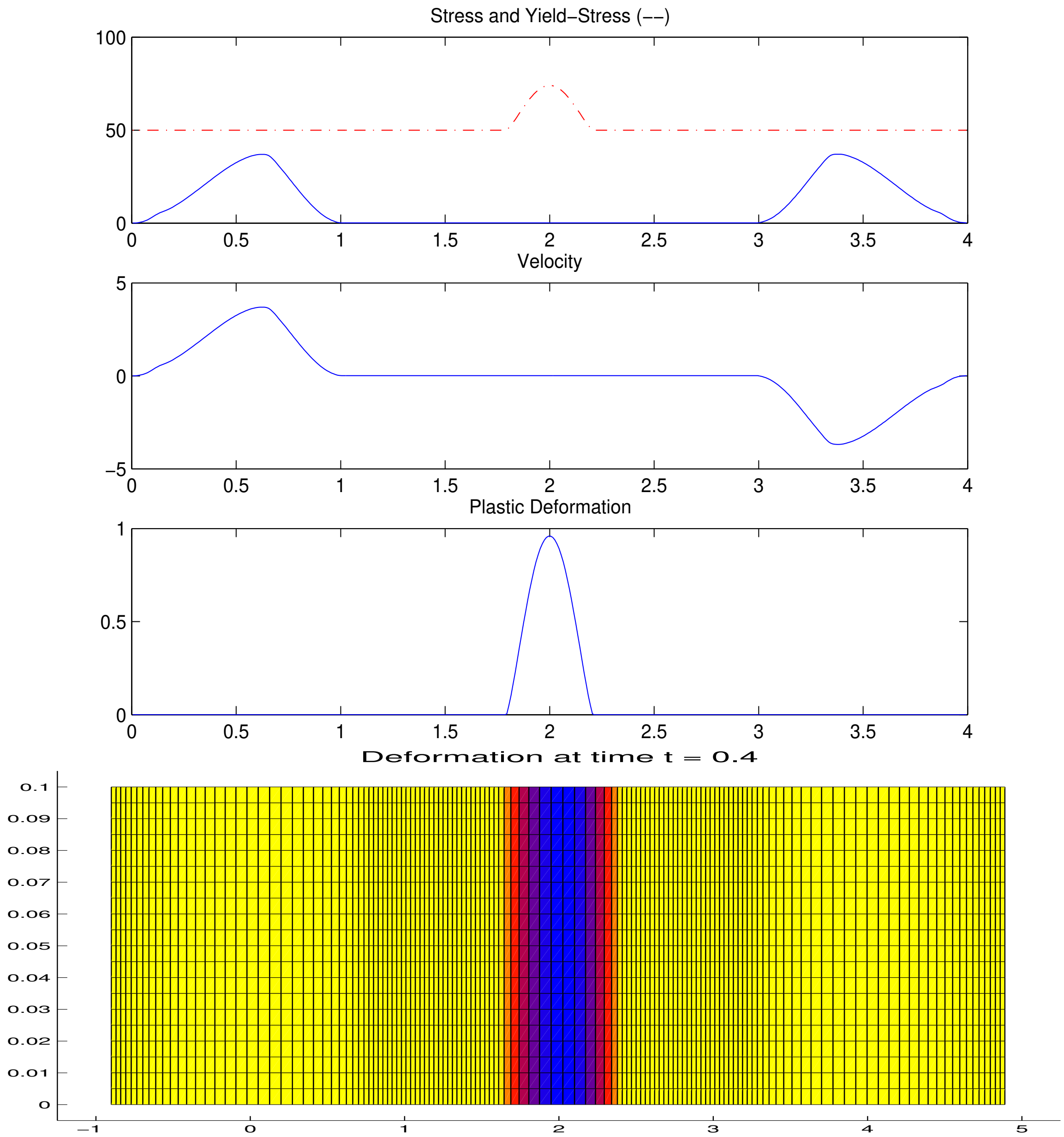

Figure 7.5: Above: Stress and Yield-Stress, Velocity, Plastic Deformation are shown in 1D and 2D (visually identical) in Lagrangian coordinates. Below: Elastic (shown by the grid) and Plastic Deformation (shown by color) in highly exaggerated Eulerian coordinates.

generated by the 1D and 2D solution methods is to constrain the 2D experiment to only have variation in the lengthwise or x-direction.

Since we want to test the 2D solution method against the 1D solution method we do not want to alter the 2D yield criterion nor the 2D yield function. To accomplish this we add the linear constraint to the 2D problem which imposes (7.3) on the solution of each call to the minimization routine. If all works as expected then this additional constraint should force the solution from the more general 2D method to only have variation in the x-direction and match the solution given by the 1D method. The imposition of this single constraint should also cause the two energy functions to give the same result. Recall that the plane-strain energy function was shown in Section 6.4.2 to be given by

$$\begin{aligned}\xi(\sigma,\pi) = [(\lambda+2\mu)((\sigma_{11}-\sigma_{11}^T)^2+(\sigma_{22}-\sigma_{22}^T)^2) - 2\lambda(\sigma_{11}-\sigma_{11}^T)(\sigma_{22}-\sigma_{22}^T) \\ +2(\lambda+\mu)(\sigma_{12}-\sigma_{12}^T)^2]/8\mu(\lambda+\mu) + \frac{1}{2}\beta_p(\pi-\pi^T)^2.\end{aligned} \tag{7.4}$$

As with the yield criterion the 1D energy function is found by imposing the relation on stress given above as 7.3. With this assumption the energy function for the 1D reduction from plane-stress is given as

$$\xi(\sigma,\pi) = \frac{(\sigma_{11}-\sigma_{11}^T)^2}{2(\lambda+2\mu)} + \frac{1}{2}\beta_p(\pi-\pi^T)^2. \tag{7.5}$$

In each of the figures, Figure 7.1-Figure 7.5, the stress, yield-stress, velocity, and plastic deformation are shown above (top three graphs) for both the 1D and 2D solutions in Lagrangian coordinates while the bottom graph shows the exaggerated elastic and plastic (color) deformation for the 2D example in Eulerian coordinates. Figure 7.1 shows the initial conditions. As in the previous 1D examples, in this example the material starts with zero deformation and both ends are pulled out and held. This generates two incoming elastic waves with amplitudes below the yield-stress until they constructively interfere. The top graph shows that initially there is zero stress everywhere and that the initial yield-stress at all points is $\sigma_y = 50$. The second graph (from the top) shows the initial velocity configuration, the third graph shows the initial plastic deformation and the bottom graph shows the initial elastic and plastic deformation in 2D. Note that in all four of the figures, Figure 7.1-Figure 7.5, the top three graphs show both the 1D results and a horizontal slice of the 2D results, which lie right on top. This shows that the 1D and 2D codes produce consistent results. Note the difference in the pulse shapes shown in this example and those shown in Section 6.6.1. Here the example shown is computed via the 1D reduction from plane-strain, while that shown in Section 6.6.1 modeled the 1D reduction from plane-stress. The two systems can be initialized to have the same elastic wave propagation with the proper choice of parameters, however it should be clear that the differences in plastic wave propagation cause the pulses to emerge from the area of plastic deformation with different shapes.

Figure 7.3 shows the examples at an early time after the elastic and plastic waves have separated. In the top graph one can see how the yield-stress is increased to match the amplitude of the plastic waves as expected. The second (from the top) graph shows the velocity distribution at this time and in the third graph one can see how the material is plastically deformed only in the region where the plastic waves have propagated. The bottom graph shows the exaggerated deformation of the material both elastically and plastically. Note that both the elastic and plastic waves cause expansion and that color represents the amount of plastic deformation in each cell. Figure 7.4 and Figure 7.5 show the computation at a further intermediate time and at the final time. Since the solution to this problem can be computed exactly, the final time has been set so that the elastic waves reach the end of the domain at the end of the computation as can be seen in Figure 7.5. It should be clear that by imposing the additional constraint (7.3) on the 2D example an excess of stress σ_{22} in the y-direction is generated which keeps the 2D material from being compressed in the vertical direction. This excess value of σ_{22} is what allows any 1D slice of the 2D experiment to be compared exactly with the 1D results. In the following section the same 2D example is re-computed with two modifications. First, the constraint (7.3) is removed from the minimization routine to allow for fully 2D behavior and secondly the initial conditions are modified so that the material is pulled apart from the ends instead of from the center. Recall that the 1D analog of this experiment was studied in Section 6.6.1.

7.1.2 Example of 2D elastic-plastic interference

In this section we explore the same 2D example as above but without the constraint on the stress that was imposed by (7.3) and instead impose no-traction boundary conditions on the edges. The six figures, Figure 7.6-Figure 7.11, show the 2D version of the 1D problem studied in Section 6.6.1. Consider again the edge on view of the table top. In either example we will have the same "view" of a 2D slab of material. In this section we examine what happens when to the material when both ends are pulled out and held. When the ends are pulled out, by giving each end an initial tug and then holding, elastic waves are generated that move inward from each end. If the tug is not too hard, then the amplitude of the induced wave is low enough that the wave propagates elastically as it moves to the right. Similarly a pull to the right, of the proper strength, on the right end of the slab generates an elastic leftward moving wave. As was seen in Figure 6.30-Figure 6.32, the constructive interference of these two elastic pulses exceeds the yield-stress and causes deformation and permanent plastic expansion in the x direction.

Note that in the following twelve figures the computation was performed on a 400 by 40 grid. The figures show (greatly exaggerated) displacement by plotting grid-lines and plastic deformation is shown as color. To avoid graphical resolution issues "the grid" is shown as 100 by 20 while all $16,000$ cells are used to plot the color. This way of plotting allows the grid to be shown without unacceptable grid-line density in some unexpanded or compressed regions but at the cost of the appearance of missing grid-lines in the expanded regions.

Expansion in the x direction for the 2D example discussed here causes compression in the y direction. Figure 7.6 shows the two initial waves as they propagate inwards towards the center of the slab. Note the expansion in the x-direction coupled with the compression in the y-direction. Also note that there is no coloring or shading (which represents plastic deformation in all of these figures) indicating that the waves are purely elastic. The waves start to interfere constructively as they reach the center of the slab. Figure 7.7 shows that when the additive amplitude of the two waves exceeds the yield-criterion the slab also undergoes plastic deformation. As is expected the area of largest amplitude interference (the center) undergoes plastic deformation first.

Figure 7.8 shows the two waves near maximum interference. Here one can see how the slab is elastically and plastically deformed by stretching or expansion in the direction of propagation while at the same time undergoing both plastic and elastic compression in the transverse direction. Figure 7.9 shows the slab at a later time where the waves have begun to leave the area of interference. Here one can see that relative to the previous time, the slab has regained more of its original configuration as the elastic part of the deformation moves out with the waves. The final two figures, Figure 7.10 and Figure 7.11, show the slab at later times. First, Figure 7.10 shows a snapshot of the waves just after they have ceased to interfere. Here one can see that the center of the slab has been permanently deformed by the passing of the two waves and that, as expected in this example, the area of greatest plastic deformation is the center of the slab. Figure 7.11 shows the slab after the two waves have moved at least a full wavelength away from the area of plastic deformation. In Figure 7.11 one can see how cells in the material neighboring the plastically deformed part of the slab have returned to a state of little or no deformation relative to the nearby cells in the plastically deformed region. In the following section we repeat the previous example but add a layer in the center of the slab which can only be elastically deformed. As we will see, this leads to a dramatically different plastic deformation pattern.

7.1.3 Example of elastic-plastic interference with a central elastic layer

The following six figures show the exact same example explored above but with with the addition of a layer of elastic material in the center of the slab. As with the previous example we begin with an undeformed 2D slab in the context of plane-strain. Recall that the initial conditions consist of pulling each end of the slab out and then holding the ends at rest. Here again we use no traction boundary conditions on the upper and lower edges. Recall that this means that the boundary can not be sheared and that the component of stress normal to the boundary (σ_{22}) is zero. As with the previous example, when the ends of the slab are pulled out elastic expansion waves are generated and move in to the right from the left edge and in to the left from the right edge. The amplitude of these waves are initialized so that each wave propagates in a purely elastic manner until the two waves constructively interfere. As with the previous example, the constructive interference of the waves causes the combined stress values to exceed the yield condition. Unlike the previous example which was homogeneous, the center of this slab has a layer of material with a very large yield-surface. Even at maximum constructive interference the stress values never exceed yield in this purely elastic layer. The following figures show how the inclusion of this layer drastically alters the deformation of the slab.

Figure 7.12 shows the two initial waves as they propagate inwards towards the center of the slab. Note that at this point in time, no plastic deformation has occurred and Figure 7.12 and Figure 7.6 are identical. Recall that expansion in the x-direction coupled with the compression in the y-direction and that there is not yet any coloring or shading indicating that the waves are purely elastic. As with the previous example, the waves start to interfere constructively as they reach the center of the slab. Figure 7.13 shows that when the additive amplitude of the two waves exceeds the yield-criterion the slab undergoes plastic deformation which is much different than that shown in Figure 7.7. Here one can see that while the layer in the center deforms in a purely elastic way, the neighboring regions are deformed both plastically and elastically. Figure 7.14 shows the two waves near maximum interference at the same point in time as the previous example shown in Figure 7.8. Here one can see how the plastically deformable section of the slab is much less resistant to deformations in the transverse direction then the purely elastic layer. Figure 7.15 shows the slab at a later time where the waves have begun to leave the area of interference. Note the compression of the elastic center of the slab compared to that shown at the same time in the previous example in Figure 7.9.

The final two figures, Figure 7.16 and Figure 7.17, show the slab at later times. First, Figure 7.10 shows a snapshot of the waves just after they have ceased to interfere. Here one can see that the elastic center of the slab has been nearly restored to the original configuration while the neighboring regions have been permanently deformed. As in the previous example, Figure 7.17 shows the slab after the two waves have moved at least a full wavelength away from the area of plastic deformation. In Figure 7.17 one can see how cells interior to the plastically deformed part of the slab have returned to a state non-zero elastic strain which causes these cells to be elastically expanded. Presumably this is caused by the neighboring material which has been plastically deformed in a new "bent" configuration. In the following section we explore our final 2D example. There we will also see how the plastic deformation of an elastic solid affects the nearby purely elastic regions.

7.1.4 Focused Expansion Wave Impinging on a Plastically Deformable Disc

Here we return to an example that is very similar to that shown in the introduction. In this example we use a phased array boundary condition to generate three focused expansion waves. The focal point of this wave is the center of a plastically deformable disc embedded in a material that is purely elastic. In the following figures we show how the expansion waves deform the disc both elastically and plastically as well as elastically deforming the surrounding material. In the following figures we show the waves as they move to the right at four different points in time. In each figure we show the exaggerated elastic and plastic deformation on the right and the normal stress σ_{11} in the x-direction on the left. Note that while this computation was done on a 400 by 400 grid, the exaggerated deformation is shown on a much coarser grid. Recall that color or shading in the grid figures represents plastic deformation and is shown with the full 400 by 400 grid. Note that in each of the four figures, the left-hand shows the exaggerated deformations of the material in Eulerian coordinates while the right-hand shows σ_{11} in Lagrangian coordinates.

Figure 7.18 shows the initial configuration of the disc embedded in an elastic solid which can not undergo plastic deformation. Here we see the expansion wave just before it hits the disc from the left. Figure 7.19 shows the deformation pattern on the left and the σ_{11} stress on the right just before the second wave hits the disc. Note how the expansion wave has nearly focused, and recall that the focal point is set to be the center of the disc. Figure 7.20 shows the experiment just as the third wave has entered the plastically deformable disc. Here in the left-hand plot we see how the disc is pulled out or "expanded" to the left. Note the increase in size of the grids cells corresponds to the darker (more plastically deformed) regions. On the right-hand plot we see how the wave is drastically slowed down (de-focused) in the region that is undergoing plastic deformation. Figure 7.21 shows a later point in time when the third wave has nearly exited the region of the disc. Again in the left-hand plot we can see the exaggerated deformation of the disc. Here we see how each successive wave causes the region of plastic deformation to migrate further and further to the right. On the right we see that the expansion wave is nearly completely de-focused by the time it exits the disc. Note also that the center of the disc is now undergoing a large elastic compression relative to its initial configuration. Figure 7.22 shows the initial and final configurations of the disc before and after the three waves have entered and exited the computational domain. Note the overall expansion in the x direction causes a compression in the y direction.

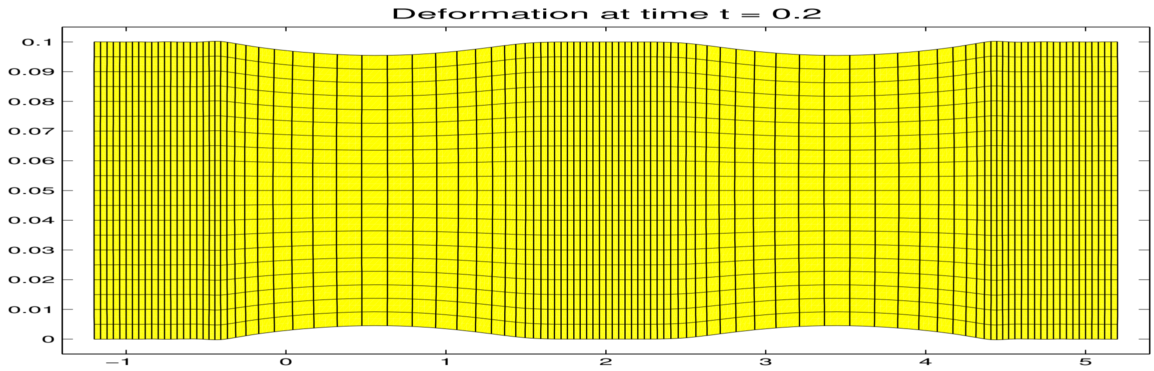

Figure 7.6: Two incoming elastic waves. The wave on the left is moving toward the right and the wave on the right is moving toward the left. Note that these waves cause elastic expansion in the x direction and compression in the y direction. As the amplitude of each wave does not exceed the yield criterion, the waves propagate elastically until they interfere (below).

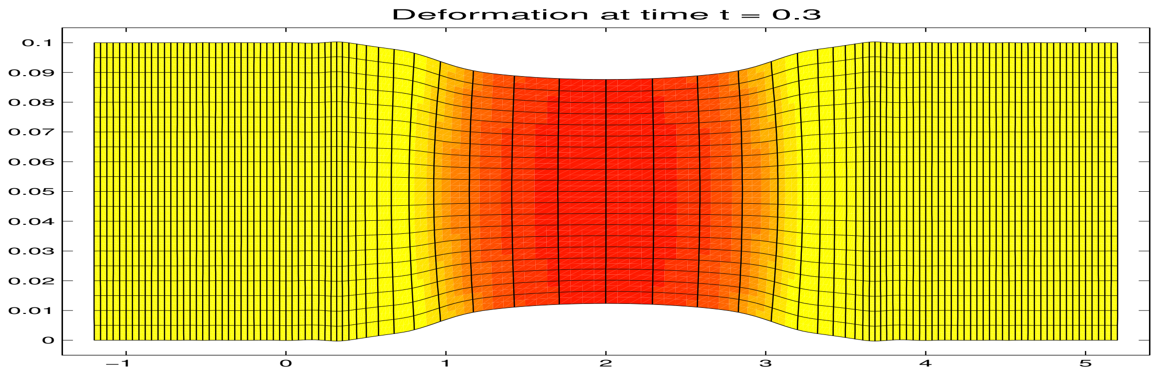

Figure 7.7: Here the waves are still moving inward and have begun to constructively interfere and cause plastic deformation (denoted by the color).

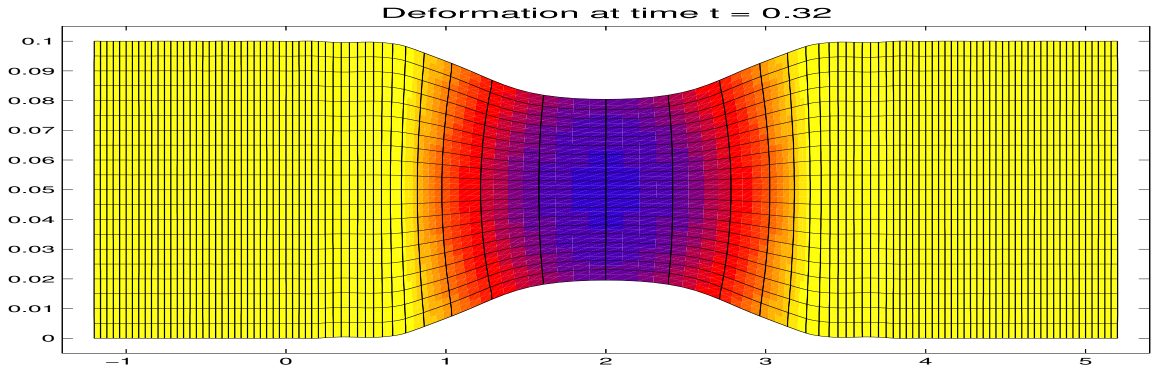

Figure 7.8: In this figure the waves have nearly reached their maximum constructive interference and the center of the "slab" is stretched in the x-direction and compressed in the y direction both elastically and plastically.

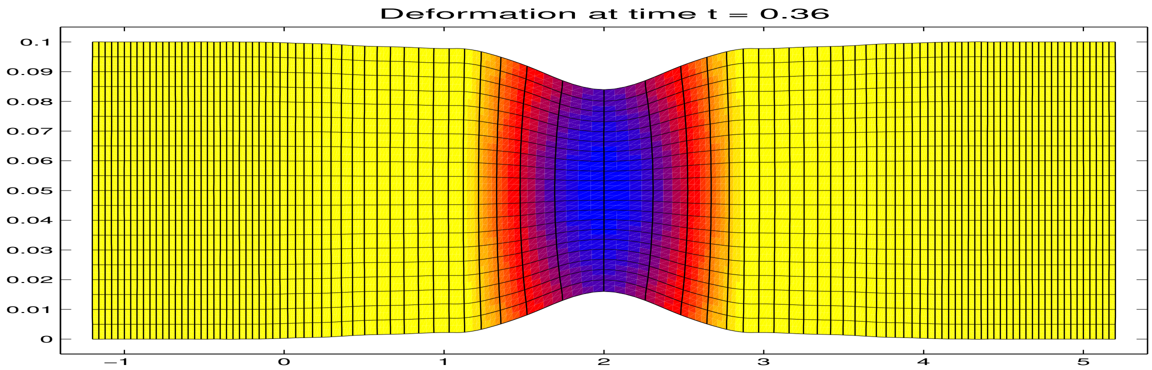

Figure 7.9: In this figure the two waves have started to pass though each other and now the expansion wave on the left is moving toward the left edge while the expansion wave on the right is moving toward the right edge. Note also that the center of the material has compressed relative to the previous figure as the elastic part of the expansion moves out with the waves.

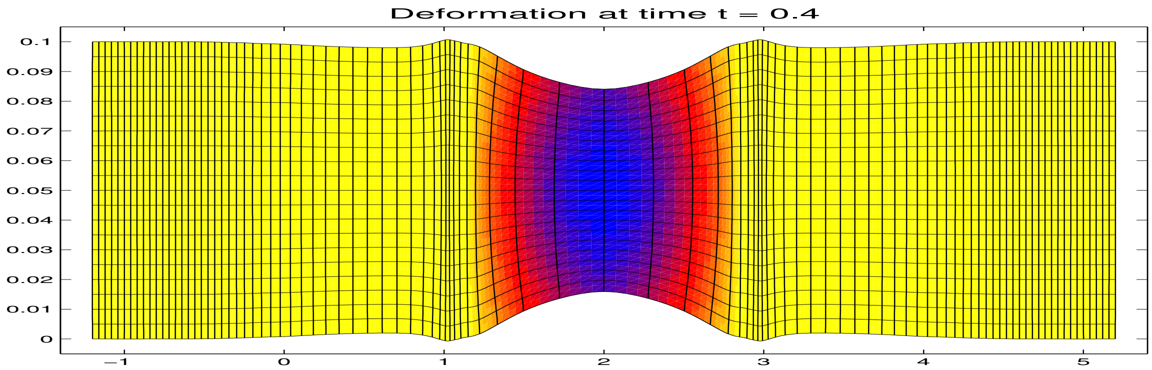

Figure 7.10: Here one can see that the expansion waves have moved out of the region of constructive interference and that the residual deformation is purely plastic.

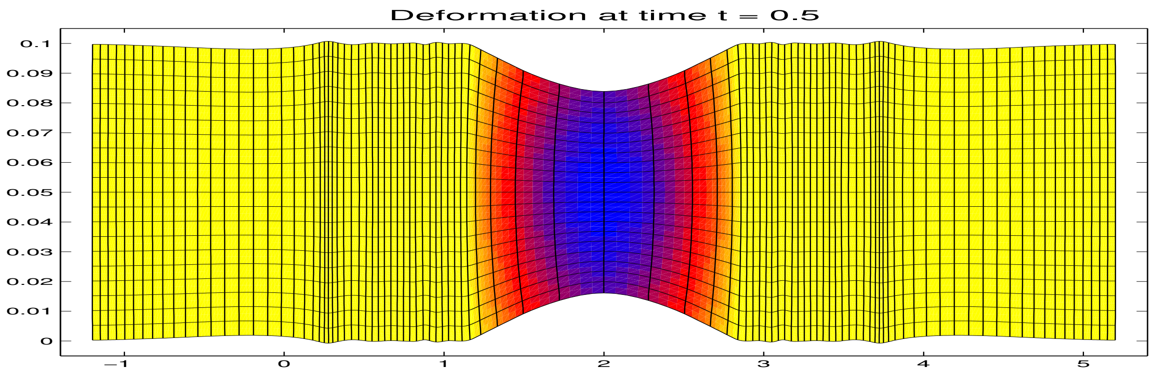

Figure 7.11: In this final time one can see how the material between the two pulses was either permanently plastically deformed or only temporarily elastically deformed. One can also see that, as expected, the cells with more plastic deformation have a darker color. Recall that color represents a measure of the total plastic deformation in each cell.

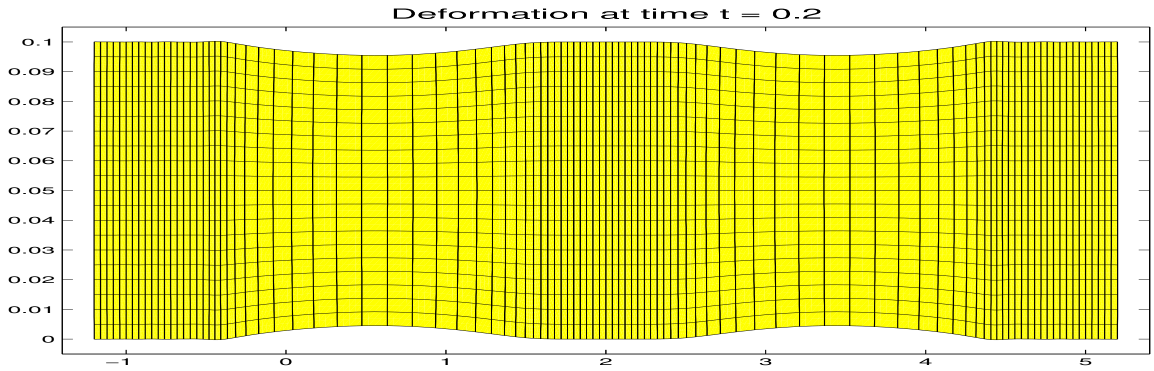

Figure 7.12: As with the previous example we have two incoming elastic (expansion) waves. The wave on the left is moving toward the right and the wave on the right is moving toward the left.

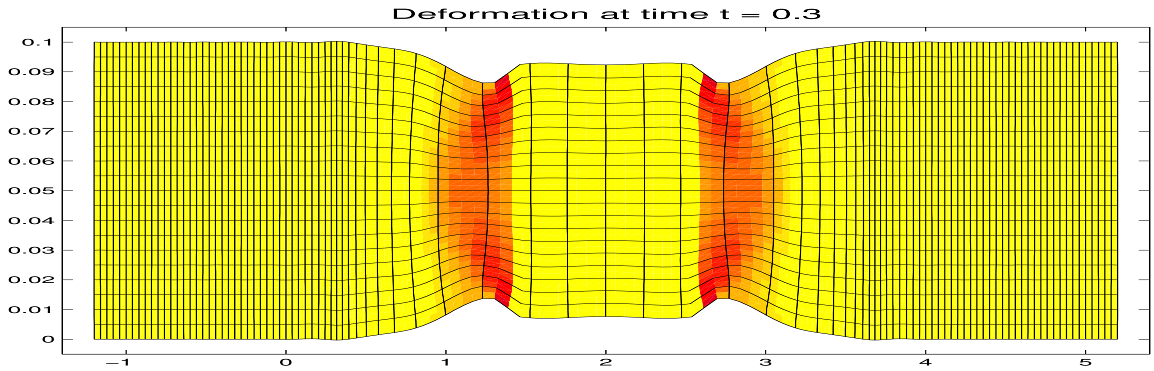

Figure 7.13: Unlike the previous example this material does not have a homogeneous yield-stress. Here we have a layer of purely elastic material embedded in the center of a material with a low elastic yield-stress. At this time step we can see the waves as they elastically deform the region with hi yield-stress while at the same time the neighboring regions are plastically deformed.

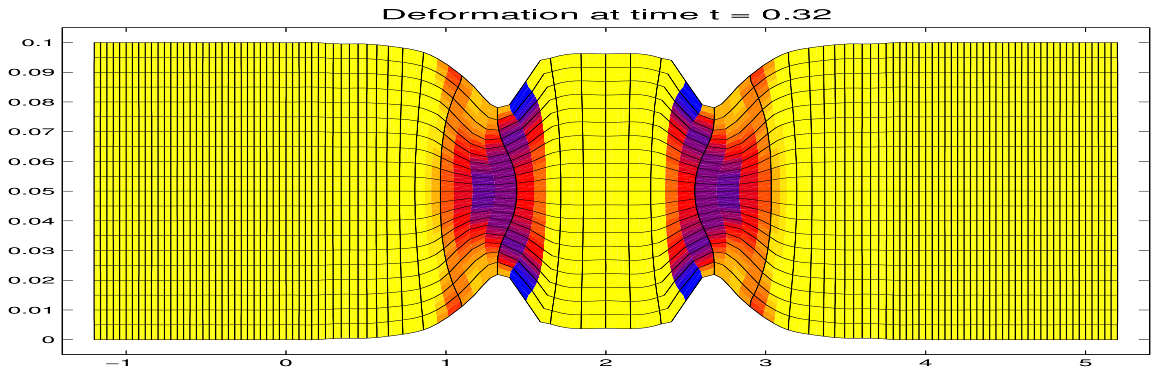

Figure 7.14: In this figure the waves have nearly reached their maximum constructive interference. Here we can see how the purely elastic center of the “slab” has caused a much different deformation pattern in the nearby material relative to the previous example.

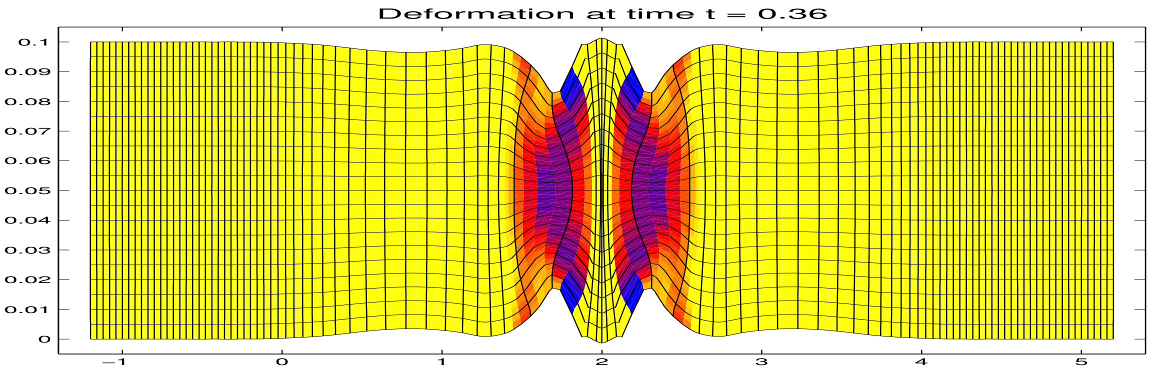

Figure 7.15: In this figure the two waves have started to pass though each other and the expansion wave on the left is moving toward the left while the expansion wave on the right is moving toward the right. Note also that the center of the material has compressed much more then in the previous example do to the neighboring regions that have been plastically expanded.

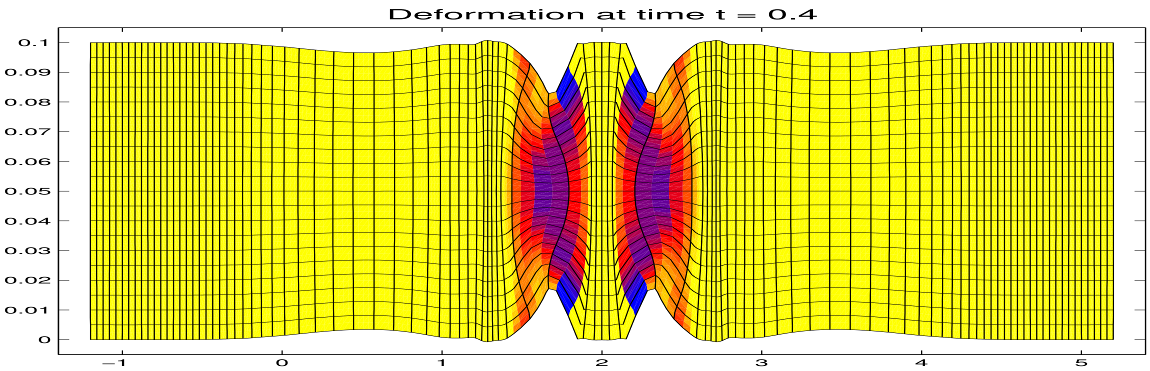

Figure 7.16: Here the expansion waves have moved out of the region of constructive interference. While the residual deformation is still purely plastic it is in a much different configuration then the previous example.

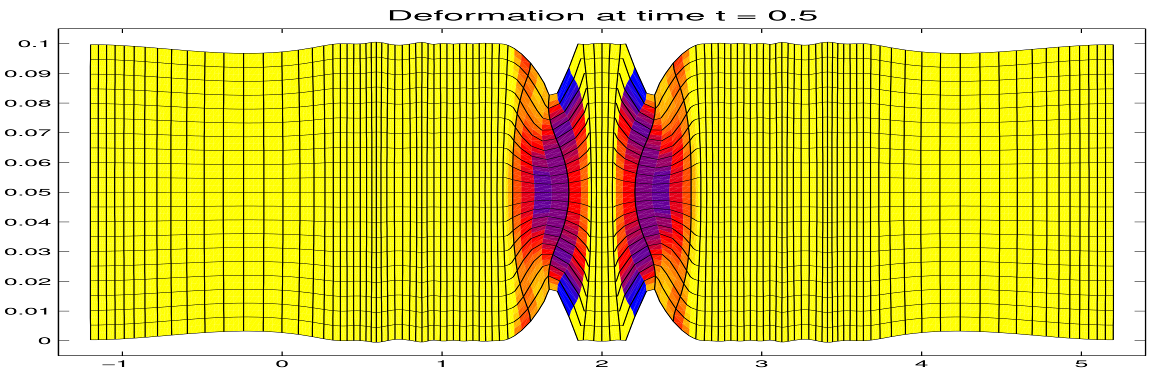

Figure 7.17: Here one can see how the material between the two pulses was either permanently plastically deformed or only temporarily elastically deformed (center layer). Unlike the previous example, here we see that the plastic deformation has a less intuitively predictable structure.

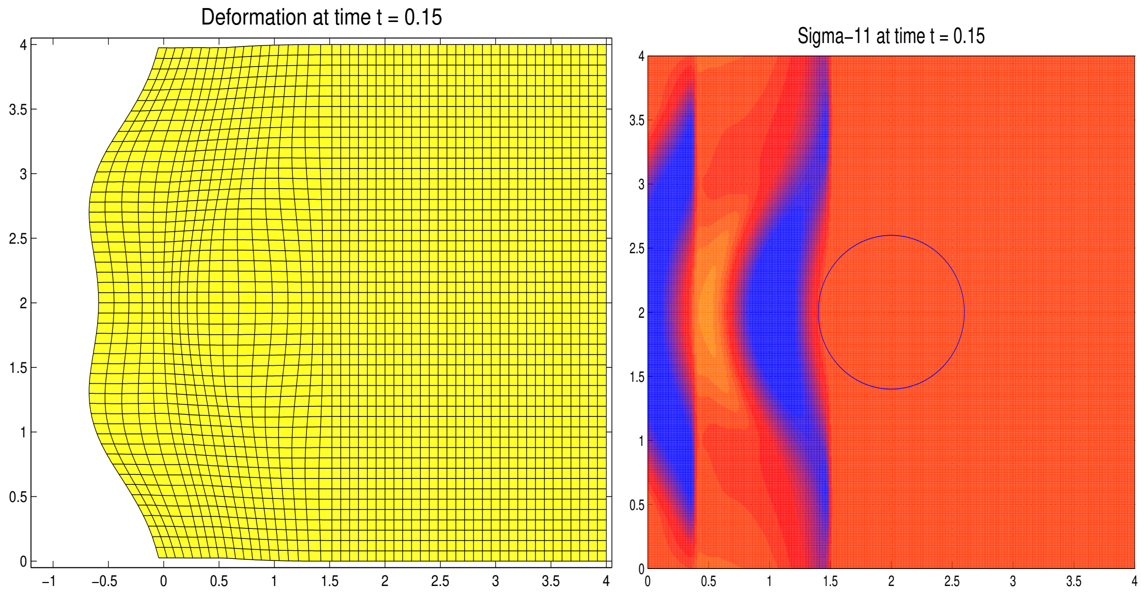

Figure 7.18: On the left the initial undeformed grid is shown just before the first expansion wave hits the disc from the left. On the right we see a plot of σ_{11}, the normal stress in the x-direction.

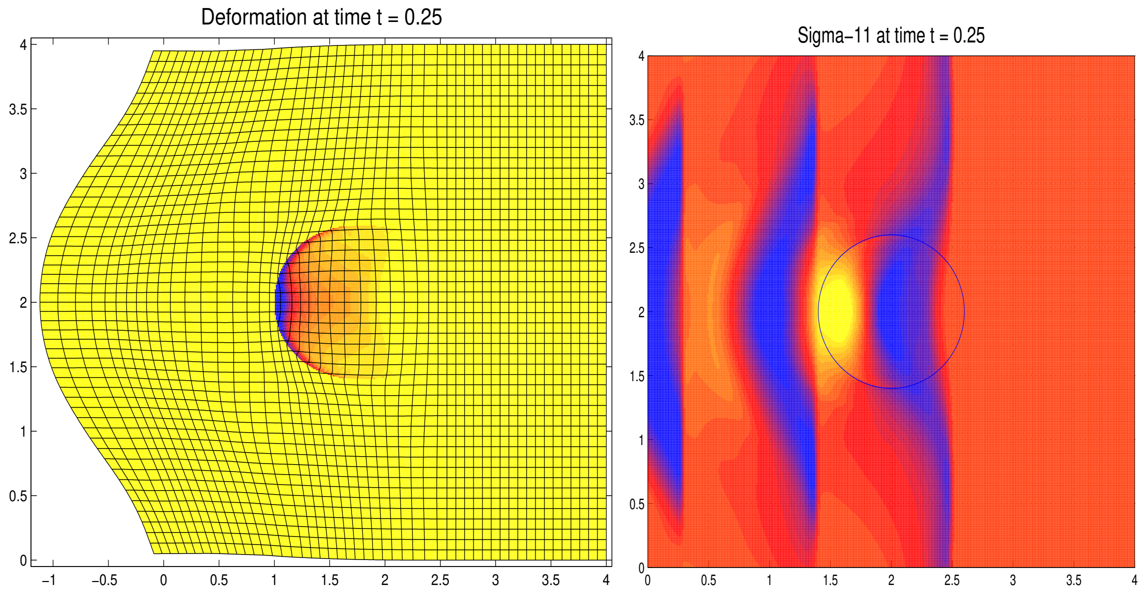

Figure 7.19: Here again on the left we see the exaggerated deformation of the material just before the second wave hits the plastically defomrable disc. On the right we again see the normal stress as it has nearly reached the focal point.

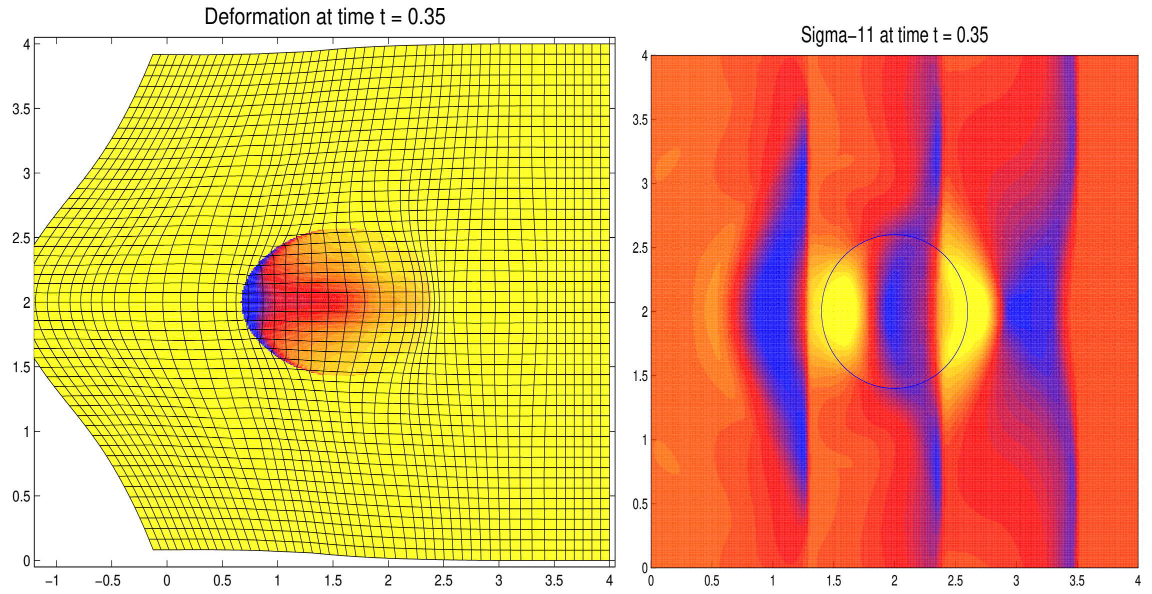

Figure 7.20: Here we see a snapshot at the time just before the third wave first enters plastically deformable disc. Note that the left-hand figure shows both how this disc is deformed as well as the regions of greatest plastic deformation (darker).

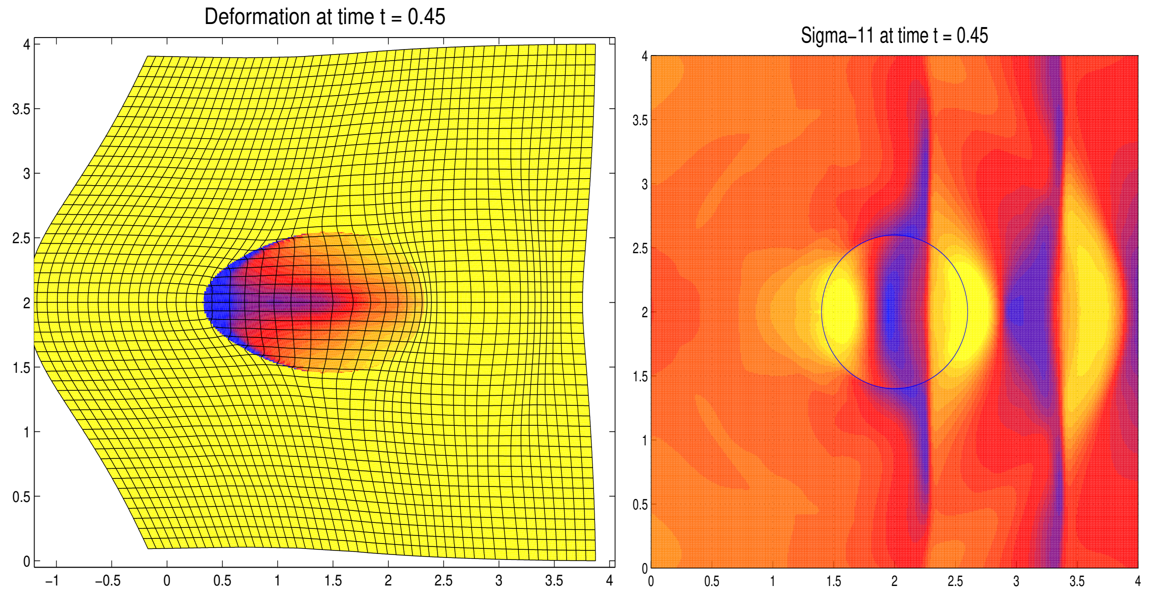

Figure 7.21: Here the first two waves have completely exited the plastically deformable region. Note that as each wave interacts with the deformable disc, the region of plastic deformation moves further in to the right. As all waves have the same amplitude, those that hit the disc first deform the left side of the disc much more then waves that come later. As such, the second and third wave cause the area of plastic deformation to move further to the right.

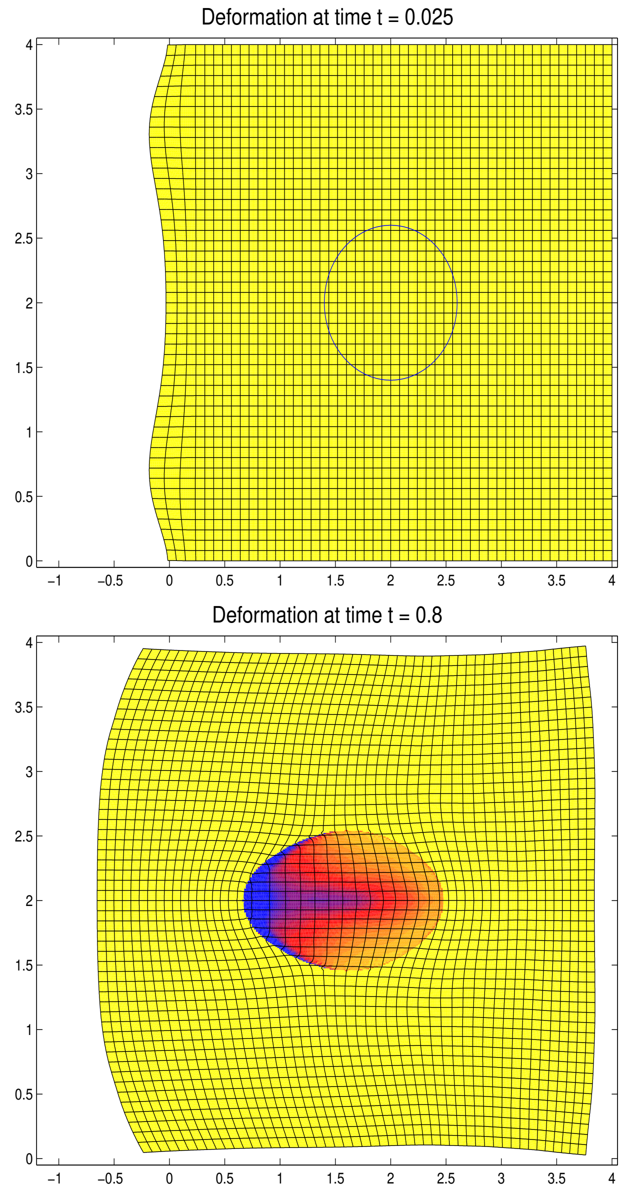

Figure 7.22: Here we see the initial and final configurations of the disc. In the upper picture the first incoming wave has not yet neared the disc and there is no plastic deformation. In the lower picture one can see the disc after the three waves have completely exited the computational domain. It is important to note that the deformation shown in all these figures is greatly exaggerated.

Chapter 8

CONCLUSIONS

8.1 Summary

In this work we have developed a numerical scheme capable of simulating time dependent elasto-plastic behavior with damage via the modeling of wave propagation. In Chapter 2, the three-dimensional linear elastic system is derived via a combination of Newton's second law, the kinematic condition, and a constitutive equation. The 3D linear elastic system is reduced to two dimensions via both the plane-strain and plane-stress assumptions. The one-dimensional linear elastic system as well as the 2D and 1D linear acoustic systems are all derived via further reductions of the 2D elastic system.

In Chapter 3, the one-dimensional linear acoustic system is used to introduce the numerical wave-propagation update software: CLAWPACK. Neighboring cell-averaged values of the state variables along with the governing differential equation define Riemann problems at each cell interface. CLAWPACK solves Riemann problems at cell interfaces to generate waves. These waves are used in an update formula in conjunction with second-order correction terms and wave limiters to create a highly effective scheme for modeling wave-propagation.

Chapter 4 and 5 have examples of 1D and 2D acoustics in a heterogeneous material that are used to show how the code works in the presence of material discontinuities. Standard limiting methods are shown to fail in the case of periodic media and a new limiting method based on reflection and transmission coefficients is introduced to correct the problem. Examples of acoustics in random media are explored and used to further validate the ability of the algorithm to handle wave propagation in discontinuous media.

Plasticity and damage are introduced in Chapter 6 in the context of one-dimensional elasticity. An exact elasto-plastic 1D-Riemann solution is introduced and used as the basis for generating numerical solutions to several 1D examples. In one dimension, the exact elasto-plastic Riemann solution is extended to solve problems that include both non-linear plasticity and damage. Solutions generated by the exact Riemann scheme are used as a basis of comparison and validation for an alternative solution method which is based on minimization techniques. Several 1D elasto-plastic examples are used to show how both solution methods are capable of solving problems in a variety of different physical regimes and with different kinds of heterogeneities.

Chapter 7 shows how the minimization solution technique can be extended to solve 2D elasto-plastic examples. First we use a special 2D example to compare results between the 1D and 2D solution methods. We then explore several examples that are fully 2D and show results given by the 2D solution method. Here we have an example of two expansion waves that constructively interfere to create a permanent plastic deformation in the center of a thin plate. We also show how a series of focused waves cause successive plastic deformation to propagate into a deformable disc in much the same way we assume must happen in lithotripsy. In this example we show that the solution method can be used in the presence of material discontinuities, and can properly model material interfaces that are not aligned with the grid.

8.2 Plans for the Future

8.2.1 Two-Dimensional Non-Linear Plasticity and Damage

In the future we hope to add to this work in several ways. While in one dimension we have demonstrated how the solution method applies to examples that include damage and non-linear plasticity, this work does not fully develop solution procedures for these two added complexities in two and three dimensions. As described above, non-linear plasticity and damage are two separate effects. We should be able to include both the effects of damage and non-linear plasticity into a multi-dimensional model by adding extra constraints to the minimization problem that is currently used for the 2D elasto-plastic system. Recall that the minimization techniques use strictly linear Riemann problems to construct the solutions. Since the Riemann solutions for 3D linear elasticity are not intrinsically any more difficult to construct then Riemann solutions for 2D elasticity, there should not be any added complexity in extending a working 2D solution technique to 3D.

8.2.2 Three-Dimensional Elasto-Plasticity and AMR

To model the 3D elasto-plastic system, we must first have a reliable 3D wave propagation algorithm and an effective way to cut down run time. CLAWPACK has been designed to model 3D wave propagation of hyperbolic systems. Recall that in 3D, the linear elastic system is described by nine state variables and three coefficient matrices. These matrices each have nine eigenvalues and eigenvectors corresponding to two pressure waves and four shear waves along with three zero speed waves. Even in three dimensions, the Riemann solutions are straight forward to construct and the only difficulty comes with the added complexity of the yield condition and energy function. However, our 1D and 2D results were derived from the general 3D energy function and yield constraints. As such, all that is needed to solve examples of 3D elasto-plasticity is already in this work. To aid in the speed of calculation we hope to adapt the solution techniques currently used in 2D to include AMR. Adaptive mesh refinement uses higher refinement in regions of activity, thus greatly decreasing the total work done on the types of calculations that tend to arise in examples of wave propagation. Note that all the algorithms we have used are written in such a way as to be directly extended to the AMRCLAW and BEARCLAW frameworks. See `http://www.amath.washington.edu/~rjl/` for more information. This software allows for the extension of all our work to include both the adaptive mesh refinement and parallelization abilities of BEARCLAW. The challenge to include AMR in an elastic-plastic model will be to properly address the way plastic deformation and the yield stress are averaged when refining or coarsening a given grid.

8.2.3 Application to Realistic Problems and Validation of Solution via Experimentation

The most important work to do in the future is to apply the methods developed here to realistic problems arising in specific applications. An additional question that will need to be addressed in any specific application is the proper constitutive equation. The goal would be to first use experimentation to properly define the constitutive relation a given material should satisfy in the force range of interest. We would then need to include this specific constitutive relation into our model and then set up both physical and numerical experiments in such a way that the results could be compared and used as verification of the numerics. We have given several examples that validate the accuracy of our solution methods. Further sources of validation will require comparison with results from other numerical methods and experimentation.

BIBLIOGRAPHY

[1] A. Bensoussan, J.L. Lions, and G. Papanicolaou. *Asymptotic Analysis for Periodic Structures.* North-Holland, Amsterdam, 1978.

[2] A. Berezovski, J. Engelbrecht, and G. A. Maugin. Thermoelastic wave propagation in inhomogeneous media. *Archive of Applied Mechanics*, pages 694–706, 2000.

[3] A. Berezovski and G. A. Maugin. Simulation of thermoelastic wave propagation by means of a composite wave-propagation algorithm. *J. of Computational Physics*, pages 249–264, 2001.

[4] J. J. Burk and V. Wiess. Shock waves and the mechanical properties of solids. In *Proddeedings of the 17th Sagamore Army Materials Research Conference.*, pages 155–185, 1970.

[5] R. Burridge, M. V. de Hoop, L. Le, and A. Norris. Waves in stratified viscoelastic media with microstructure. *J. Acoustical Society of America*, pages 2884–2894, 1993.

[6] R. Burridge, G. S. Papanicolaou, and B. S. White. One-dimensional wave propogation in a highly discontinuous medium. *Wave Motion*, pages 19–44, 1988.

[7] R. E. Caflisch, M. J. Miksis, G. C. Papanicolaou, and L. Ting. Effective equations for wave propagation in bubbly liquids. *J. Fluid Mechanics*, pages 259–273, 1985.

[8] G. T. Camacho and M. Ortiz. Computational modelling of impact damage in brittle materials. *Int. J. Solids Structures*, pages 2899–2938, 1996.

[9] A. Capsoni and L. Corradi. A plane strain formulation of the elastic-plastic constitutive law for hardening von Mises materials. *Int. J. Solids Structures*, 32:3515–3531, 1995.

[10] A. Capsoni and L. Corradi. Variational formulations for the plane strain elastic-plastic problem for materials governed by the von mises criterion. *International Journal of Plasticity*, 12:547–560, 1996.

[11] T. J. Chen and C. H. Cooke. On the Riemann problem for liquid or gas-liquid media. *International Journal for Numerical Methods in Fluids*, pages 529–541, 1994.

[12] W. F. Chen. Concrete plasticity: macro and microapproaches. *Int. J. Mechanical Science*, pages 1097–1109, 1993.

[13] C. C. Church. A theoretical study of cavitation generated by an extracorporeal shock wave lithotripter. *J. Acoustical Society of America*, pages 215–227, 1989.

[14] W. C. Elmore and M. A. Heald. *Physics of Waves.* Dover, 1985.

[15] G. Etse and K. Willam. Failure analysis of elastoviscoplastic material models. *J. of Engineering Mechanics*, pages 60–69, 1999.

[16] T. Fogarty. Wave-propagation algorithms for acoustics in a rapidly varying heterogeneous medium. Masters' thesis, University of Washington, 1997. (`ftp://amath.washington.edu/pub/rjl/students/fogarty:masters.ps.gz`).

[17] T. Fogarty and R. J. LeVeque. High-resolution finite-volume methods for acoustic waves in periodic and random media. *Journal of The Acoustical Society of America*, pages 17–28, 1999.

[18] E. Godlewski and P. Raviart. *Numerical Approximation of Hyperbolic Systems of Conservation Laws.* Springer, 1996.

[19] W. Han and B. D. Reddy. *Plasticity, Mathematical Theory and Numerical Analysis.* Springer, 1999.

[20] L. A. Janosik and S. F. Duffy. A viscoplastic constitutive theory for monolithic ceramics. *Journal of Engineering for Gas Turbines and Power*, pages 155–161, 1998.

[21] J. B. Jones-Oliveira. Transient analytic and numerical results for the fluid-solid interaction of prolate spheroidal shells. *J. Acoustical Society of America*, pages 392–407, 1996.

[22] J. Kevorkian and D. L. Bosley. Multiple-scale homogenization for weakly nonlinear conservation laws with rapid spatial fluctuations. *Stud. Appl. Math.*, 101:127–183, 1998.

[23] A. S. Khan and S. Huang. *Continuum Theory of Plasticity.* John Wiley and Sons, Inc., 1995.

[24] H. Lammer and Ch. Taskmakis. Discussion of coupled elastoplasticity and damage constitutive equations for small and finite deformations. *International Journal of Plasticity*, 16:495–523, 2000.

[25] H. Lammer and Ch. Tsakmakis. Discussion of coupled elstoplasticity and damage constitutive equations for small and finite deformations. *Plasticity*, pages 285–308, 2000.

[26] L. D. Landau and E. M. Lifshitz. *Theory of Elasticity.* Pergamon Press, 1959.

[27] J. O. Langseth and R. J. LeVeque. A wave propagation method for three-dimensional hyperbolic conservation laws. Revised and accepted, 2000, J. Comput. Phys.

[28] P. D. Lax and X. D. Liu. Solution of two dimensional Riemann problem of gas dynamics by positive schemes. *SIAM J. Sci. Comput.*, 19:319–340, 1998.

[29] T. Lay and T. C. Wallace. *Modern Global Seismology.* Academic Press, 1995.

[30] E. H. Lee and D. T. Liu. Finite-strain elastic-plastic theory with application to plane-wave analysis. *Journal of Applied Physics*, pages 19–27, 1967.

[31] E. H. Lee and Wei H. Yang. On waves in composite material with periodic structure. *SIAM J. Appl. Math.*, 25:492–499, November 1973.

[32] J. Lemaiture. *A Course on Damage Mechanics.* Springer, 1996.

[33] R. J. LeVeque. *Numerical Methods for Conservation Laws.* Birkhauser, 1992.

[34] R. J. LeVeque. Wave propagation algorithms for multi-dimensional hyperbolic systems. *J. Comput. Phys.*, 131:327–353, 1997.

[35] R. J. LeVeque. *Finite Volume Methods for Conservation Laws and Hyperbolic Systems.* To be published by Cambridge University Press, Draft Version 2001.

[36] R. J. LeVeque and D. S. Bale. Wave propagation methods for conservation laws with source terms. In *7'th Intl. Conf. on Hyperbolic Problems, Zurich*, pages 9–13, 1998.

[37] X. Lin and J. Ballmann. A Riemann solver and second-order Godunov method for elastic-plastic wave propagation in solids. *Int. J. of Impact Engng.*, pages 463–478, 1993.

[38] X. D. Liu and P. D. Lax. Positive schemes for solving multi-dimensional hyperbolic systems of conservation laws. *Computational Fluid Dynamics Journal*, 5:133–156, 1996.

[39] G. H. Miller and P. Colella. A high-order Eulerian Godunov method for elastic/plastic flow in solids. Submitted to Journal of Computational Physics, 2000.

[40] M. Ortiz. A constitutive theory for the inelastic behavior of concrete. *Mechanics of Materials*, pages 67–93, 1985.

[41] G. Papanicolaou. Mathematical problems in geophysical wave propagation. *Documenta Mathematica*, 1998.

[42] A. Philipp, M. Delius, C. Scheffczyk A. Volgel, and W. Lauterborn. Interaction of lithotripter-generated shock waves with air bubbles. *J. Acoustical Society of America*, pages 2496–2509, 1993.

[43] B. J. Plohr and D. H. Sharp. A conservative formulation for plasticity. *Adv. Appl. Math*, 13:462–493, 1992.

[44] N. Ramakrishnan, K. M. Singh, R.K.V. Suresh, and N. Srinivasan. An algorithm based on the total-elastic-incremental-plastic strain for large deformation plasticity. *Journal of Materials Processing Technology*, pages 190–199, 1999.

[45] K. Rink, G. Delacretaz, G. Pittomils, R. Boving, and J. P. Lafaut. Incidence of cavitation in the fragmentation process of extracorporeal shock wave lithotriptors. *Applied Physics Letters*, pages 2596–2598, 1994.

[46] E. Sanchez-Palencia. *Non-Homogeneous Media and Vibration Theory.* Springer-Verlag,Berlin Heidelberg New York, 1980.

[47] F. Santosa and W. W. Symes. A dispersive effective medium for wave propagation in periodic composits. *SIAM J. Appl. Math.*, 51:984–1005, 1991.

[48] M. A. Van Schaack, J. M. Harris, and K. P. Bube. Crosswell reflection traveltime tomography: a field data demonstration. In *65th Annual International SEG Meeting*, pages 65–68, 1995.

[49] J. C. Simo and T. J. R. Hughes. *Computational Inelasticity.* Springer, 1998.

[50] J. C. Simo and M. Ortiz. A unified approach to finite deformation elstoplastic analysis based on the use of hyperelastic constitutive equations. *Computer Methods in Applied Mechanics and Engineering*, pages 221–245, 1985.

[51] Sokolnikoff. *Mathematical Theory of Elasticity.* Brown University, 1941.

[52] H. J. Stam and A. T. De Hoop. Theoretical considerations on a finite-element method for the computation of three-dimensional space-time elastodynamic wave fields. *Wave Motion*, pages 67–80, 1990.

[53] H. S. Tang and F. Sotiropoulos. A second-order Godunov method for wave problems in coupled solid-water-gas systems. *J. of Computational Physics*, pages 790–815, 1999.

[54] J. N. Tjotta and S. Tjotta. Nonlinear equations of acoustics, with application to perametric acoustic arrays. *J. Acoustical Society of America*, pages 1644–1652, 1981.

[55] J. N Tjotta and S. Tjotta. Nonlinear equations of acoustics. In *Frontiers of Nonlinear Acoustics: Proceedings of the 12th ISNA*, pages 80–97, 1990.

[56] J. A. Trangenstein and P. Colella. A higher-order Godunov method for modeling finite deformation in elastic-plastic solids. Larence Livermore National Laboratory.

[57] J. A. Trangenstein and R. B. Pember. Numerical algorithms for strong discontinuities in elastic-plastic solids. submitted to J. of Computational Physics, 1990.

[58] J. A. Trangenstein and R. B. Pember. The Riemann problem for longitudinal motion in an elastic-plastic bar. *Siam J. Sci. Stat. Comput.*, 12(1):180–207, January 1991.

[59] F. De Veubeke. *Course in Elasticity.* Springer-Verlag, 1979.

[60] G. Z. Voyiadjis and T. Park. The kinematis of damage for finite-strain elasto-plastic solids. *Int. J. of Engineering Science*, pages 803–830, 1999.

[61] F. Wang, J. G. Glimm, J. W. Grove, B. J. Plohr, and D. H. Sharp. A conservative Eulerian numerical scheme for elasto-plasticity and application to plate impact problems. *Impact Comput. Sci. Engrg.*, 5:285–308, 1993.

[62] C. Xuanhui and L. Yongqi. Damage process in hardened cement paste. *ACI Materials Journal*, pages 378–385, 1996.

[63] D. Yong and J. Kevorkian. Solving boundary-value problems for systems of hyperbolic conservation laws with rapidly varying coefficients. *To Appear in Studies in Applied Mathematics*, November 2000.

[64] P. Zhong and C. J. Chuong. Propagation of shock waves in elastic solids caused by cavitation microjet impact. I: Theoretical formulation. *J. Acoustical Society of America*, pages 19–28, 1993.

VITA

EDUCATION

Ph.D, Applied Mathematics, 2001, University of Washington, Seattle, WA. Topic: *Finite Volume Methods for Acoustics and Elasto-plasticity with Damage in a Heterogeneous Medium*

M.S., Applied Mathematics, 1997, University of Washington, Seattle, WA. Topic: *High-Resolution Finite Volume Methods for Acoustics in a Rapidly-Varying Heterogeneous Medium*

B.S., Mathematics 1995. University of Washington, Seattle, WA

B.S., Physics 1995. University of Washington, Seattle, WA

B.S., Astronomy 1995. University of Washington, Seattle, WA

PUBLICATIONS

High-Resolution Finite Volume Methods for Acoustics in Periodic and Random Media. Tiernan R. Fogarty and Randall J. LeVeque, Journal of the Acoustical Society of America, vol. 106, no. 1, July 1999, pp. 17-28.

High-Resolution Finite Volume Methods for Acoustics in a Rapidly-Varying Heterogeneous Medium, Tiernan R. Fogarty and Randall J. Leveque, Proc. 4'th Intl. Conf. on Wave Propagation, Golden,Colorado, June 1–5, 1998.